REDUCED FIDELITY ANALYSIS OF COMBUSTION INSTABILITIES USING FLAME TRANSFER FUNCTIONS IN A NONLINEAR EULER SOLVER

A Dissertation

Submitted to the Faculty

of

Purdue University

by

Gowtham Manikanta Reddy Tamanampudi

In Partial Fulfillment of the

Requirements for the Degree

of

Doctor of Philosophy

August 2019

Purdue University

West Lafayette, Indiana

THE PURDUE UNIVERSITY GRADUATE SCHOOL

STATEMENT OF DISSERTATION APPROVAL

Dr. William E. Anderson, Chair

School of Aeronautics and Astronautics

Dr. Gregory Blaisdell

School of Aeronautics and Astronautics

Dr. Carlo Scalo

School of Mechanical Engineering

Dr. Swanand Sardeshmukh

School of Aeronautics and Astronautics

Dr. Cheng Huang

School of Aeronautics and Astronautics

Approved by:

Dr. Weinong Wayne Chen

Head of the School Graduate Program

To my family.

ACKNOWLEDGMENTS

I would first like to thank my advisor, Prof. William Anderson for giving me this opportunity to do research in the field of combustion instabilities. He has been an exceptional mentor going above and beyond to help me understand the concepts and guide me through the research. He has been very patient and was always there when I needed help. I would also like to thank Dr. Cheng Huang, and Dr. Swanand Sardeshmukh for being exceptional mentors, and for guiding me throughout. They provided valuable advice and played a key role in the model formulation and subsequent improvements. I extend my thanks to Prof. Carlo Scalo and Prof. Gregory Blaisdell, for serving on my committee. I am also grateful to Dr. Merkel, and Dr. Venkateswaran Sankaran for their guidance and support throughout my research. I would also like to thank my family and friends for their continuous support and belief in me. It would not have been possible for me to stand where I am today without their well wishes and support. I must thank Kashmira Samel for being very supportive and there for me at all the times.

TABLE OF CONTENTS

Page

LIST OF TABLES

LIST OF FIGURES

Figure Page

Figure Page

Figure Page

ABBREVIATIONS

CFD	Computational Fluid Dynamics
CVRC	Continuously Variable Resonance Combustor
DES	Detached Eddy Simulation
DMD	Dynamic Mode Decomposition
FTF	Flame Transfer Function
FDF	Flame Describing Function
GEMSMA	Generalized Equation and Mesh Solver with Multiple Approaches
LES	Large Eddy Simulation
POD	Proper Orthogonal Decomposition
PSD	Power Spectral Density
RANS	Reynolds Averaged Navier Stokes
1L, 2L, ...	First Longitudinal Mode, Second Longitudinal Mode, ...
SVD	Singular Value Decomposition

ABSTRACT

Tamanampudi, Gowtham Manikanta Reddy Ph.D., Purdue University, August 2019. Reduced Fidelity Analysis of Combustion Instabilities Using Flame Transfer Functions in a Nonlinear Euler Solver. Major Professor: William E. Anderson.

Combustion instability, a complex phenomenon observed in combustion chambers is due to the coupling between heat release and other unsteady flow processes. Combustion instability has long been a topic of interest to rocket scientists and has been extensively investigated experimentally and computationally. However, to date, there is no computational tool that can accurately predict the combustion instabilities in full-size combustors because of the amount of computational power required to perform a high-fidelity simulation of a multi-element chamber. Hence, the focus is shifted to reduced fidelity computational tools which may accurately predict the instability by using the information available from the high-fidelity simulations or experiments of single or few-element combustors. One way of developing reduced fidelity computational tools involves using a reduced fidelity solver together with the flame transfer functions that carry important information about the flame behavior from a high-fidelity simulation or experiment to a reduced fidelity simulation.

To date, research has been focused mainly on premixed flames and using acoustic solvers together with the global flame transfer functions that were obtained by integrating over a region. However, in the case of rockets, the flame is non-premixed

and distributed in space and time. Further, the mixing of propellants is impacted by the level of flow fluctuations and can lead to non-uniform mean properties and hence, there is a need for reduced fidelity solver that can capture the gas dynamics, nonlinearities and steep-fronted waves accurately. Nonlinear Euler equations have all the required capabilities and are at the bottom of the list in terms of the computational cost among the solvers that can solve for mean flow and allow multi-dimensional modeling of combustion instabilities. Hence, in the current work, nonlinear Euler solver together with the spatially distributed local flame transfer functions that capture the coupling between flame, acoustics, and hydrodynamics is explored.

In this thesis, the approach to extract flame transfer functions from high-fidelity simulations and their integration with nonlinear Euler solver is presented. The dynamic mode decomposition (DMD) was used to extract spatially distributed flame transfer function (FTF) from high fidelity simulation of a single element non-premixed flame. Once extracted, the FTF was integrated with nonlinear Euler equations as a fluctuating source term of the energy equation. The time-averaged species destruction rates from the high-fidelity simulation were used as the mean source terms of the species equations. Following a variable gain approach, the local species destruction rates were modified to account for local cell constituents and maintain correct mean conditions at every time step of the nonlinear Euler simulation. The proposed reduced fidelity model was verified using a Rijke tube test case and to further assess the capabilities of the proposed model it was applied to a single element model rocket combustor, the Continuously Variable Resonance Combustor (CVRC), that exhibited self-excited combustion instabilities that are on the order of 10% of the mean pressure. The results showed that the proposed model could reproduce the unsteady behavior of the CVRC predicted by the high-fidelity simulation reasonably well. The effects of control parameters such as the number of modes included in the FTF, the number of sampling points used in the Fourier transform of the unsteady heat release, and mesh size are also studied. The reduced fidelity model could reproduce the limit cycle amplitude within a few percent of the mean pressure. The successful constraints on the model include good spatial resolution and FTF with all modes up to at least one dominant frequency higher than the frequencies of interest. Furthermore, the reduced fidelity model reproduced consistent mode shapes and linear growth rates that reasonably matched the experimental observations, although the apparent ability to match growth rates needs to be better understood. However, the presence of significant heat release near a pressure node of a higher harmonic mode was found to be an issue. This issue was rectified by expanding the pressure node of the higher frequency mode. Analysis of two-dimensional effects and coupling between the local pressure and heat release fluctuations showed that it may be necessary to use two dimensional spatially distributed local FTFs for accurate prediction of combustion instabilities in high energy devices such as rocket combustors. Hybrid RANS/LES-FTF simulation of the CVRC revealed that it might be necessary to use Flame Describing Function (FDF) to capture the growth of pressure fluctuations to limit cycle when Navier-Stokes solver is used.

The main objectives of this thesis are:

1. Extraction of spatially distributed local flame transfer function from the high fidelity simulation using dynamic mode decomposition and its integration with nonlinear Euler solver

2. Verification of the proposed approach and its application to the Continuously Variable Resonance Combustor (CVRC).

3. Sensitivity analysis of the reduced fidelity model to control parameters such as the number of modes included in the FTF, the number of sampling points used in the Fourier transform of the unsteady heat release, and mesh size.

The goal of this thesis is to contribute towards a reduced fidelity computational tool which can accurately predict the combustion instabilities in practical systems using flame transfer functions, by providing a path way for reduced fidelity multi-element simulation, and by defining the limitations associated with using flame transfer functions and nonlinear Euler equations for non-premixed flames.

1. INTRODUCTION

1.1 Overview of combustion instability

Combustion instability is a phenomenon that arises due to coupling between heat release and other unsteady processes [1–3]. It is observed in rocket engines, gas turbine engines and many other devices like the blast furnace and heating units. A small perturbation in pressure caused by any of the processes like vortex shedding, atomization and chemical kinetics, when coupled with heat release oscillations can lead to amplification of pressure oscillations. The level of oscillations can be very small and harmless or very large and damaging. The level of pressure oscillations depends on the operating parameters and the geometry of the device.

The "singing flame", where a flame produces sound when a tube of sufficient length is used, observed by Byron Higgins in 1777 is one of the earliest references to combustion instability. Another important reference to combustion instability was found in the work by Rijke [4], where a flame located at the quarter length from the inlet of the tube, which is open at both ends, showed self-excited pressure oscillations that are coupled with the heat release fluctuations. It was Rayleigh [1], who proposed the famous Rayleigh criterion,

$$\int_0^{\tau} \int_0^{V} p'(x,t) q'(x,t) dv dt > \int_0^{\tau} \int_0^{V} \phi(x,t) dv dt \tag{1.1}$$

where p' and q' are the unsteady pressure and heat release fluctuations, τ is the time period, v is the volume of the combustor and ϕ is the wave energy dissipation, that instabilities occur when Eq. 1.1 is satisfied, i.e., when the energy entering the system is greater than the energy leaving the system. It also states that pressure oscillations continue to grow when the pressure and heat release oscillations are coupled in phase and damp when they are coupled out of phase. The system, however, may reach a limit cycle, where there is no growth or decay of oscillations due to nonlinearities and losses through the boundaries.

The most prominent reference to the combustion instabilities observed in a practical system dates to the Saturn F-1 engine development in 1960s. During the testing phase, the instability levels that exceed the threshold of safe engine operation were observed [5]. To control the observed instabilities a series of tests were performed by trial and error approach by using different configurations of baffles and fuel injectors. After rigorous testing over two years, the best arrangement of injectors and baffles that allows stable operation of the engine by damping any transverse and tangential instability modes was found. The final design of the F-1 injector plate with baffles is shown in Fig. 1.1.

Combustion instability is one of the main risks associated with rocket and gas turbine engine development [6–8]. A rocket engine which did not show any kind of pressure oscillations during the test phase can suddenly start to show high pressure oscillations due to a minor change in the operating conditions or design alterations, which could end the mission. In rocket engines, it can be very difficult to identify the

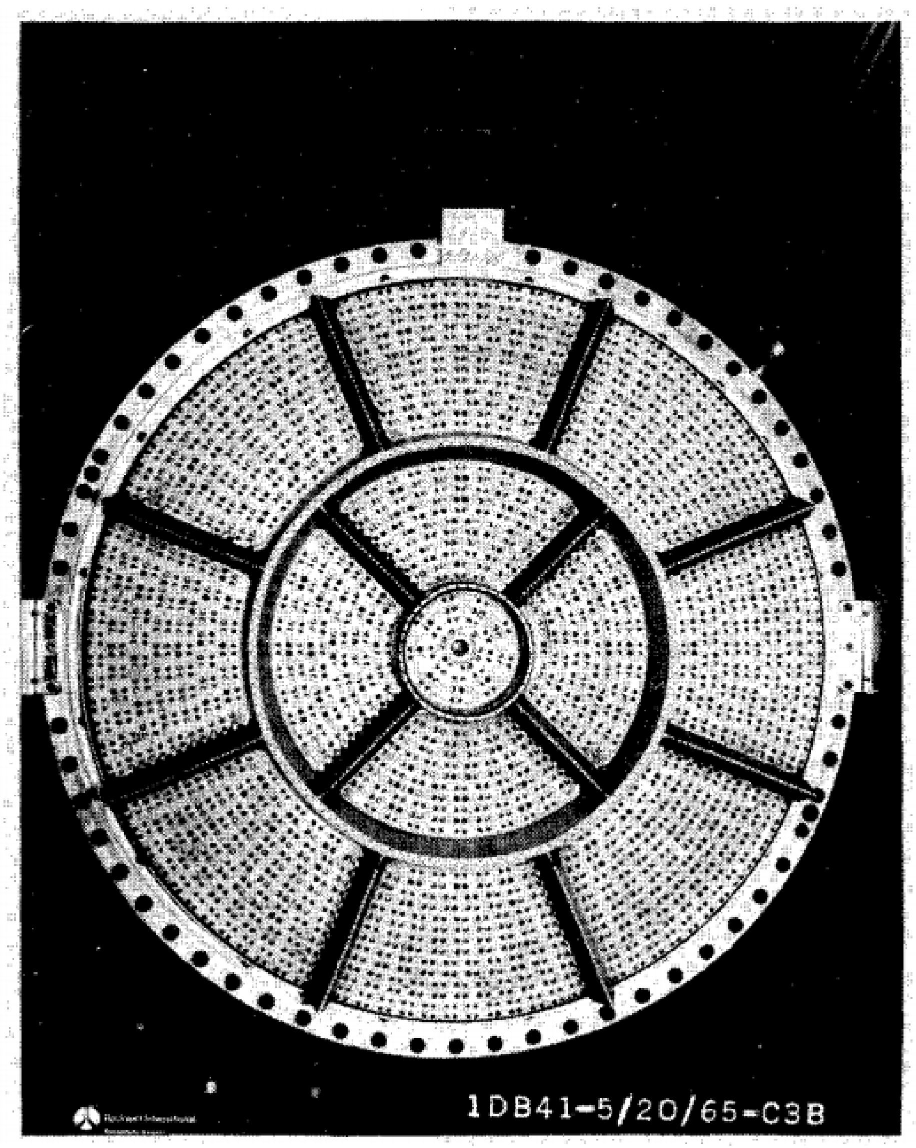

Fig. 1.1. The Saturn F-1 engine with baffles installed to prevent combustion instabilities [5]

source of combustion instabilities given the complexity of the flow field. Also, it could cost many millions of dollars in full-scale testing of the engine to identify and control the instabilities. Affordability being one of the main objectives of new rocket engine development programs, combustion instability and the underlying mechanisms must be well understood to reduce the cost and to increase the margin of safety.

1.2 Types of instability

Although there is no exact dividing line between the various regimes of combustion instability, based on the frequency at which combustion oscillations occur, they are classified into three types: 1. Chugging [9] is a low-frequency combustion instability that occurs at several hundreds of Hz due to coupling between the bulk mode and mass flow oscillations, 2. Buzzing [10] is an intermediate frequency combustion instability that occurs around higher hundreds to low thousand Hz due to the interaction between the propellant feed system and combustion chamber and, 3. Screeching [11] is the high-frequency combustion instability generally observed in rockets due to coupling between acoustics, injection flow oscillations and other sub-process of combustion. The source of high-frequency combustion instabilities is difficult to determine due to the complex flow field associated with the rocket engines.

Based on the system to which they are coupled, Barrere and Williams [12] classified the combustion instabilities as: 1. instabilities that occur only in the combustion chamber without coupling to other parts of the engine (combustion-chamber instabilities), 2. instabilities that occur due to interaction with other parts of the engine such as the feed system (system instabilities), and 3. instabilities that occur due to chemical reactants (intrinsic instabilities).

Combustion instabilities are further classified based on the type of oscillations: 1. self-excited combustion instabilities that initiate due to a self-induced perturbation in the system, such as a small change in pressure drop across the injector that leads to mass flow fluctuations which in-turn causes heat release fluctuations. These fluctuations continue to grow until they reach a limit cycle due to inherent coupling between the heat release fluctuations and other flow processes [13–15] such as flame-vortex interactions [16] [17], and flame-acoustic interactions as shown in Fig. 1.2. The instabilities observed in the Saturn F-1 engine are self-excited combustion instabilities. 2. forced combustion instabilities are initiated by an external forcing that causes the flow perturbations. External forcing is often used as a stability rating tool, and in experiments as an independent test variable.

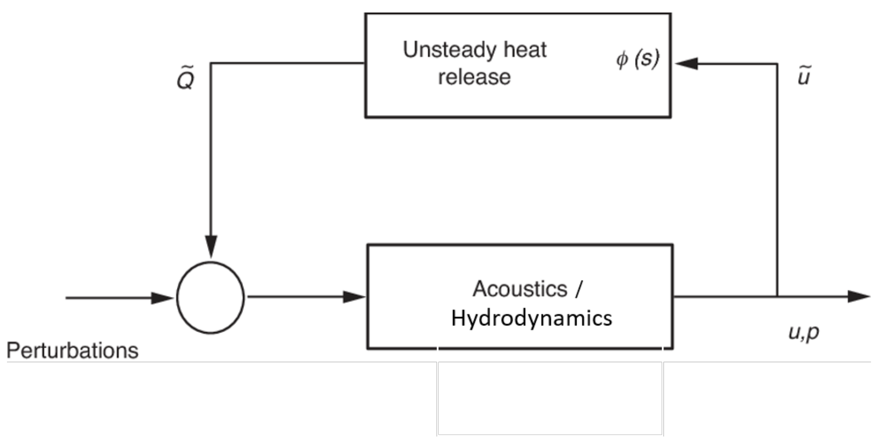

Fig. 1.2. Block diagram showing closed loop of self-excited combustion instability

1.3 Governing mechanism of combustion instability

Combustion instabilities in any device are mainly governed by two types of mechanism, linear and nonlinear mechanism. If combustion instabilities in a system are governed by linear mechanism, the fluctuations either grow or decay exponentially as shown in Fig. 1.3. However, the fluctuations in a practical system reach a limit cycle instead of growing forever as shown in Fig. 1.4. The initial growth of fluctuations at low amplitudes is typically characterized by linear mechanisms, but as the amplitude of fluctuations increase, the nonlinear mechanisms take over restricting the exponential growth of fluctuations. Although there is no clear boundary, the nonlinear mechanisms become prominent when the oscillation levels are more than 5% of the mean pressure.

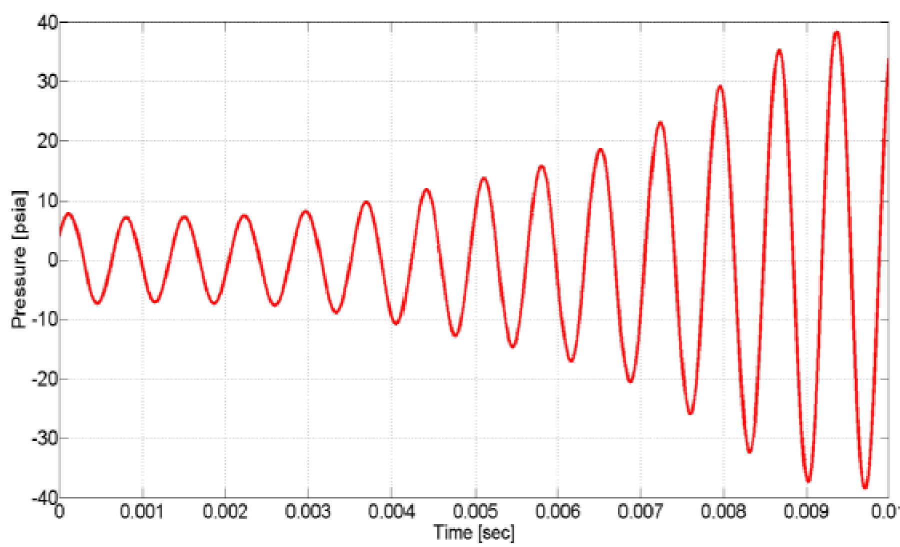

Fig. 1.3. Pressure variation with time showing linear growth regime

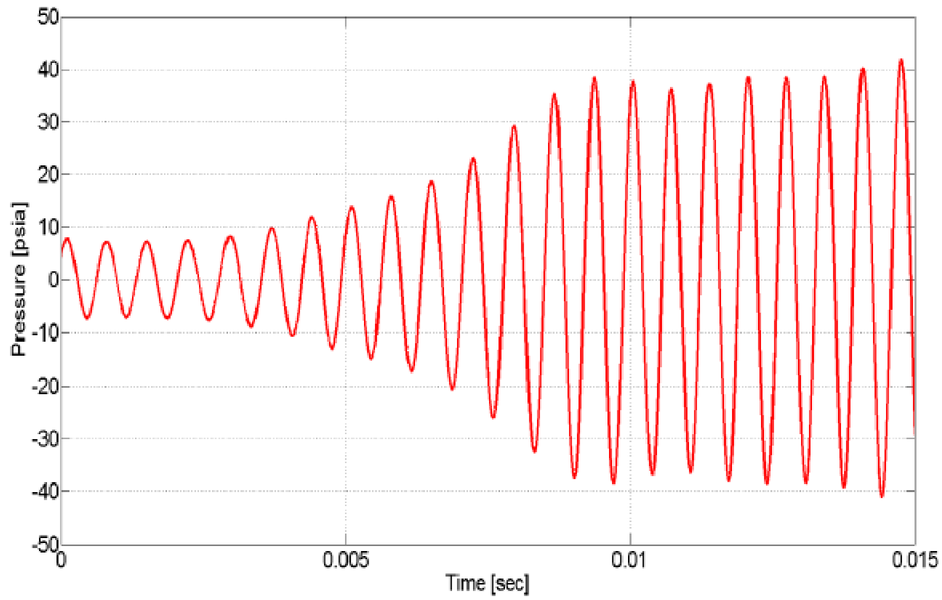

Fig. 1.4. Pressure variation with time showing limit cycle

1.4 Modeling approaches

Combustion instability is being studied both experimentally [10, 18–23] and computationally [24–30] for the past several decades. A majority of the studies are restricted to a single element combustion chamber. As of today, no feasible experimental procedure or computational tool exists that can predict the combustion instabilities in full scale engine.

It is of utmost importance to be able to predict the combustion instabilities in a full-size combustor. That is, one should be able to predict the level and growth rate of instabilities that can be expected in a combustor during the design phase itself so that necessary modifications can be made to the engine design to prevent the instabilities in an engine while in operation. Once developed and tested, the predictive tools would help reduce the uncertainty factor associated with engine operation and the cost associated with engine testing.

1.4.1 high-fidelity simulations

In the present day, there are many high-fidelity computational techniques such as large eddy simulations (LES), detached eddy simulations (DES), and direct numerical simulations (DNS) that provide a great amount of detail about the phenomena under study, which cannot be observed through experiments. These methods solve the multi-dimensional Navier Stokes Equations accounting for chemical reactions, mean flow, flame dynamics, vortex interactions, turbulence, viscosity, boundary effects, etc,. The high-fidelity techniques can be used to study complex flow fields such as the gas turbines and rocket combustors. Tucker et al. [31] simulated the rocket combustor using LES, unsteady Reynolds Averaged Navier Stokes (URANS), and steady Reynolds Averaged Navier Stokes (RANS) and pointed out the modeling challenges associated with these simulations. They observed that the results of URANS and fine grid LES compared well with each other. However, the work by Tucker et al. did not focus on combustion instability modeling. Brookes et al. [32] modeled bluff body stabilized simplified gas turbine system using URANS to study combustion instabilities associated with the system. LES [33, 34] is being used widely to study combustion instabilities in gas turbine systems. Angelberger et al. [33] studied combustion instabilities in backward facing step using LES and observed that the large eddies play a prominent role in the combustion instability of the system under study. Shipley et al. [35] investigated combustion instabilities in a seven element Transverse Instability Chamber (TIC) using DES. The results provided a deeper insight into the phenomenon leading to combustion instabilities. Heat release contour of the seven element TIC obtained through DES is shown in Fig. 1.5. Although the high-fidelity simulations provide valuable and detailed information, they require an enormous amount of computational power. Especially, this situation becomes worse in the simulation of complex fields which require three-dimensional modeling and detailed chemical kinetics. In addition, one of the key parameters that characterize the instabilities, their growth rate, is difficult to obtain using high-fidelity simulations, as it would require enormous computational power to be able to capture the entire growth period and limit cycle of the system. Hence, the use of high-fidelity computational techniques to predict combustion instabilities in full-size combustors can take a very long time and is not preferred in situations that demand a quick turnaround time. An alternative to high-fidelity simulations is the reduced fidelity simulations that solve wave equation, linearized Euler equation, or nonlinear Euler equations. A block diagram showing the various approaches of combustion instability modeling arranged in term of fidelity and associated cost is shown in Fig. 1.6.

1.4.2 Reduced fidelity simulations

Reduced fidelity simulations based on the wave equation and Euler equations [37] [38] require considerably less time to obtain a solution compared to the high-fidelity models. The reduced fidelity methods can be broadly classified into linear and non-

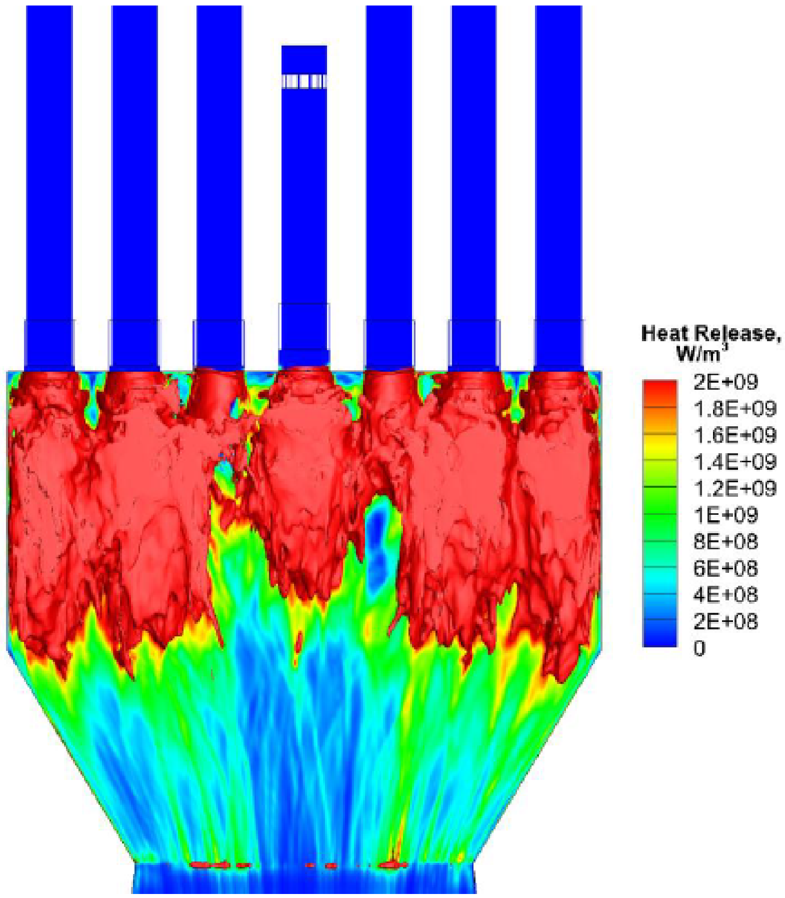

Fig. 1.5. Heat release contour of a 7 element Transverse Instability Chamber obtained from a 3D high-fidelity simulation [35]

linear methods. The linear methods use simple equations and are based on wave equation or linearized Euler equations. Using linear methods, the eigen-modes and eigen-frequencies can be predicted. However, the growth rates predicted correspond to the linear system where the pressure fluctuations grow exponentially without any bounds. Using linear methods, the limit cycle amplitudes cannot be predicted. To overcome the limitations of the linear models, work has been done on the nonlinear modeling of combustion instability by accounting for nonlinear acoustics and com-

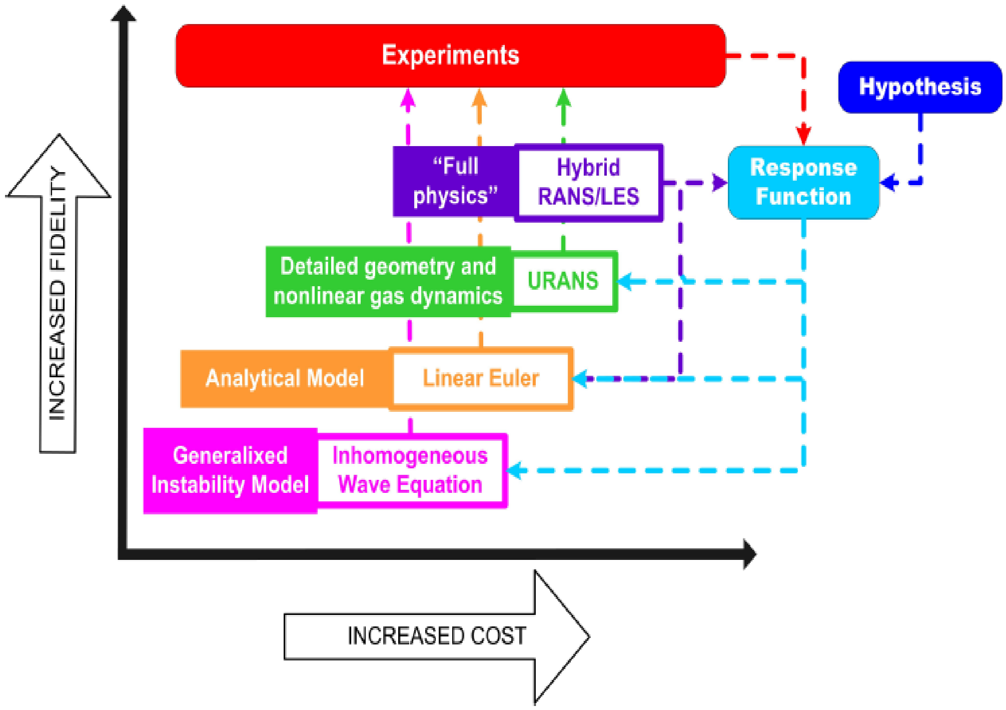

Fig. 1.6. Block diagram showing various approaches of combustion instability modeling arranged in terms of fidelity and associated cost [36]

bustion [39–42]. Nonlinear modeling of combustion instability is significantly more challenging than the linear analysis. The reduced fidelity models despite being able to accurately capture the resonant modes of the chamber do not account for all the physics involved and cannot predict the combustion instabilities to the full extent. In order to use these reduced fidelity models to study combustion instabilities, additional information about the interaction of flame and acoustics of the chamber must be provided externally as a source term. Using the reduced fidelity approach, some of the important parameters such as the resonant frequency, growth rate of resonant modes can be predicted to help characterize the combustion instabilities associated with the system to a certain extent. However, the reduced fidelity models cannot inherently account for the coupling between unsteady heat release fluctuations and flow fluctuations. Hence the unsteady heat release response needs to be specified as an input to the reduced fidelity techniques.

The $n - \tau$ time-lag approach proposed by the Crocco [2] has been widely used to account for unsteady combustion in the reduced fidelity models. The time lag model characterizes the global heat release fluctuations in the combustion chamber to a reference pressure or velocity fluctuations using the two parameters n and τ. It is expressed as,

$$\frac{q'}{\bar{q}} = n\frac{p'(t-\tau)}{\bar{p}} \tag{1.2}$$

where n is the interaction index and τ is the time lag between the global (integrated over the entire combustion chamber) heat release fluctuations and reference pressure fluctuations. Although the $n - \tau$ model has shown success in capturing reasonable growth rate and frequencies, the main drawback of the model is the lack of generality of the parameters n and τ. They must be determined for every system to perform reduced fidelity analysis. Over the years the time-lag model proposed by Crocco has undergone many changes in the way the n and τ are calculated but its form remain unchanged. Similar time-lag models were developed by Dowling and Stow [43].

The other frameworks used to describe the flameacoustic interactions in the reduced fidelity models are: 1. The transfer matrix approach, and 2. The flame transfer function approach. In the transfer matrix approach [44] [45], which can also be termed as acoustic network model, the flame is represented as black box and the flow upstream and downstream of the flame are connected through the transfer matrix,

$$\begin{pmatrix} p'_{down} \\ \\ u'_{down} \end{pmatrix} = \mathbf{M}(f) \begin{pmatrix} p'_{up} \\ \\ u'_{up} \end{pmatrix}, \mathbf{M}(f) = \begin{pmatrix} M_{pp}(f) & M_{pu}(f) \\ \\ M_{up}(f) & M_{uu}(f) \end{pmatrix}, \tag{1.3}$$

where ( )' indicates the fluctuating quantities, $(\ )_{down}$ down indicates the downstream variables and $(\ )_{up}$ indicates the upstream variables and $\mathbf{M}(f)$ is the transfer matrix.

In this approach of acoustic network model, each part of the system is considered as a lump and are connected to each other through the transfer matrix. Although this approach is being used widely, considering the flame as a black box makes this approach less appealing than the approach using flame transfer function.

Using flame transfer function (FTF) [46] approach, the information about flame is externally provided to the reduced fidelity model in the form of unsteady source term or unsteady heat release fluctuations,

$$FTF(\omega) = \frac{\frac{\dot{q}'}{\bar{q}}}{\frac{p'}{\bar{p}}} \ or \ FTF(\omega) = \frac{\frac{\dot{q}'}{\bar{q}}}{\frac{u'}{\bar{u}}}. \tag{1.4}$$

Flame transfer function is a carrier function that provides information about the unsteady flame response. When used together with reduced fidelity models, FTFs can help characterize the combustion instabilities of a system to a certain extent using limited computational power. In this thesis, the main emphasis is on the flame transfer functions.

The flame transfer functions are being extensively used to study the combustion instabilities of premixed flames [47–50]. However, their application to non-premixed flames is very limited [51] [52]. Flame transfer functions were calculated both for the laminar [53] [54] and turbulent [55–57] premixed flames involving complex geometries. However, the studies related to the FTFs of turbulent premixed flame are limited given the complexities associated with their extrapolation and complex acoustic/flame coupling. The flame transfer functions have been calculated experimentally [58–62], computationally [48, 53, 55, 63] and analytically [64–66]. The flame transfer functions are most extensively extracted from the experiments following the global flame transfer function approach in which the FTF is obtained by using the volume integrated heat release measurements and the velocity measured at the inlet of the combustor [58] [61]. Some studies have been dedicated to obtaining spatially distributed flame transfer function from the experiments [67] following the local flame transfer function approach in which the local heat release measurements were used for the FTF extraction. The heat release measurements in the combustor are usually based on the CH* and OH* chemiluminescence measurements. In addition to being used in the reduced fidelity models, FTFs also help shed information on how the flame responds to various flow parameters. Various studies dedicated to the investigation of the influence of various flow/flame parameters on the FTF can be found throughout the literature [68]. Through these studies, it is possible to unlink the coupling between various phenomenon leading to combustion instabilities. Preetham et al. [56] through their investigation on the effect of flame structure on FTF, found that the average area of turbulent flame is less compared to the laminar flame as the small turbulent scales will help disseminate larger fluctuations in the flame area and hence it leads to a lower gain of the FTF. The flame transfer function data obtained from the experiments is further used to develop an analytical flame transfer function dispersion relation given by Noiray et al. [65],

$$H(\omega_r + i\omega_i) = F(\omega_r), \tag{1.5}$$

where,

$$H(\omega) = \frac{4\pi h}{\alpha\omega}\frac{\bar{u}P}{(E-1)\bar{A}}\frac{c}{S_L}(cotan(\frac{\omega L}{c}) - \frac{\omega l}{cP}(1+\frac{l_v}{r_p}(1+i))), \tag{1.6}$$

and $F(\omega_r)$ is the flame transfer function, which can be solved to predict the Eigen modes and growth rate of resonant modes. In this approach, the original FTF measured from the experiments or computations can be assumed to be a combination of several Gaussian functions with varying time delays in order to better fit the data as given by Kaess et al. [51]

$$F(\omega) = (1+a)e^{-i\omega\tau_1 - \frac{\omega^2\sigma_1^2}{2}} - ae^{-i\omega\tau_2 - \frac{\omega^2\sigma_2^2}{2}}, \tag{1.7}$$

where, the unknowns $\tau 1, \tau 2, \sigma 1, \sigma 2$ can be calculated based on the available data. Using similar approach, Kim et al. [67] showed that the global flame transfer function can accurately predict the resonant modes and growth rates if the flame length is less than 10% of the acoustic wavelength. Otherwise, local flame transfer function was found to be more accurate.

The extraction of the flame transfer function from high-fidelity simulations is less common compared to the extraction from experiments. However, there is growing interest in this area and several studies can be found throughout the literature [48]

[53] [55] [69] [70]. Most of the studies involving extraction of the FTF from CFD simulation can be categorized into two based on the approach used, 1. Generic FTF approach, in which the global FTF in frequency domain was simply obtained by taking the ratio of the Fourier transform of the global heat release fluctuations and Fourier transform of pressure or velocity fluctuations [53], 2. Extraction of FTF using impulse response function, in which the FTF is extracted in the time domain using the Weiner - Hopf method, which is based on correlation of the data, as given by Luis et al. [70],

$$\Gamma_{ij} h_i = c_i, \tag{1.8}$$

where Γ is the auto-correlation matrix of the input signal (pressure or velocity measured at the reference location) and c is the cross-correlation of the input signal and heat release signal, h is the unit impulse response function obtained by inverting the above equation. The unit impulse response in the time domain can be converted into the frequency domain by taking z- transform, which then takes the form,

$$F(\omega) = \sum_{k=0}^{L} h_k e^{-i\omega k \delta t}, \tag{1.9}$$

given by Luis et al. [70] and Scarpato et al. [63]. Using the generic FTF approach, Duchaine et al. [53] investigated the effect of flame speed, the expansion angle of burnt gases, inlet air temperature, inlet duct temperature and combustor wall temperature on laminar premixed flame by characterizing the flame response through FTFs obtained from DNS simulations and found that laminar flames are more sensitive to flame speed and inlet duct temperature. Similarly, Preetham et al. [56] investigated the response of turbulent premixed flames to harmonic forcing and found that the average flame area is less when the turbulent flame is subjected to higher amplitudes of excitation, because of the small turbulent scales that disseminate the flame area fluctuations. The second approach of using impulse function was mainly used in studies where the intention was to integrate the developed FTF with acoustic solvers. Scarpato et al. [63] investigated a reheat combustor considering flame as a multiple input single output system using the Weiner- Hopf method to unlink the coupling between the effects of various flow parameters on combustion instability. The main assumption of the Weiner-Hopf method is that the system is linear, which is true only at small fluctuation levels and is well applicable to the gas turbine systems but not to the rocket systems. Further, the FTF is only a frequency dependent function and hence it cannot characterize the flame response at all fluctuation levels, especially in a system with higher fluctuation levels. Flame Describing Function (FDF) is an amplitude dependent flame transfer function and can be expressed as

$$FDF(\omega, p') = \frac{\frac{\dot{q}'}{\bar{q}}}{\frac{\dot{p}'}{\bar{p}}} \ or \ FDF(\omega, u') = \frac{\frac{\dot{q}'}{\bar{q}}}{\frac{\dot{u}'}{\bar{u}}}. \tag{1.10}$$

Flame describing function helps predict the limit cycle amplitude in addition to the resonant modes and growth rate when integrated with a nonlinear solver. Several studies can be found in the literature in which FDF was extracted from the experiments and a dispersion relation was developed to implement the FDF in acoustic solver [65] [71] [66] [64]. Flame describing function also helps study the limit cycles of multiple flame combustors [71].

One of the recent works on FTF/FDF in premixed flames is done by Han et al. [72]. In their study, a bluff body stabilized partially premixed flame combustor was simulated using an LES solver. Further, the flame describing function was extracted from the high-fidelity simulations and was used in the reduced fidelity thermo-acoustic modeling network tool developed in-house. Han et al. [72] successfully analyzed the limit cycle behavior of the combustor using the flame describing function. This is one of the first attempts where a flame describing function extracted from high-fidelity simulations was successfully implemented in a reduced fidelity acoustic tool. The FDF obtained by Han et al. showing the gain and phase for various flow fluctuation levels and frequencies is shown in Fig. 1.7. The use of FDF/FTF extracted from high-fidelity simulations in reduced fidelity tools is only at the beginning stage.

Among the very limited studies on the extraction of FTF from non-premixed flames [51] and application of combustion response models to study non-premixed flames [52], particular interest is a recent attempt on combustion instability prediction of non-premixed flames by Frezzotti et al. using quasi one-dimensional Euler equations. In her work, the response functions were extracted from two different simulations, DES and URANS, and two flame response models similar to Crocco's $n-\tau$ model, one based on pressure and the other based on velocity for each reference sim-

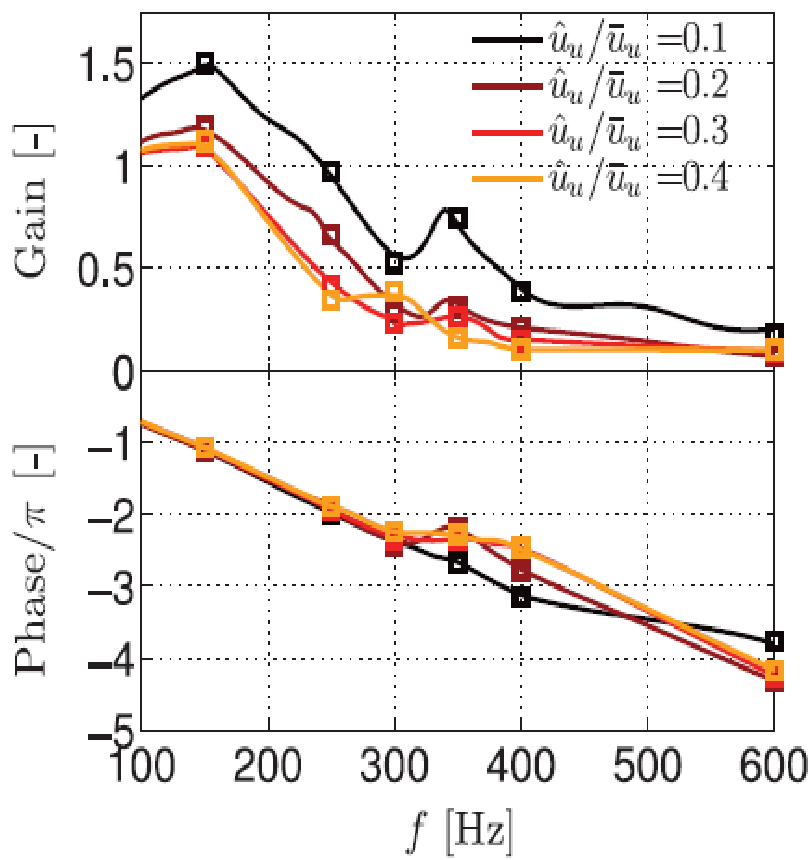

Fig. 1.7. The FDF obtained by Han et al. showing the gain and phase for various flow fluctuation levels and frequencies [72]

ulation were developed. The velocity-time lag response function used by Frezzotti et al. is,

$$\dot{q}_{us}(x,t) = g_u(x)\alpha_u A(x)[u(x_u, t - \tau_u) - \bar{u}(x_u)], \tag{1.11}$$

where,

$$g_u(x) = \frac{e^{-\frac{(x-\mu_u)^2}{2\sigma_u^2}}}{\sqrt{2\pi\sigma_u^2}}, \tag{1.12}$$

α_u is the coefficient of proportionality, τ_u is time lag, μ_u is mean of Gaussian distribution, σ_u is the standard deviation of Gaussian distribution. It was assumed that the flame transfer function follows Gaussian distribution close to the dump plane and is zero elsewhere. The parameters such as mean, and variance were modeled such that the assumed Gaussian profile closely represents the mean heat release profile observed in the high-fidelity simulations. Further, two important parameters, the time lag, and coefficient of proportionality were determined using cross-correlation and the least square method respectively. Although the response function was distributed, only a particular value of time lag and proportionality constant were used in accordance with Crocco's $n - \tau$ model [2]. The combustion response models were then used with quasi one-dimensional Euler equations and the results obtained agreed well with the reference DES simulation as shown in Fig. 1.8.

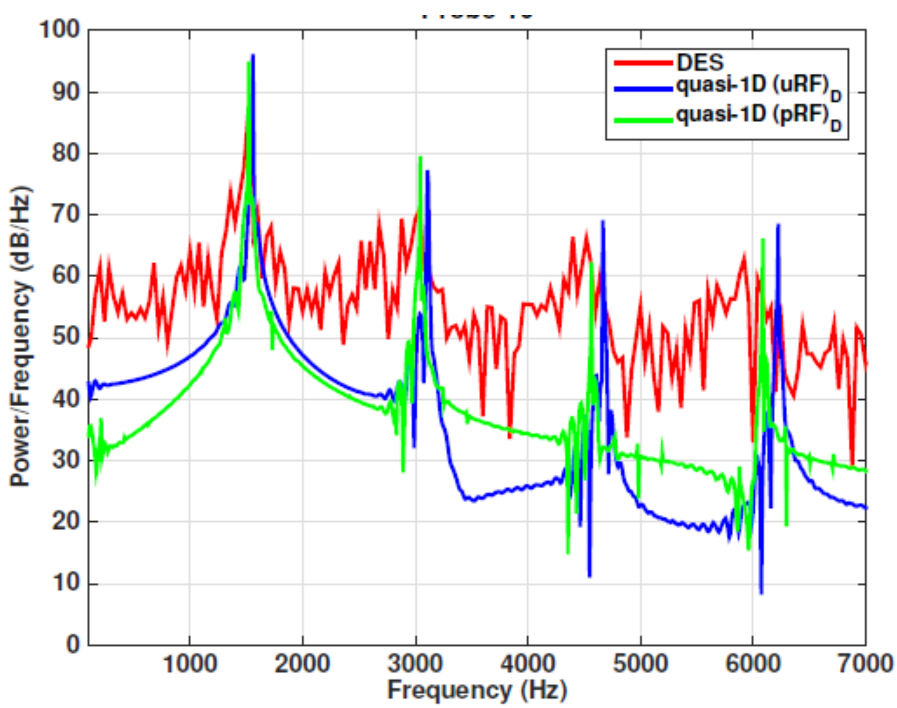

Fig. 1.8. Comparison of a) pressure trace, and b) Power Spectral Density (PSD) between the DES simulation, one-dimensional pressure and velocity lag models [52]

Although a good agreement was obtained using one-dimensional solver, the application of this approach is limited to axial instability and transverse instability modes in a multi-element chamber cannot be predicted. Also, employing a one-dimensional solver, one of the main assumptions made by Frezzotti et al. in calculating the steady state conditions was that the oxidizer burns instantaneously in the chamber following a prescribed sinusoidal pattern and produces corresponding reactants. This assumption has made the flame appear to be more of a distributed premixed flame with a specified rate of production of products that varies spatially in the region specified, rather than a non-premixed flame where the flow mixes on its own and produces products accordingly. Further, the mixing of propellants is impacted by the level of flow fluctuations and can lead to non-uniform mean properties and hence, there is a need for reduced fidelity solver that can capture the gas dynamics, nonlinearities and steep-fronted waves accurately.

1.5 Objectives

Based on the literature review, it is clear that there has not been a lot of research in the area of using FTFs to study non-premixed flames. To model the non-premixed flames, acoustic solvers [73] [74] are limited as they do not account for flow mixing, cannot capture steep-fronted waves, and cannot be applied to complicated geometries. Nonlinear Euler equations have all the required capabilities that are necessary to model the non-premixed flames and are at the bottom of the table in terms of the computational cost among the solvers that can solve for mean flow and account for flow mixing. The NLE solver can capture steep-fronted waves, allow multi-dimensional modeling, allow modeling of complicated geometries and realistic boundaries. Although viscous effects are not included in the NLE equations, NLE solver accounts for flow mixing through the numerical viscosity associated with it. However, the impact of viscous terms on the results obtained through this approach needs to be evaluated.

The literature review also reveals that most of the FTF studies involve reference pressure/velocity based global FTFs due to compact and continuous nature of the premixed flame. However, in case of non-premixed flames, especially in rocket combustors, the flame is very energetic, erratic, detached, intermittent and extends far into the chamber [75] [76]. This behavior of flame could impact the local coupling between the heat release and pressure fluctuations and hence a spatially distributed local FTF may be necessary to accurately study the combustion instabilities in non-premixed flames using FTF and NLE solver.

The present thesis uses multi-dimensional nonlinear Euler equations together with spatially distributed local flame transfer functions, where the constant of proportionality and time lag are spatially resolved and calculated locally, to study and predict the combustion instabilities of non-premixed flames. This procedure will presumably allow us to treat the coupling between heat release and pressure fluctuations more accurately. Also, using multi-dimensional nonlinear Euler equations will allow us to study transverse instabilities in rectangular and cylindrical chambers using multiple elements.

In summary, the main objectives of this thesis are

1. Extraction of spatially distributed local flame transfer function from the high-fidelity simulation using dynamic mode decomposition and its integration with nonlinear Euler solver.

2. Verification of the proposed approach and its application to the Continuously Variable Resonance Combustor (CVRC).

3. Sensitivity analysis of the reduced fidelity model to control parameters such as the number of modes included in the FTF, number of sampling points used in the Fourier transform of the unsteady heat release, and mesh size.

1.6 Outline

In this thesis, the reduced fidelity approach that uses flame transfer functions together with the nonlinear Euler equations is proposed and the numerical aspects of the proposed model were verified using a Rijke tube test case and was subsequently applied to the CVRC. Sensitivity analysis of the reduced fidelity model to important control parameters was studied. This thesis is organized as follows:

In chapter 1, a short background on combustion instability and the problem statement were presented. The concept of the flame transfer function and its use in the field of combustion instability was introduced. Also, a brief review of the literature related to the current thesis was presented. Further, a clear distinction between work done by others and the work proposed in this thesis was presented. In this thesis, the NLE solver was used as a reduced fidelity solver that uses the spatially resolved local FTF as the combustion response function. The NLE solver is at the bottom of the table among the solvers that can solve for the mean flow and allow multi-dimensional modeling. Unlike acoustic solvers, NLE solver accounts for flow mixing (through numerical viscosity) that characterizes the non-premixed flows and captures the steep-fronted waves in addition to accounting for compressibility effects. Through this solver, complicated geometries can be modeled and realistic boundaries similar to high-fidelity simulations can be simulated. NLE solver also allows for modeling of transverse instability waves and rectangular chambers. However, the impact of the viscous terms on the performance of this model may need to be evaluated. The choice of spatially resolved local FTF was made based on the fact that flame in non-premixed combustor extends far into the chamber, unlike the premixed flames which are compact. Also, in the systems under consideration, the rocket combustors, in addition to high energy levels, the flame is erratic, detached and intermittent. This behavior of the flame can affect the local coupling between the heat release and pressure fluctuations and hence a spatially distributed local FTF was used in this thesis.

In Chapter 2, the background on the reference experiment and simulation is provided. The reference experiment, Continuously Variable Resonance Combustor (CVRC) is a single element model rocket combustor developed at Purdue University to study longitudinal combustion instabilities. This system is equipped with a movable oxidizer post whose length can be varied from 0.089 m to 0.1905 m either continuously during a test or fixed for a particular test. The stability behavior of the

CVRC ranged from 8% to 40% when the oxidizer post length was changed from 0.089 m to 0.1905 m. Numerous tests of the CVRC revealed that this system exhibited a consistent and repeatable behavior of pressure oscillations that are 8% of the mean pressure when the oxidizer post length was fixed at 0.089 m. Hence this weakly nonlinear case of CVRC with 0.089 m oxidizer post length was chosen as the reference case. The high-fidelity simulation of the same case, a two-dimensional axisymmetric hybrid RANS/LES simulation, was performed using an in-house solver GEMS. This simulation was performed using a mesh consisting of 100k nodes and a single step global chemistry. The high-fidelity simulation predicted a limit cycle pressure oscillation on the order of 10.5% of the mean pressure. This high-fidelity reference simulation was used as the source to extract the data necessary to perform a reduced fidelity NLE-FTF simulation. Further, an overview of the decomposition techniques, Proper Orthogonal Decomposition (POD) and the Dynamic Mode Decomposition (DMD) is presented along with the justification for using DMD to extract the flame transfer functions.

In chapter 3, a brief literature review on the flame transfer function is presented. The approach to extract flame transfer function from high-fidelity simulations and their integration with nonlinear Euler solver is presented. The flame transfer functions were extracted from high-fidelity simulations by applying the Dynamic Mode Decomposition (DMD) technique to the pressure and heat release fluctuations in the time domain to isolate frequency content. DMD is a dimensionality reduction technique similar to Proper Orthogonal Decomposition (POD) [77] which reduces a high dimensional complex raw data set into lower dimensions (modes) that represent dominant features of the raw data set. POD reduces the raw data with a focus on error minimization between the reduced and original data set. POD organizes the reduced data set based on the energy content of each mode. Each POD mode comprises of multiple frequencies. In contrast, DMD assumes a linear relationship in time between the snapshots of raw data and thereby reduces the raw data set into modes that are associated with a distinct frequency. This feature of DMD helps to identify the relationship between variables at a particular frequency. Hence DMD was employed to extract the FTF from high-fidelity simulation. This is also the first step in integrating the FTF and NLE solver. In the next step, the time-averaged species destruction rates from the high-fidelity simulation were imported to the NLE solver. In the NLE solver, the source term was split into the mean and fluctuating part. The mean source term comprises of the time averaged species destruction rates from the hybrid RANS/LES simulation. In the final step, the FTF obtained in the first step is integrated with the NLE solver as the fluctuating source term of the energy equation. The imported FTFs make use of the evolving pressure data of the NLE solver and calculate appropriate unsteady heat release.

In chapter 4, the verification of the proposed approach using a Rijke tube test case and its application to the CVRC is presented. The proposed approach was verified using a Rijke tube of length 0.5 m with a head addition zone 0.125 m from the inlet of the tube. Crocco's n-τ model was used to generate the unsteady heat release fluctuations. This model allows for accurate verification of the numerical aspects of the proposed approaches of FTF extraction and its integration with NLE solver. The results obtained revealed that the gain of the FTF extracted is equal to n imposed and the phase of the FTF is equal to the τ imposed. The obtained FTFs when integrated with the NLE solver were able to reproduce the mean variables and limit cycle statistics to a good extent verifying the proposed approaches. Upon successful verification, the proposed approaches were applied to the CVRC. During the initial runs, although the NLE-FTF simulation reached a limit cycle, non-physical temperature was observed close to the dump plane due to constant addition of mean heat without considering the local cell constituents. However, imposing a restriction on the mean heat based on the local cell constituents lead to pressure and temperature drop. This issue was corrected by following a variable gain approach which maintains the correct amount of heat in the system while considering the local cell constituents. Through the variable gain approach, accurate mean conditions in the chamber were obtained and the NLE-FTF simulation was able to reproduce the limit cycle to a good extent. The pressure cycle analysis revealed that the NLE-FTF simulation was able to predict global pressure trends however it could not capture all the details of hybrid RANS/LES simulation. The fuel cycle analysis revealed that the NLE-FTF simulation was able to capture the fuel accumulation near the dump plane during the compression cycle and its destruction during the expansion cycle. However, the temperature cycle analysis revealed that the NLE-FTF simulation showed a broader temperature range as expected because the unsteady heat release does not consider the local cell constituents. Although the results motivated the application of the proposed approach to transverse instability chamber, before any further application it is imperative to understand the effects of control parameters on the proposed model.

In chapter 5, the sensitivity analysis of the reduced fidelity model is presented. The sensitivity of the model to the number of modes in the FTF, the number of sampling points used in the Fourier transform of unsteady heat release fluctuation and the mesh size was studied. When high-frequency modes, which has a pressure node in the heat release zone were included in the NLE-FTF simulation, it resulted in numerical instability since the FTF was defined as the ratio of heat release fluctuations to pressure fluctuations. To eliminate this issue, the modes were stretched at the location of a pressure node. However, it resulted in a slight increase in the limit cycle amplitude of the NLE-FTF simulations. As the number of modes included in the FTF was increased, the limit cycle amplitudes of the NLE-FTF simulation approached the reference high-fidelity simulation. However, the 4- and 5- mode simulations showed a slightly higher limit cycle amplitude due the node issues. The NLE-FTF simulation was able to reproduce the high-fidelity simulation to a good extent under the constraints of good spatial resolution and an FTF that includes all modes up to at least one higher dominant frequency than the frequencies of interest. In addition to limit cycle amplitudes, the NLE-FTF simulations were also able to reproduce the mode shapes and linear growth rates observed in the experiment. Further analysis using a reference point based two-dimensional FTF resulted in higher limit cycle amplitudes revealing that it is necessary to account for local coupling between the heat release and pressure fluctuations. Also, the simulation with one-dimensional local FTF resulted in higher limit cycle amplitudes and lower growth rates indicating that the two-dimensional effects are important.

In chapter 6, a summary of the work done, and objectives achieved are presented. In addition, the recommendations for future work are also presented. Finally, the contribution of this thesis to the scientific body is presented.

This thesis will attempt to make a significant contribution towards a computational tool which can accurately predict the combustion instabilities in practical systems in a reasonable amount of time using limited computational power. It will provide a pathway for performing reduced fidelity multi-element simulations and by defining the limitations associated with using flame transfer functions and nonlinear Euler equations for non-premixed combustors.

2. BACKGROUND ON CONTINUOUSLY VARIABLE RESONANCE COMBUSTOR

In this chapter, a brief overview of the experimental setup of the reference case and results corresponding to that experiment are presented. The reference experiment used in this thesis is a single element model rocket combustor, the Continuously Variable Resonance Combustor (CVRC), with an oxidizer post length of 0.089 m. This case exhibited pressure fluctuations on the order of 8% of the mean pressure and its behavior is found to be very consistent and repeatable during the experiments. The high fidelity simulation of this case, two-dimensional axisymmetric hybrid RANS/LES simulation, was performed using the in-house compressible flow Navier-Stokes solver GEMS. The framework of the GEMS solver and the results obtained in the high fidelity simulation are also presented. In addition, an overview of the modal decomposition techniques and the reason for choosing DMD is explained.

2.1 Experiment

The reference experiment selected for the present work is Continuously Variable Resonant Chamber (CVRC), a single element combustion chamber with a gas-gas coaxial injector, capable of exhibiting self-excited longitudinal instabilities [22] [78] [79]. The schematic of the CVRC is shown in Fig. 2.1. The CVRC has a variable length oxidizer post which can be adjusted by using an actuator connected to the post. The oxidizer post is choked at the inlet to maintain constant mass flow rate and at the end, it is connected to a dump combustion chamber of length 0.381 m, which ends in a choked nozzle. The oxidizer post length can be varied from 0.089 m to 0.1905 m either continuously during an experiment or can be fixed at any particular post length of interest between 0.089 m and 0.1905 m. This feature helps to study the effect of acoustic resonance on combustion instability. The CVRC is very highly instrumented and is equipped with a set of high-frequency pressure transducers to measure the pressure. It is also equipped with a quartz window to perform optical measurements such as CH* and OH* chemiluminescence.

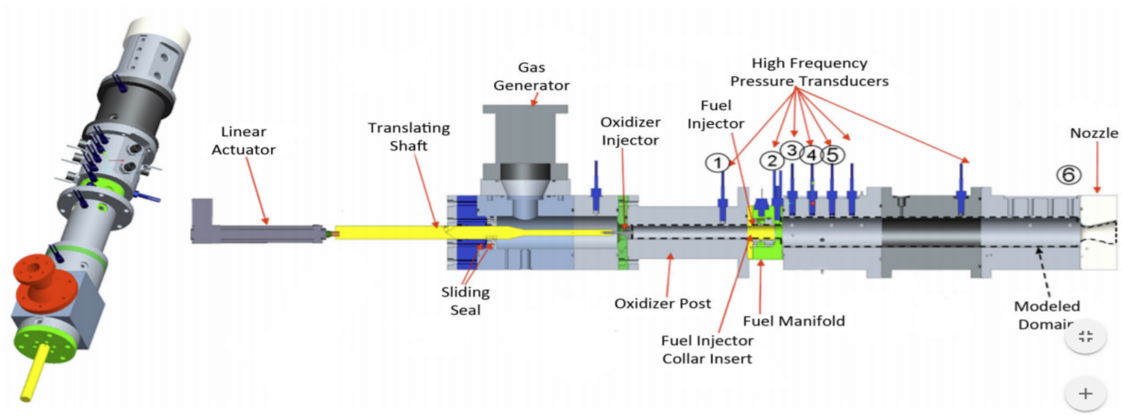

Fig. 2.1. Experimental setup of the Continuously Variable Resonance Chamber (CVRC)

The CVRC uses 90% hydrogen peroxide as the oxidizer, which when passed over a catalyst bed decomposes into 42.35% oxygen and 57.65% water vapor at

1030K. Methane at 298 K is used as the fuel. The CVRC is operated at an equivalence ratio of 0.8. The test conditions are summarized in Table. 2.1.

Table 2.1.
Operating conditions of CVRC

Parameter	Value
Fuel mass flow rate, kg/s	0.024
Fuel temperature, K	300
Oxidizer mass flow rate, kg/s	0.3175
Oxidizer temperature, K	1030
Equivalence ratio	0.8
Chamber Pressure, MPa	1.4
Chamber length, m	0.381
Oxidizer post length, m	0.089 0.190

The current version of CVRC was developed and extensively studied by Yu et al. [22] following the earlier the work with fixed-geometry combustors by Miller et al. [78] [79]. Several experiments were performed by Yu et al. both by translating the post length continuously during an experiment and by fixing the post length. Yu et al. observed that the CVRC exhibited varying levels of instability when the oxidizer post length was changed. The most stable case was observed when the oxidizer post length was 0.089 m, with pressure fluctuations around 8-10% of the mean pressure. The most unstable case was observed when the oxidizer post length was 0.1397 m, with pressure fluctuations around 40% of the mean pressure. At oxidizer post length 0.1905 m, the system was found stable during some runs and unstable during the rest.

A comparison of the high-passed pressure traces between the 0.089 m oxidizer post length case and 0.1397 m oxidizer post length case, measured 0.368 m downstream of the dump plane is shown in Fig. 2.2. A clear distinction in the amplitude of pressure fluctuations between the two cases can be seen in Fig. 2.2. Also, a comparison of power spectral densities (PSDs) of pressure traces between the 0.089 m oxidizer post length case and 0.1397 m oxidizer post length case, measured 0.368 m downstream of dump plane is shown in Fig. 2.3. The first three dominant modes in the 0.089 m oxidizer post length case were observed at 1440 Hz, 2844 Hz, and 3722 Hz, whereas in the 0.1397 m oxidizer post length case the first three dominant modes were observed at 1355 Hz, 2716 Hz and 4071 Hz.

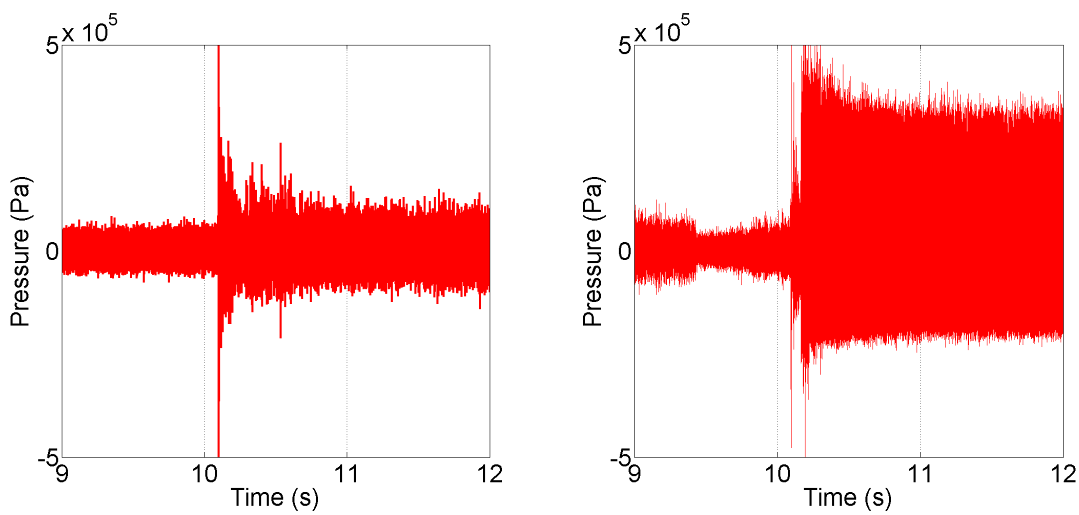

(a) (b)

Fig. 2.2. High passed pressure trace comparison between CVRC a) 0.089 m, and b) 0.1397 m oxidizer post length cases

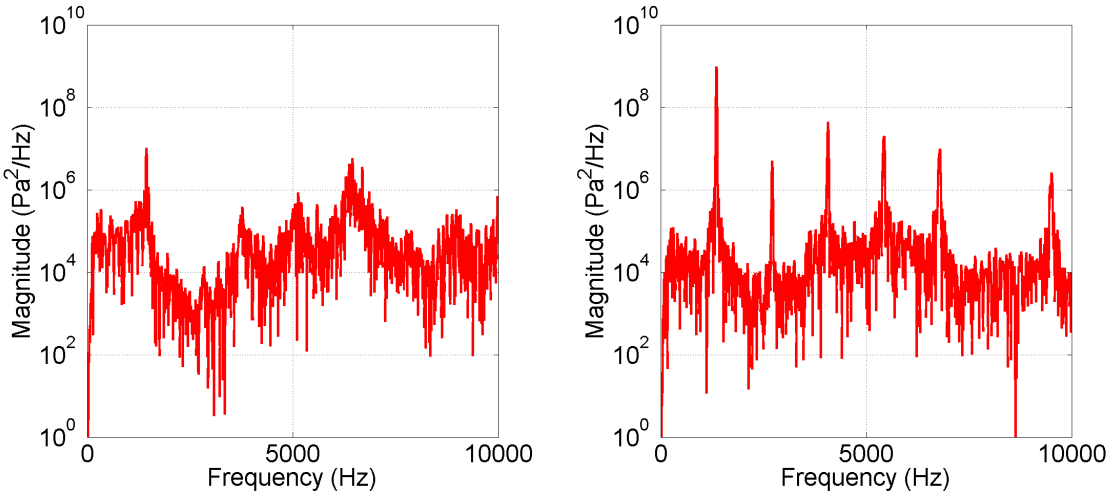

(a) (b)

Fig. 2.3. Comparison of PSDs between CVRC a) 0.089 m, and b) 0.1397 m oxidizer post length cases

During the experimental runs, as shown in Fig. 2.4, it was observed that the system's behavior was found to be consistent and repeatable for the oxidizer post length of 0.089 m. Also, the instability levels on the order of 8% - 10%, considered to be in the "weakly nonlinear regime", represents a realistic system near the transition of what is generally regarded as unstable operation whereas the instability levels of 40% are rarely observed. Further, it is believed that at such high amplitudes the nonlinear interactions between the flame and acoustics play a very important role. he FTF is a linear function and its applicability to high amplitude cases is yet to be evaluated. Hence, for the aforementioned reasons, the CVRC case with 0.089 m post length case was chosen to be the reference case for the work presented in this thesis.

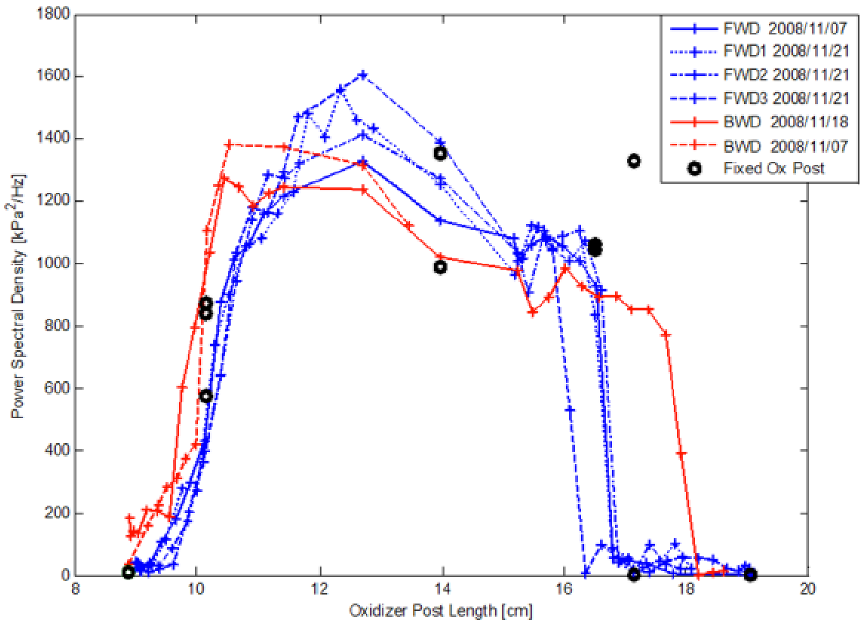

Fig. 2.4. Variation of instability amplitude with oxidizer post length as observed in experiments [80]

2.2 Simulation

The reference simulation selected for the present work is Continuously Variable Resonance Chamber (CVRC) described in section 2.1. The CVRC was extensively studied numerically [28] [29,81–85] by employing several high fidelity techniques such as the detached eddy simulation (DES). Harvazinski et al. [81] performed three dimensional DES simulations of the CVRC with 0.089 m, 0.1397 m and 0.1905 m oxidizer post lengths and compared them with two dimensional DES simulations. They observed that both two-dimensional and three-dimensional simulations could predict the limit cycle behavior. Further, Harvazinski et al. [86] studied the impact of inlet boundary conditions by performing the simulation of CVRC with choked slots and no slots. They observed only a minor difference between the two cases. Sardeshmukh et al. [29] performed two dimensional axisymmetric DES simulations of the CVRC with 0.089 m, 0.1397 m and 0.1905 m oxidizer post lengths using detailed chemistry, GRI 1.2 set, for methane-oxygen reaction. A comparison of the pressure traces and power spectral densities between the experiment and detailed chemistry simulations for the CVRC 0.089 m oxidizer post length simulation is shown in Fig. 2.5.

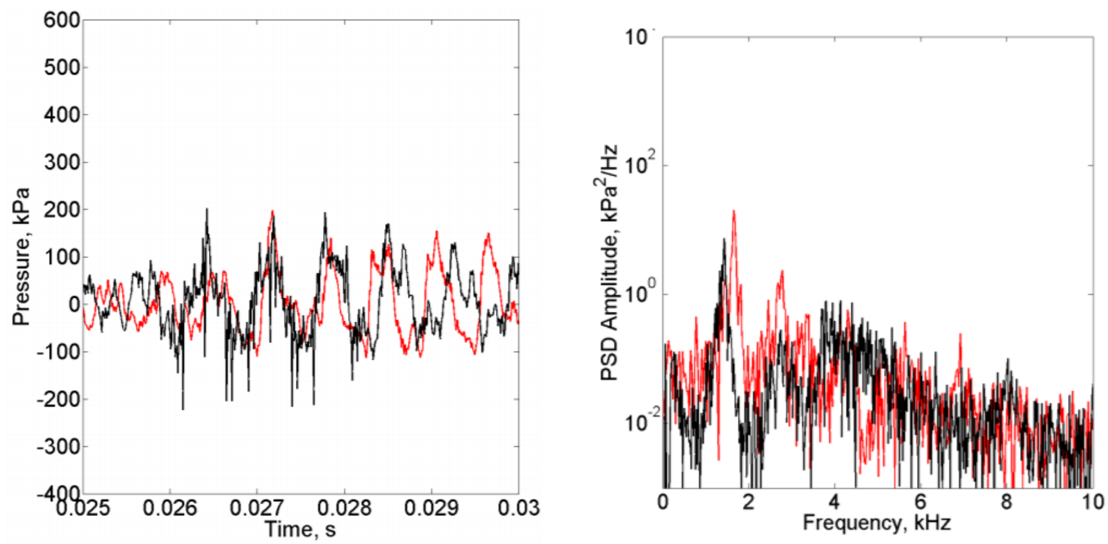

(a) (b)

Fig. 2.5. Comparison of a) pressure trace and b) PSD between the experiment and hybrid RANS/LES with detailed chemistry

2.2.1 Computational framework

The numerical simulations of the CVRC were performed using Generalized Equation and Mesh Solver - GEMS, an in-house Fortran based finite volume compressible flow solver. The GEMS solver being a three dimensional compressible Navier-Stokes solver, it solves the continuity, momentum equations for u, v, and w, energy, k, ω, and species equations. The partial differential equations that are being solved are

$$\frac{\partial Q}{\partial t} + \frac{\partial E}{\partial x} + \frac{\partial F}{\partial y} + \frac{\partial G}{\partial z} + \frac{\partial E_v}{\partial x} + \frac{\partial F_v}{\partial y} + \frac{\partial G_v}{\partial z} = H \tag{2.1}$$

where, Q is a vector of conserved variables,

$$Q = \begin{pmatrix} \rho \\ \rho u \\ \rho v \\ \rho z \\ \rho h^0 - p \\ \rho k \\ \rho \omega \\ \rho Y_l \end{pmatrix} \tag{2.2}$$

where ρ is density, u, v, w are the velocities in x, y and z direction respectively, p is the pressure, $\frac{h^0-p}{\rho}$ is the total internal energy, k is the turbulent kinetic energy, ω

is the dissipation rate, Y_l is the species mass fraction of l^{th}species, E, F, and G are vectors of inviscid fluxes,

$$E = \begin{pmatrix} \rho u \\ \rho u^2 + p \\ \rho uv \\ \rho uw \\ \rho uh^0 \\ \rho uk \\ \rho u\omega \\ \rho uY_l \end{pmatrix}, F = \begin{pmatrix} \rho v \\ \rho uv \\ \rho v^2 + p \\ \rho vw \\ \rho vh^0 \\ \rho vk \\ \rho v\omega \\ \rho vY_l \end{pmatrix}, G = \begin{pmatrix} \rho w \\ \rho uw \\ \rho vw \\ \rho w^2 + p \\ \rho wh^0 \\ \rho wk \\ \rho w\omega \\ \rho wY_l \end{pmatrix}, \tag{2.3}$$

E_v, F_v, and G_v are vectors of viscous fluxes,

$$E = \begin{pmatrix} \tau_{xx} \\ \tau_{yx} \\ \tau_{zx} \\ u\tau_{xx} + v\tau_{yx} + w\tau_{zx} + q_x \\ (\mu + \sigma * \frac{\rho k}{\omega})\frac{\partial k}{\partial x} \\ (\mu + \sigma\frac{\rho k}{\omega})\frac{\partial \omega}{\partial x} \\ \rho D_i \frac{\partial Y_i}{\partial x} \end{pmatrix}, F = \begin{pmatrix} \tau_{xy} \\ \tau_{yy} \\ \tau_{zy} \\ u\tau_{xy} + v\tau_{yy} + w\tau_{zy} + q_y \\ (\mu + \sigma^* \frac{\rho k}{\omega})\frac{\partial k}{\partial y} \\ (\mu + \sigma\frac{\rho k}{\omega})\frac{\partial \omega}{\partial y} \\ \rho D_i \frac{\partial Y_i}{\partial y} \end{pmatrix},$$

$$G = \begin{pmatrix} \tau_{xz} \\ \\ \tau_{yz} \\ \\ \tau_{zz} \\ \\ u\tau_{xz} + v\tau_{yz} + w\tau_{zz} + q_z \\ \\ (\mu + \sigma^* \frac{\rho k}{\omega}) \frac{\partial k}{\partial z} \\ \\ (\mu + \sigma \frac{\rho k}{\omega}) \frac{\partial \omega}{\partial z} \\ \\ \rho D_i \frac{\partial Y_i}{\partial z}, \end{pmatrix} \tag{2.4}$$

where σ and σ^* are the parameters of the k-ω turbulence model, D_i is the mass diffusivity of the i^{th} species, the heat flux term q_i is

$$q_i = -K \frac{\partial T}{\partial x_i} + \rho \sum_{l=1}^{N} V_{i,l} Y_l h_l + Q, \tag{2.5}$$

where the shear stress term τ_{ij} is

$$\tau_{ij} = (\mu + \mu_t)(\frac{\partial u_i}{\partial x_j} + \frac{\partial u_j}{\partial x_i} - \frac{2}{3} \frac{\partial u_m}{\partial x_m} \delta_{ij}), \tag{2.6}$$

the source term H is

$$H = \begin{pmatrix} 0 \\ \\ 0 \\ \\ 0 \\ \\ 0 \\ \\ 0 \\ \\ \rho \tau_{ij} \frac{\partial u_i}{\partial x_j} - \beta^* k \omega \\ \\ \gamma \frac{\rho \omega}{k} \tau_{ij} \frac{\partial u_i}{\partial x_j} - \rho \beta \omega^2 + \rho \frac{\sigma_d}{\omega} \frac{\partial k}{\partial x_j} \frac{\partial \omega}{\partial x_j} \\ \\ \dot{\omega}_l \end{pmatrix}, \tag{2.7}$$

β, σ_d,$\beta*$ are the parameters of the $k-\omega$ turbulence model, where $\dot{\omega}_l$ is the chemical source term of species l.

If the chemical mechanism has N species and M reactions, the species production rate of species l is

$$\dot{\omega}_l = W_l \sum_{m=1}^{M} (v''_{lm} - v'_{lm}) r_m \tag{2.8}$$

where W_l is the molecular weight of species l, r_m is the rate of reaction m,

$$r_m = k_{f,m} \Pi_{l=1}^{N} [X_l]^{v'_{l,m}} - k_{r,m} \Pi_{l=1}^{N} [X_l]^{v''_{l,m}} \tag{2.9}$$

where v''_{lm}, v'_{lm} are the stoichiometric coefficients of species l on the right and left side of reaction m,

$$\sum_{l=1}^{N} v'_{lm} X_l \underset{k_{r,m}}{\overset{k_{f,m}}{\Longleftrightarrow}} \sum_{l=1}^{N} v''_{lm} X_l \tag{2.10}$$

$k_{f,m}$ is the rate of forward reaction of reaction m,given in Arrhenius form,

$$k_{f,m} = AT^b exp(\frac{-E_a}{RT}) \tag{2.11}$$

where E_a is the activation energy, A and b are the Arrhenius constants of a given reaction. The reverse reaction rate $k_{r,m}$ is determined using the equilibrium constant

$$k_{r,m} = \frac{k_{f,m}}{K_{C,m}} \tag{2.12}$$

where the equilibrium constant is

$$K_{C,m} = (\frac{1bar}{RT})^{\sum_{l=1}^{N} v''_{l,m} - \ v'_{l,m}} \ X \ exp(\frac{\delta s^0}{R} - \frac{\delta h^0}{RT}) \tag{2.13}$$

The DES model requires the flow variables to be decomposed into the mean and fluctuating component in time. To avoid the additional complex terms involving density and velocity that needs to be modeled, Favre averaging was used in GEMS. The complete set of equations, the Jacobians, and the numerical schemes employed were explained in detail by Harvazinski [87]. In brief, the governing equations given in this section were solved in GEMS following finite volume methodology, employing a second order implicit scheme in time with dual time method to reduce factorization errors. In GEMS, spatial fluxes are evaluated using a second order approximate Riemann solver.

2.2.2 Computational setup

For the current thesis, a two-dimensional axisymmetric hybrid RANS/LES simulation of the CVRC 0.089 m oxidizer post length case was performed with a single step global chemistry using the in-house solver GEMS. In this hybrid RANS/LES simulation, the k-ω turbulence model was used to model the flow near the walls and in the regions where the grid resolution can resolve the length scales DES mode calculations were performed. The computational setup of the CVRC with a close-up view of the computational mesh is shown in Fig. 2.6. The mesh consists of 100k nodes.

Both the oxidizer and fuel inlets were modeled as the constant mass flow boundaries and the exit of the chamber was modeled using the static pressure boundary. In terms of species mass fraction, the fuel inlet was modeled as 100% CH_4 and the oxidizer inlet was modeled as 42% O_2 and 58% H_2O. The chemical kinetics were modeled using a single step global chemistry reaction

$$CH_4 + 2O_2 \rightarrow CO_2 + 2H_2O \tag{2.14}$$

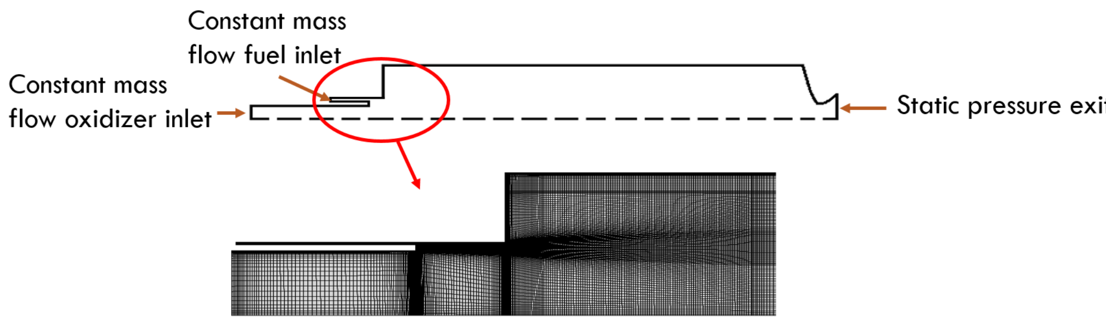

Fig. 2.6. Computational setup of the CVRC

where the constants of the production rate described by the Arrhenius form are given in Table. 2.2.

$$\dot{\omega} = AT^b \, e^{-\frac{E_a}{RT}} [Fuel]^m [Oxidizer]^n \tag{2.15}$$

Table 2.2.
Single step global reaction constants

Parameter	Units	Value
A	$(\frac{kmol}{m^3})^{1-n-m})\frac{1}{s}\frac{1}{k^b}$	0.636e11
b	-	0.0
$\frac{E_a}{R}$	K	24356.0
m	-	0.2
n	-	1.3

The hybrid RANS/LES simulation with the above computational setup exhibited limit cycle pressure oscillations with peak-to-peak amplitude around 10.5% of the

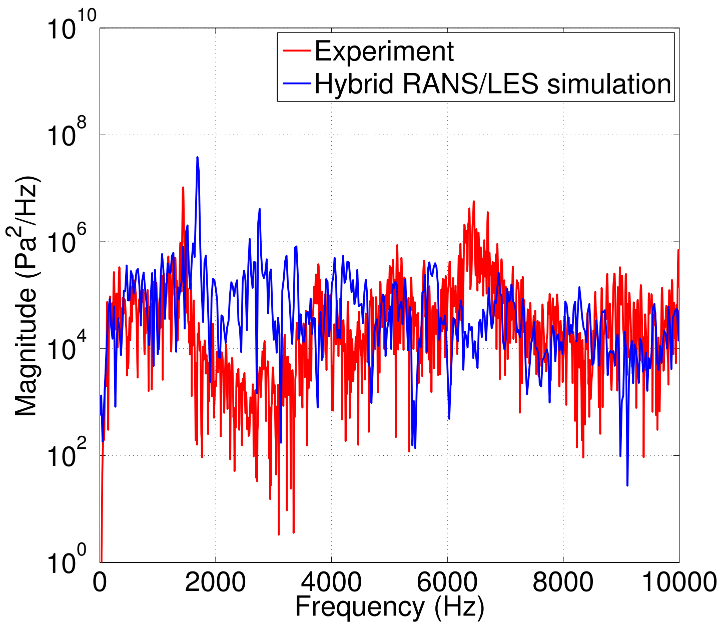

Fig. 2.7. Comparison of Power Spectral Density (PSDs) between the experiment and hybrid RANS/LES simulation with global chemistry

mean pressure. A comparison of the Power Spectral Densities (PSDs) of the pressure trace measured 0.368 m downstream of the dump plane is shown in Fig. 2.7. The hybrid RANS/LES simulation exhibited dominant modes at frequencies 1700 Hz, 2750 Hz, and 3350 Hz, which are slightly higher than the frequencies observed in the experiment. It is believed that the higher frequencies are due to slightly higher adiabatic flame temperature observed in the simulation. The data obtained in this simulation were used as the reference high fidelity simulation to extract flame transfer function.

To reduce the dimensionality of the complex raw data obtained from the high-fidelity simulations the data reductions techniques such as the Proper Orthogonal Decomposition (POD) and Dynamic Mode Decomposition (DMD) are being widely employed. POD was originally developed by Kosambi in 1943 whereas the DMD was developed by Schmid [77] in 2010. The early application of these techniques was limited to turbulent cold flow studies to identify the coherent turbulent structures that are otherwise difficult to observe [88] [89]. As the techniques gained popularity, the application of these techniques now extends to identifying the flame dynamics in the combustion chamber [75] [90] [91]. Both the POD and DMD reduce the high dimensional data set into lower dimensions (modes) but they differ in the way the data is reduced. POD reduces the data with a focus on error reduction between the original and reduced dimension data set. POD organizes the data based on the energy content of each mode. Each POD mode comprises of multiple frequencies. In contrast, DMD assumes a linear relationship in time between the snapshots of raw data and thereby reduces the raw data set into modes that are associated with a distinct frequency. This feature of DMD helps to identify the relationship between variables at a particular frequency. Unlike the traditional post processing techniques such as band-pass filtering which require a priori knowledge of the dominant frequencies and are susceptible to the various parameters used for the filtering, the decomposition techniques provide a systematic approach to identify the dominant features of the system.

2.2.3 Proper orthogonal decomposition

In general, a random function $R(x,t)$ varying in two dimensions, say, x - spatial coordinate and t - time, can be approximated as a finite sum

$$R(x,t) = \sum_{k=1}^{M} a_k(t)\phi_k(x), \tag{2.16}$$

with the assumption that the original function $R(x,t)$ can be recovered for a large M. Based on the choice of $\phi_h(x)$, which can be chosen from Fourier series, Chebyshev polynomial, Legendre polynomials, and so on, the $a_k(t)$ varies accordingly. In case of POD, the $\phi_k(x)$ is chosen to be orthonormal, that is,

$$\int_x \phi_{k1}(x)\phi_{k2}(x)dx = \begin{cases} 1, & \text{if } k_1 = k_2 \\ 0, & \text{otherwise} \end{cases} \tag{2.17}$$

then $a_k(t)$ can be calculated using $\phi_k(x)$,

$$a_k(t) = \int_x R(x,t)\phi_k(x)dx, \tag{2.18}$$

instead of using all other ϕ's.

Consider a matrix D representing the data set with N rows and m columns, where each column contains data corresponding to N spatial locations measured at time t. So, m columns represent the data collected from time t to $t + dt\ m$, where dt is the time interval. Singular Value Decomposition (SVD) of matrix D yields,

$$D = U\Sigma V^T, \tag{2.19}$$

where U is an $N\ X\ N$ orthogonal matrix, V is an $m\ X\ m$ orthogonal matrix, Σ is an $N\ X\ m$ diagonal matrix with $N_p = \min(N,m)$ diagonal elements and all other elements except the diagonal elements zero, the superscript T indicates the transpose of a matrix. The diagonal elements of Σ, called the singular values of A, are unique non-negative numbers, σ_i, arranged in the descending order. Let $Q = U\Sigma$, then $D = QV^T$. Letting q_k be the kth column of Q and v_k be the kth column of V, we can write the D as,

$$D = QV^T = \sum_{k=1}^{N_p} q_k {v_k}^T. \tag{2.20}$$

In the above representation, if $N > m$, i.e, the number of spatial locations are greater than the number of time snapshots, we will get $N_p = m$ POD modes and q_k, the kth column of Q represents the temporal mode of kth POD mode and v_k, the kth column of V or the kth row of V^T represents the spatial mode of the kth POD mode. The kth POD can be expressed as,

$$D_k = q_k {v_k}^T = u_k \sigma_k {v_k}^T. \tag{2.21}$$

D_k is the low-order representation of the original data set D approximated using the kth POD mode. σ_k represents the relative energy associated with the kth POD mode.

2.2.4 Dynamic mode decomposition

Consider a situation where the data set of N snapshots is represented as

$$\mathbf{V_1}^N = \mathbf{v}_1, \mathbf{v}_2, \mathbf{v}_3, \ldots, \mathbf{v}_N, \tag{2.22}$$

where $\mathbf{v}_i$ represents the i^{th} snapshot or flow field. Assuming a linear relationship between two consecutive snapshots, $\mathbf{v}_i$ and $\mathbf{v}_{i+1}$, i.e,

$$\mathbf{v}_{i+1} = \mathbf{A}\mathbf{v}_i, \tag{2.23}$$

the matrix $\mathbf{v_1}^N$ can be expressed as,

$$\mathbf{V_1}^N = \mathbf{v}_1, \mathbf{A}\mathbf{v}_1, \mathbf{A}^2\mathbf{v}_1, \ldots, \mathbf{A}^{N-1}\mathbf{v}_1. \tag{2.24}$$

Also, assuming that beyond a critical number of snapshots, adding more snapshots will not improve the vector space represented by $\mathbf{V_1}^N$, i.e, beyond the critical limit, the vector $\mathbf{v}_N$ can be represented as linear combination of the previous vectors,

$$\mathbf{v}_N = a_1\mathbf{v}_1 + a_2\mathbf{v}_2 + \ldots + a_{N-1}\mathbf{v}_{N-1} + \mathbf{r} \tag{2.25}$$

where $\mathbf{r}$ is the residual vector. In matrix form, it can be represented as,

$$\mathbf{v}_N = \mathbf{v_1}^{N-1}\mathbf{a} + \mathbf{r}, \tag{2.26}$$

where $\mathbf{a}^T = a_1, a_2, \ldots, a_{N-1}$. Hence,

$$\mathbf{A}\mathbf{V}_1^{N-1} = \mathbf{V}_2^N = \mathbf{V}_1^{N-1}\mathbf{S} + \mathbf{r}\mathbf{e}_{N-1}^T \tag{2.27}$$

where, $\mathbf{e}_{N-1}$ is the $(N\text{-}1)^{th}$ unit vector and $\mathbf{S}$ is the companion matrix,

$$\mathbf{S} = \begin{pmatrix} 0 & & & & a_1 \\ 1 & 0 & & & a_2 \\ & \ddots & \ddots & & \vdots \\ & & 1 & 0 & a_{N-2} \\ & & & 1 & a_{N-1} \end{pmatrix}. \tag{2.28}$$

Applying QR-decomposition on $\mathbf{V}_1^{N-1}$, we get,

$$\mathbf{V}_1^{N-1} = \mathbf{QR}. \tag{2.29}$$

The last column of the companion matrix $\mathbf{S}$, $(N-1)$ component vector $\mathbf{a}$, can be calculated as,

$$\mathbf{a} = \mathbf{R}^{-1}\mathbf{Q}^T\mathbf{v}_N \tag{2.30}$$

Instead of computing the companion matrix by calculating the vector $\mathbf{a}$ as shown above, a robust implementation that results in full matrix $\tilde{S}$, that is related to $\mathbf{S}$ through similarity transformation, can be achieved through Singular Value Decomposition (SVD) of $\mathbf{V}_1^{N-1}$, given by,

$$\mathbf{V}_1^{N-1} = U\Sigma W^T. \tag{2.31}$$

Then,

$$\mathbf{V}_2^N = \mathbf{A}\mathbf{V}_1^{N-1} + \mathbf{r}e_{N-1}^T = \mathbf{A}\mathbf{U}\Sigma\mathbf{W}^T + \mathbf{r}e_{N-1}^T. \tag{2.32}$$

Choosing $\mathbf{A}$ such that,

$$\mathbf{V}_2^N = \mathbf{A}\mathbf{U}, \tag{2.33}$$

and minimizing residual,

$$\mathbf{U}^T\mathbf{r} = 0, \tag{2.34}$$

we get,

$$\mathbf{U}^T\mathbf{A}\mathbf{U} = \mathbf{U}^T\mathbf{V}_2^N\mathbf{W}\Sigma^{-1} \equiv \tilde{\mathbf{S}}. \tag{2.35}$$

The dynamic modes can be constructed as

$$\phi_i = \mathbf{U}\mathbf{y}_i, \tag{2.36}$$

were, $\mathbf{y}_i$ is the i^{th} eigenvector of $\tilde{S}$. In matrix form, it can be expressed as,

$$\Phi = \mathbf{U}\mathbf{T} \tag{2.37}$$

where, $\mathbf{T}$ is the eigenvector matrix of $\tilde{\mathbf{S}}$, obtained by eigen decomposition,

$$\tilde{\mathbf{S}} = \mathbf{T}^{-1}\Lambda\mathbf{T}. \tag{2.38}$$

The POD and DMD techniques were applied to the CVRC data obtained from the hybrid RANS/LES simulation. The relative mode energy of the POD modes of static pressure is shown in Fig. 2.8. The figure shows that the contribution of modes

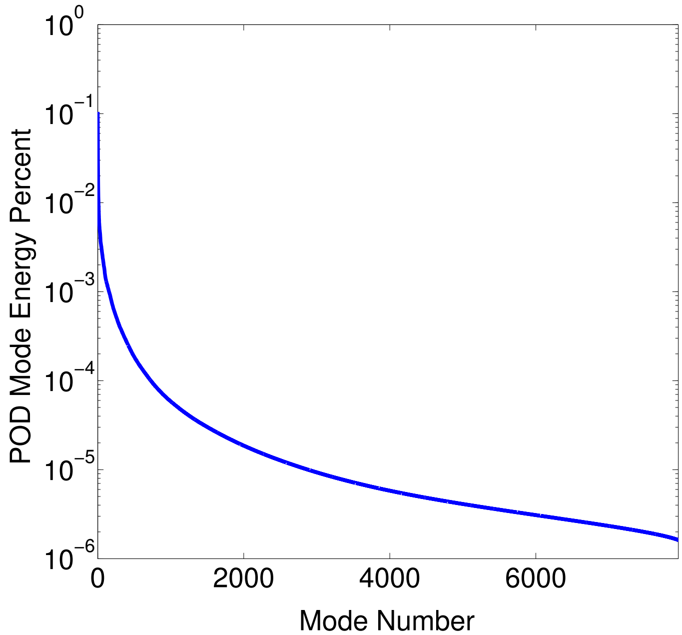

Fig. 2.8. POD mode energy variation of the static pressure

to the full energy spectrum drops rapidly for the initial tens of modes and then flattens out as the mode number increases. This is expected since the POD arranges the eigenvalues in the descending order. It also means that by reconstructing the data using the first tens of modes we may be able to recover most of the original raw data. A comparison of the PSDs of a pressure trace between the original data and the reconstructed data using five POD modes and ten POD modes is shown in

Fig. 2.9. It can be observed from the plot that five mode POD reconstruction was

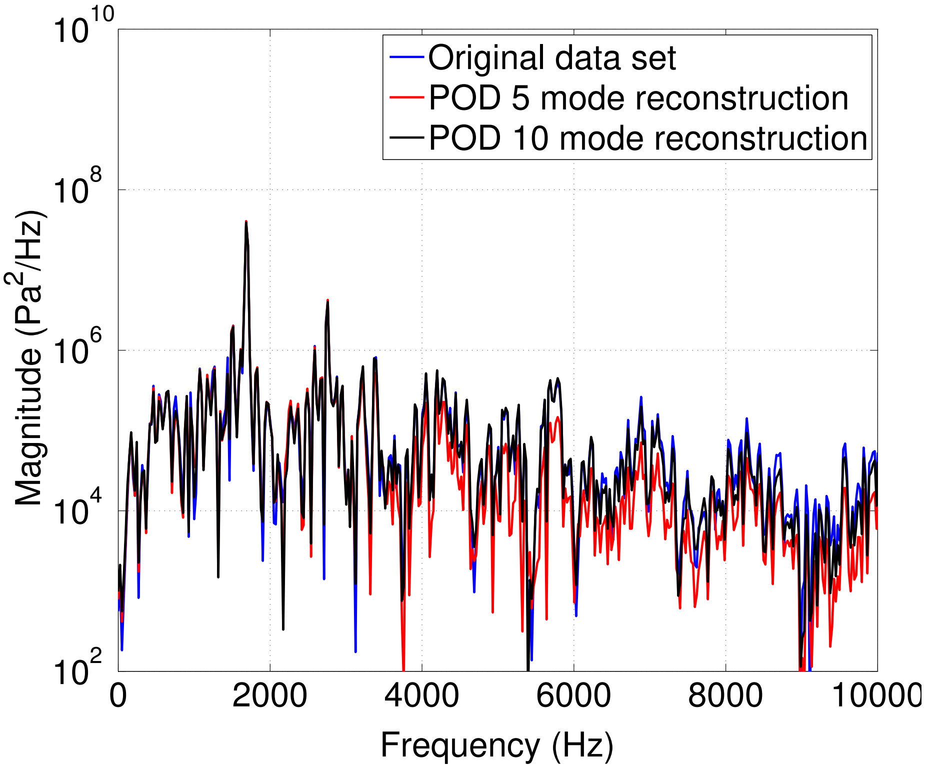

Fig. 2.9. Comparison of PSDs of POD reconstructed data and original data

able to reproduce the PSD accurately up to 3000 Hz, whereas the ten mode POD reconstruction was able to reproduce the PSD up to 6000 Hz. This is in accordance with the expected POD behavior that the more the number of POD modes included, the better will be the reconstructed data. A detailed study of the impact of number of POD modes used in the reconstruction of original data set is performed by Huang et al. [92]. A sample PSD of a POD mode of the static pressure obtained from the 2D axisymmetric hybrid RANS/LES simulation of the CVRC 0.089 m oxidizer post length case is shown in Fig. 2.10.

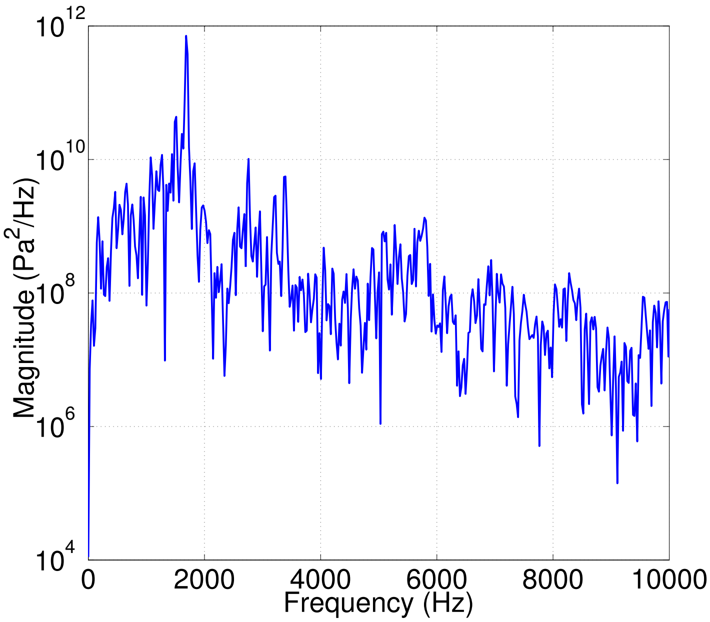

Fig. 2.10. A sample PSD of a POD mode of the static pressure obtained from hybrid RANS/LES simulation of the CVRC

It can be observed from the PSD that the POD mode contains multiple frequencies. However, to extract the FTFs we need the information at particular frequencies of interest. The DMD power spectrum of static pressure obtained from the same simulation data is shown in Fig. 2.11. Using the DMD energy spectrum, dominant modes can be identified, and the information related to those particular frequencies can be extracted. The PSD of the data set reconstructed using five dominant DMD modes is compared with the PSDs of reconstructed POD data set and original data in Fig. 2.12.

From the figure, it can be seen that the reconstructed DMD data only reproduced the five dominant modes included in the reconstruction. Hence DMD was used in this thesis to extract the flame transfer functions at frequencies of interest. Also,

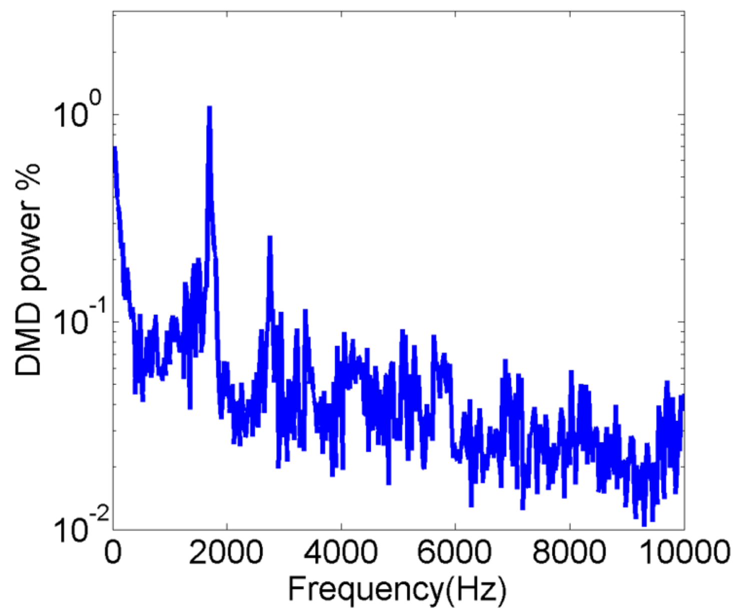

Fig. 2.11. DMD power spectrum of the static pressure obtained from hybrid RANS/LES simulation of the CVRC

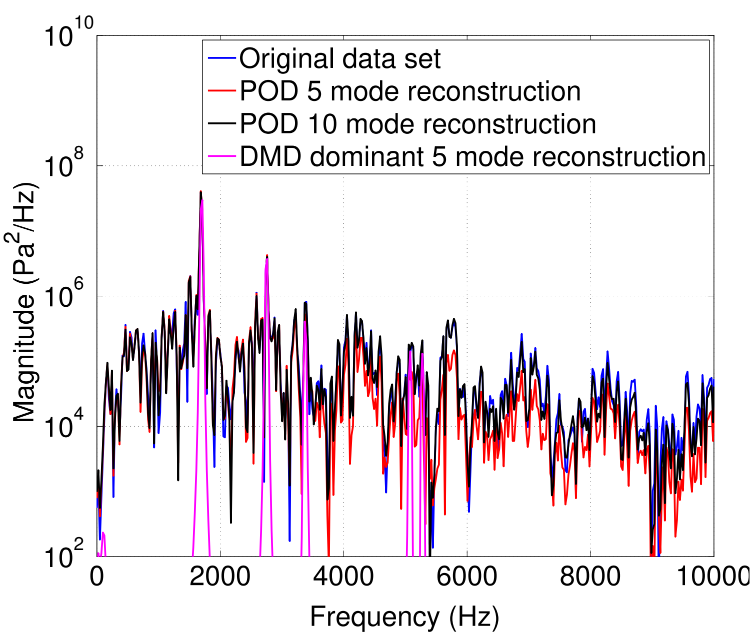

Fig. 2.12. Comparison of the PSDs between the reconstructed POD, DMD data set and original data

Huang et al. [75] investigated the application of POD and DMD to study self-excited combustors and found that DMD is superior to POD. Huang et al. observed that POD analysis is susceptible to the spatial information provided. POD was not able to capture the dominant mode accurately when only part of the full chamber was analyzed. Also, it is often difficult to provide physical interpretation of the POD modes due to the presence of multiple frequencies in a given POD mode. In contrast, DMD provides cleaner mode shapes and can provide better physical interpretation of the mode shapes corresponding to various dominant frequencies. So, DMD was found to a better tool to study combustion instabilities.

3. FRAMEWORK OF NONLINEAR EULER SOLVER AND FLAME TRANSFER FUNCTION

In this chapter, a brief literature review on the flame transfer function is presented. The approach to extract the flame transfer function from high fidelity simulations and their integration with nonlinear Euler solver is presented. The flame transfer functions were extracted from high fidelity simulations by applying the DMD technique to pressure and heat release fluctuations in the time domain to isolate frequency content. In the NLE solver, the source term was split into the mean and fluctuating part. The mean source term comprises the time averaged species destruction rates from the hybrid RANS/LES simulation. The FTF obtained from high-fidelity simulations is integrated with the NLE solver as the fluctuating source term of the energy equation. The imported FTFs make use of the evolving pressure data of the NLE solver and calculate appropriate unsteady heat release.

The flame transfer function (FTF) is a simple function which takes pressure or velocity fluctuations as input and gives heat release fluctuations as the output. It can be simply represented as shown in Fig. 3.1. The flame transfer function characterizes the response of the flame to pressure or velocity perturbations. The flame transfer functions are used to reproduce the unsteady flame behavior in reduced order simulations [73] [93] that inherently do not account for the flame response to pressure or velocity perturbations through the mathematics involved unlike the high fidelity simulations. Thus, a reduced fidelity model accounts for unsteady flame response necessary to accurately characterize and predict the combustion instabilities.

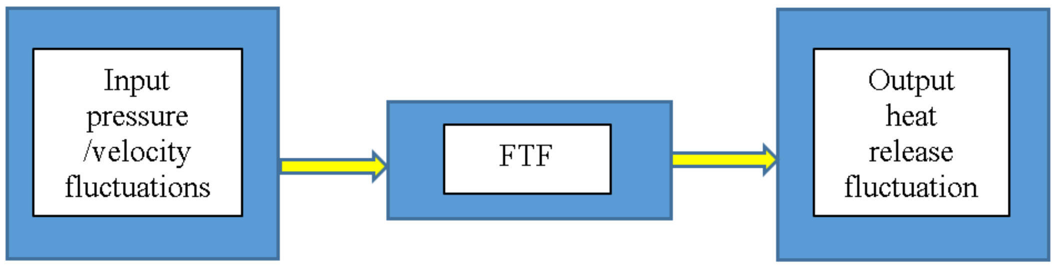

Fig. 3.1. Block diagram representation of FTF

The flame transfer function, by definition, is only dependent on the frequency of the input fluctuations,

$$q'''(\omega) = FTF(p'(\omega)) \tag{3.1}$$

The above expression can be interpreted as, when pressure fluctuations (p') at frequency ω are input through the FTF, the output will be heat release fluctuations (q''') heat release fluctuations at the same frequency.

The output heat release fluctuations will be zero for pressure fluctuations at a frequency other than the frequency at which FTF was developed. In brief, to obtain heat release fluctuations at various frequencies, FTFs need to be extracted at all those frequencies. Every flame transfer function is associated with certain magnitude and phase information to transform the input pressure fluctuations to the corresponding heat release fluctuations with appropriate magnitude and phase.

Historically, the flame transfer functions have been calculated experimentally [50] [67] [94] , computationally [48] [53] [55] [63] and analytically [64] [65] [66] [95] . Once extracted, the flame transfer function can be used together with low order models (e.g., acoustic models) to analyze combustion instabilities. However, the flame transfer function, by definition, being a linear function that depends only on frequency, limits its application to study systems that exhibit low level combustion instabilities. In case of systems that exhibit high level of instabilities, nonlinear effects dominate, and the response of the flame can vary drastically with the amplitude of pressure fluctuations. This necessitates the need for multiple flame transfer functions at different forcing amplitudes.

3.1 Integration of FTF with nonlinear Euler solver

To implement the FTF, a nonlinear Euler (NLE) solver with three species - oxidizer, fuel and products - was chosen. Although three species are being solved in the NLE, their destruction/production rates are obtained from the time averaged reference hybrid RANS/LES solution to reduce the computational cost. The governing equations that are being solved are

$$\frac{\partial Q}{\partial t} + \frac{\partial E}{\partial x} + \frac{\partial F}{\partial y} = H_{mean} + H_q, \tag{3.2}$$

where,

$$Q = \begin{pmatrix} \rho \\ \rho u \\ \rho v \\ \rho h^0 - p \\ \rho Y_f \\ \rho Y_{ox} \end{pmatrix}, E = \begin{pmatrix} \rho u \\ \rho u^2 + p \\ \rho uv \\ \rho u h^0 \\ \rho u Y_f \\ \rho u Y_{ox} \end{pmatrix}, F = \begin{pmatrix} \rho v \\ \rho uv \\ \rho v^2 + p \\ \rho v h^0 \\ \rho v Y_f \\ \rho v Y_{ox} \end{pmatrix},$$

$$H_{mean} = \begin{pmatrix} 0 \\ 0 \\ 0 \\ 0 \\ \bar{\dot{\omega}}_f \\ \bar{\dot{\omega}}_{ox} \end{pmatrix} and, H_q = \begin{pmatrix} 0 \\ 0 \\ 0 \\ \dot{q}''' \\ 0 \\ 0 \end{pmatrix} \tag{3.3}$$

H_{mean} is the mean source term; H_q is the unsteady source term; ρ is the density; u, v are the components of velocity in x and y direction respectively; h^0 is the stagnation enthalpy; p is the pressure; Y_f , Y_{ox} are the mass fraction of fuel and oxidizer respectively; $\bar{\dot{\omega}}_f$, $\bar{\dot{\omega}}_{ox}$ are the mean species production and destruction rates obtained by time averaging LES data; $\dot{q}'''$ is the fluctuating heat release given by FTF.

The fluctuating heat release, $\dot{q}'''(\overrightarrow{\mathbf{x}}, t)$, is obtained by performing inverse Fourier transform on the product of the FTF and pressure fluctuations in the frequency domain obtained by performing Fourier transform on time domain data,

$$q'''(\overrightarrow{\mathbf{x}}, t) = F^{-1}(p'(\overrightarrow{\mathbf{x}}, \omega) * FTF(\overrightarrow{\mathbf{x}}, \omega)), \tag{3.4}$$

where F^{-1} is inverse Fourier transform. The procedure followed in integrating the flame transfer function with the nonlinear Euler solver assumes that the time averaged species destruction/production rates obtained from hybrid RANS/LES simulation will maintain proper mean conditions in the nonlinear Euler simulation.

The integration procedure of the nonlinear Euler solver and the FTF mainly involves three steps: 1. Extract the flame transfer function from the high-fidelity simulation data of the combustor under study, 2. Obtain the time averaged species destruction rates from the high-fidelity simulation and add them to the nonlinear Euler equations as source terms to species equations and initiate the NLE simulation using time averaged hybrid RANS/LES solution and run the simulation until sufficient data (frequency resolution) necessary to activate the FTF are obtained, and 3. Activate the FTF and continue the NLE simulation.

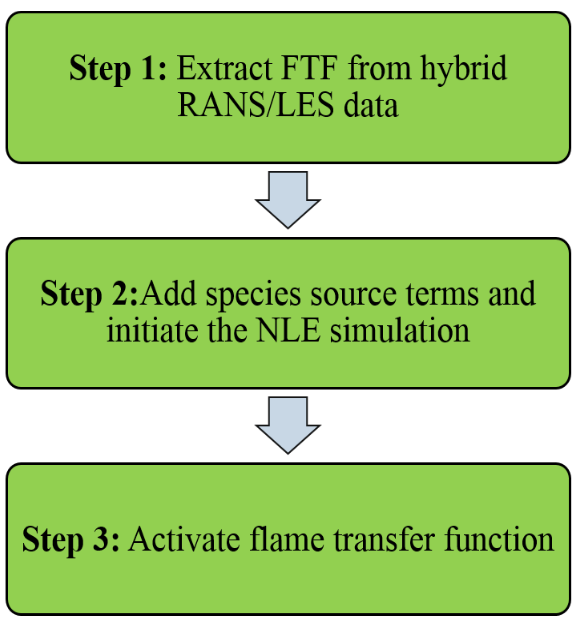

Fig. 3.2. Flow chart showing the steps involved in NLE-FTF simulation

In this thesis, in step-2, the NLE simulation without the FTF was run for 4ms to record the pressure data of the NLE simulation. For the baseline simulation of the CVRC presented in chapter 4, the recorded time domain pressure data of the NLE simulation was converted into frequency domain by choosing 1024 pressure points at equal intervals of time from the recorded data. The effect of number of pressure points used for the conversion of time domain pressure data into frequency domain on the prediction capability of the proposed reduced fidelity model is presented in chapter 5. A moving window of 4ms of pressure data in the time domain was used throughout the NLE simulation to obtain the pressure data in the frequency domain at every time step, which is necessary to calculate corresponding heat release fluctuations in the time domain. The length of pressure data obtained determines the frequency resolution. Hence, if sufficient length of pressure data is not obtained, one possibility is that the FTF applied may have no effect. The other possibility is that the FTF may produce spurious oscillations. Hence, it is critical to obtain sufficient data (frequency resolution) to activate the FTF.

If preferred, in step-2, instead of initiating the NLE simulation from time averaged hybrid RANS/LES solution, the NLE simulation can be initiated on its own, similar to hybrid RANS/LES simulation. In such case, the NLE simulation may be allowed to reach a steady state before forcing the inlet mass flow or back pressure, to record the pressure data necessary to activate the FTF are obtained. If forcing is used in step - 2, it must be turned off before activating the FTF in step 3. In the approach presented in this paper, heat release fluctuations are obtained by performing an inverse Fourier transform on the product of the FTF and pressure fluctuation data in the frequency domain. The approach to extract FTF from the high-fidelity simulations is outlined in the next section.

3.2 Extraction of FTF from high-fidelity simulation

The flame transfer function (FTF), is a linear function that uses pressure and/or velocity fluctuations as an input and gives heat release fluctuations as the output. It is used in reduced fidelity models to account for unsteady combustion by characterizing the response of the flame to pressure or velocity fluctuations. In the present work, pressure is used as the reference fluctuating input. The FTF is associated with a gain $G(\overrightarrow{\mathbf{x}},\omega)$ and phase $\phi(\overrightarrow{\mathbf{x}},\omega)$ to transform the input fluctuations to a corresponding heat input fluctuation with appropriate magnitude and phase. Using pressure as the fluctuating parameter, the spatially resolved FTF, $FTF(\overrightarrow{\mathbf{x}},\omega)$, can be mathematically expressed as

$$FTF(\overrightarrow{\mathbf{x}},\omega) = \frac{\frac{q'''(\overrightarrow{\mathbf{x}},\omega)}{\bar{q}(\overrightarrow{\mathbf{x}})}}{\frac{p'(\overrightarrow{\mathbf{x}},\omega)}{\bar{p}(\overrightarrow{\mathbf{x}})}} = G(\overrightarrow{\mathbf{x}},\omega)e^{i\phi(\overrightarrow{\mathbf{x}},\omega)} \tag{3.5}$$

The above expression can be interpreted as, when pressure fluctuations p' at frequency ω are input through the FTF, the output will be heat release fluctuations q''' at the same frequency. The ratio of magnitudes of heat release and pressure fluctuations at a particular frequency and location give gain $G(\overrightarrow{\mathbf{x}},\omega)$ of the FTF and the difference of phases between the heat release and pressure fluctuations at that frequency and location gives the local phase of FTF, $\phi(\overrightarrow{\mathbf{x}},\omega)$. The Dynamic Mode Decomposition

(DMD) technique [77] can be applied on the reference fluctuation and heat release fluctuation in the time domain to isolate the frequency content. Mathematically, it can be expressed as

$$FTF(\overrightarrow{\mathbf{x}},\omega) = \frac{|q'''(\overrightarrow{\mathbf{x}},\omega)|e^{i\phi_{q'''(\overrightarrow{\mathbf{x}},\omega)}}}{|p'(\overrightarrow{\mathbf{x}},\omega)|e^{i\phi_{p'(\overrightarrow{\mathbf{x}},\omega)}}}_{@\omega} = G(\overrightarrow{\mathbf{x}},\omega)e^{i\phi(\overrightarrow{\mathbf{x}},\omega)} \tag{3.6}$$

$$|q'''(\overrightarrow{\mathbf{x}},\omega)| = \sqrt{\frac{1}{T_2 - T_1}\int_{T_1}^{T_2}[q'''(\overrightarrow{\mathbf{x}},t)]^2 dt}_{@\omega} \tag{3.7}$$

$$|p'(\overrightarrow{\mathbf{x}},\omega)| = \sqrt{\frac{1}{T_2 - T_1}\int_{T_1}^{T_2}[p'(\overrightarrow{\mathbf{x}},t)]^2 dt}_{@\omega} \tag{3.8}$$

$$\phi(\overrightarrow{\mathbf{x}},\omega) = \phi_{q'''(\overrightarrow{\mathbf{x}},\omega)} - \phi_{p'(\overrightarrow{\mathbf{x}},\omega)} \tag{3.9}$$

Through the above procedure, the magnitude of the FTF and the local phase difference between the heat release and reference fluctuation can be obtained. This approach results in a spatially resolved FTF in the frequency domain. For reference fluctuations at frequencies that lie outside the frequency range associated with the FTFs developed, the output heat release fluctuations will be zero. To obtain the heat release fluctuations that interact with the combustor modes, FTFs need to be extracted at each frequency that corresponds to a mode of interest.

4. APPLICATION OF THE REDUCED FIDELITY MODEL TO THE CVRC

In this chapter, the verification of the proposed approach using a Rijke tube test case and its application to the CVRC are presented. The proposed approach was verified using a Rijke tube of length 0.5 m with a heat addition zone 0.125 m from the inlet of the tube. Crocco's n-τ model was used to generate the unsteady heat release fluctuations. The results obtained showed that the proposed approach was able to reproduce the mean variables and limit cycle statistics to a good extent verifying the proposed approaches. Upon successful verification, the proposed approach was applied to the CVRC. During the initial runs, although the NLE-FTF simulation reached a limit cycle, non-physical temperature was observed. The corrective measures employed to resolve the temperature issues are also discussed in this chapter. Through the variable gain approach, accurate mean conditions in the chamber were obtained and the NLE-FTF simulation was able to reproduce the limit cycle to a good extent. A comparison of the pressure, temperature and fuel cycle between the NLE-FTF simulation and the hybrid RANS/LES simulation is also presented. The results showed that the NLE-FTF approach was able to reproduce global pressure and fuel cycle, but it could not capture all the details. The temperature cycle analysis revealed that a broader temperature range was observed in the NLE-FTF simulation.

4.1 Rijke tube

A Rijke tube is a simple open-open end thermoacoustic device that generates sound when an appropriate amount of temperature gradient was applied in the lower half of the tube. This behavior was first observed by Rijke in 1859 [4] and hence the device was named after him. The original Rijke tube is a vertical pipe that is open to atmosphere at both ends and a gauze located in the lower half of the pipe as shown in Fig. 4.1. The gauze when heated by a flame creates a mean flow in the tube due to natural convection. It was found that a high intensity tonal sound is generated when a sufficient temperature gradient was applied at a one quarter length from the bottom end of the tube. The expansion of gas near the flame and its compression near the ends was believed to be the reason for the sound generation in the tube. Later, it was found that the Rijke tube satisfies the Rayleigh criterion and is the main reason for exhibiting thermoacoustic instability.

Although the original Rijke tube setup is simple it does not allow for an independent control of the mean flow and the amount of heat added to the flow. Hence, a horizontal version of the Rijke tube came into existence. In this version of Rijke tube, the mean flow is provided by a blower and an electric heater whose heat settings can be adjusted independently replaced the gauze. This setup allows for a better control of the parameters governing the behavior of Rijke tube [96].

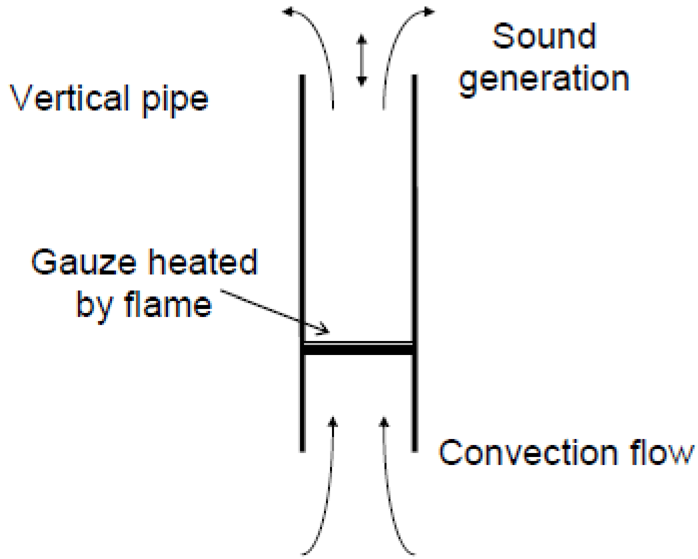

Fig. 4.1. Original vertical Rijke tube [96]

4.2 Verification of the reduced fidelity model

The proposed approach of extracting the FTF and integrating it with the nonlinear Euler solver were verified using a Rijke tube test case. A Rijke tube of length 0.5 m and radius 0.0225 m was considered. In this test case, unsteady heat release was added 0.125 m from the inlet of the tube following Crocco's [2] $n-\tau$ model

$$q' = np'(t-\tau) \tag{4.1}$$

where n = 2.8e-5 W/Pa and $\tau = 0$. The heat addition zone was spread across a length of 9 mm. Imposing constant pressure at both inlet and outlet in the absence of an acoustic isolation is an ill-defined boundary condition, hence the surrounding atmosphere is modeled. The pressure boundary conditions were imposed at the inlet and outlet of the surrounding domain as shown in Fig. 4.2. For all calculations and results reported henceforth, only the interior tube is considered [97].

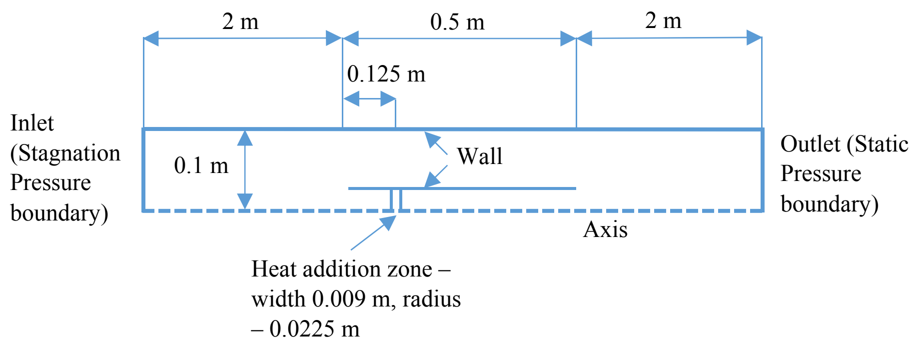

Fig. 4.2. Rijke tube setup

The raw pressure measured 0.125 m from the inlet of the tube and the DMD power spectrum of the pressure are shown in Fig. 4.3. The peak-to-peak pressure oscillations in the limit cycle of this system were found to be around 10.5% of the mean pressure. A single dominating mode at 650 Hz corresponding to the 1L mode of the tube was observed from the DMD power spectrum. Following the procedure outlined in section 3.1, the flame transfer function corresponding to 650 Hz was extracted and the gain and phase of the FTF is shown in Fig. 4.4. The gain of the extracted flame transfer function was 2.8e-5 W/Pa, equal to the n of the Crocco's n-τ model imposed, and the phase lag was zero, equal to the τ imposed. This verified that the approach followed to extract the gain and phase of the FTF is mathematically correct.

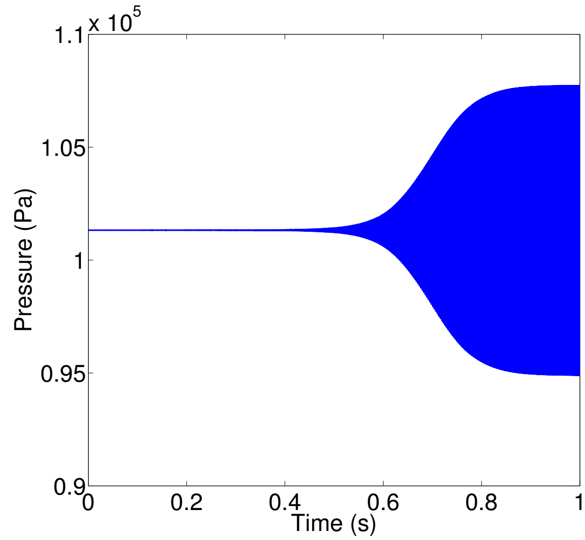

(a)

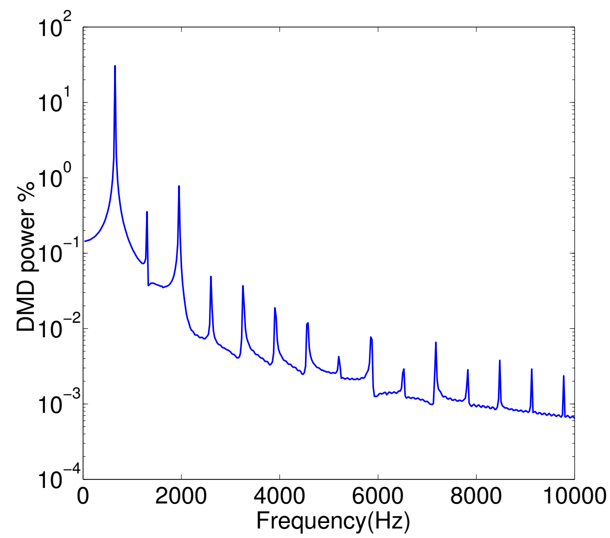

(b)

Fig. 4.3. a) Pressure trace measured 0.125 m from the inlet of the tube, and b) the DMD power spectrum of pressure

The FTF was integrated with the nonlinear Euler solver following the procedure outlined in section 3.1. The raw pressure measured 0.125 m from the inlet of the tube

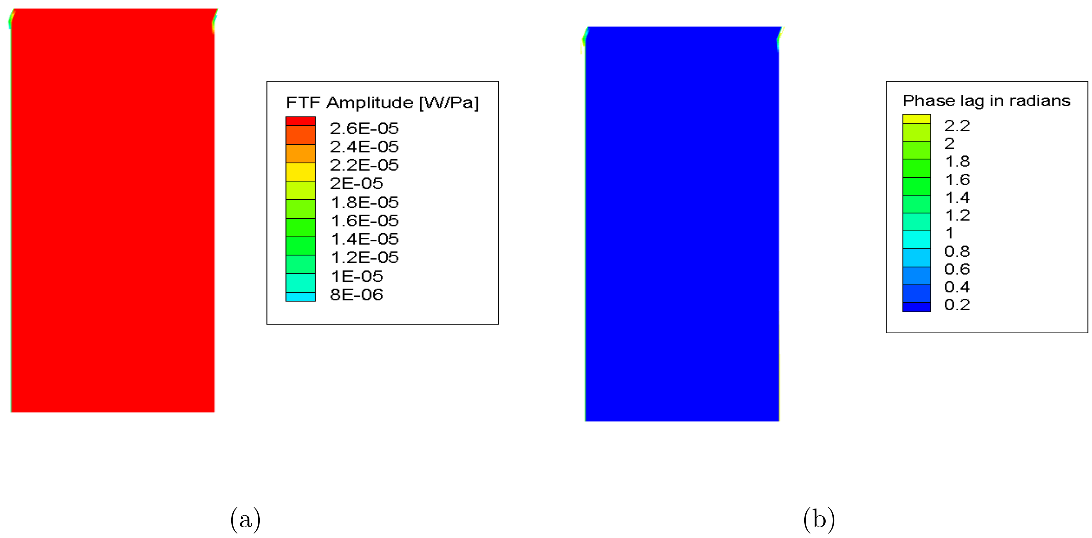

Fig. 4.4. a) Gain of the flame transfer function, and b) phase of the flame transfer function (Only the zone of heat addition is shown in the figure)

in the nonlinear Euler simulation with the FTF is shown in Fig. 4.5. The peak-to-peak pressure oscillations in the limit cycle were found to be 10.8 % of the mean pressure, which is in very good agreement with the original simulation data. A comparison of the limit cycle pressure and Power Spectral Density (PSD)s between the original simulation and the simulation with FTF is shown in Fig. 4.6. A very good agreement between the limit cycle pressure fluctuations and PSDs was observed. Also, a very good agreement in terms of the mean flow variables was also observed between the original simulation and the simulation with FTF.

The one-dimensional mean temperature and pressure obtained by time averaging the limit cycle data and then volume averaging along the radius of the tube are shown in Fig. 4.7.

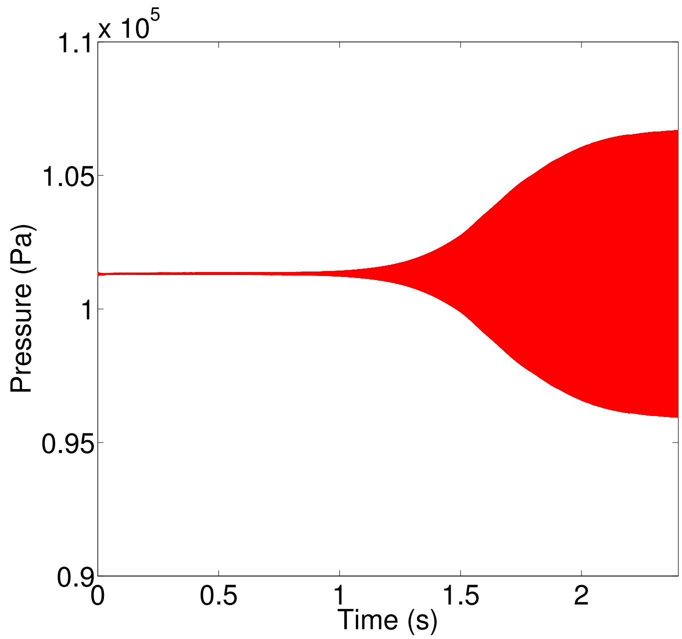

Fig. 4.5. Pressure trace measured 0.125 m from the inlet of the tube in the simulation with the FTF

From the results obtained, i.e., accurate limit cycle amplitude and mean variables, it can be inferred that the approach proposed to extract the spatially distributed local flame transfer function and its integration with nonlinear Euler solver is verified. Successful verification of the proposed approach motivated its application to a model rocket combustor that demonstrates repeatable self-excited instability.

4.3 Application of the reduced fidelity model to the CVRC

The dynamic mode decomposition power spectrum of pressure and heat release signals of CVRC 0.089 m oxidizer post length case is shown in Fig. 4.8. The DMD spectrum of pressure shows that the first three dominant modes were observed at

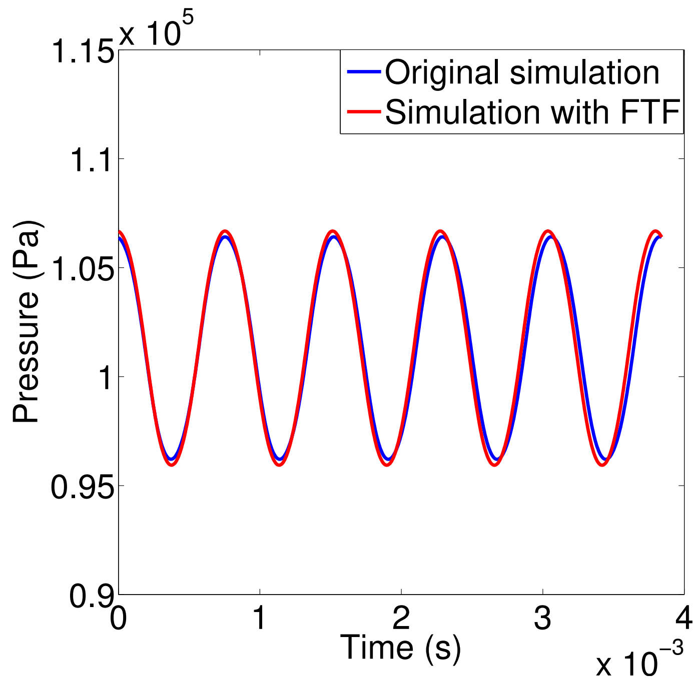

(a)

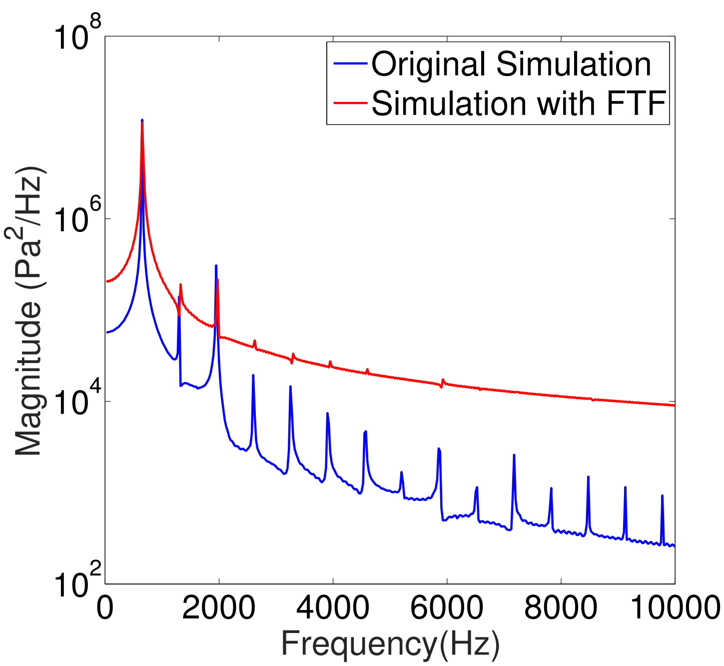

(b)

Fig. 4.6. Pressure trace and PSDs comparison between original simulation and simulation with FTF

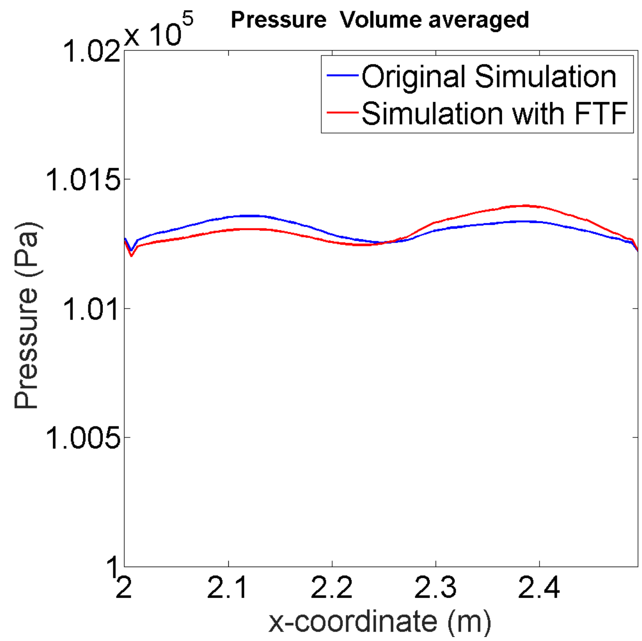

(a)

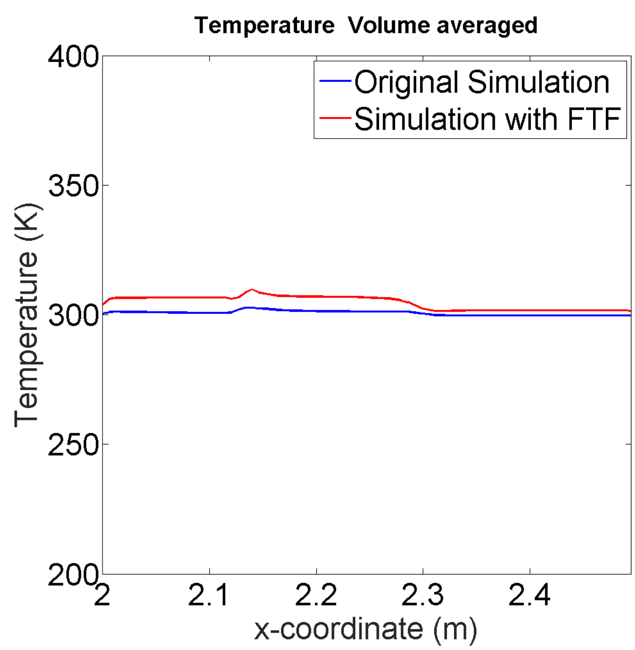

(b)

Fig. 4.7. Comparison between the original simulation and simulation with FTF a) Mean Pressure, and b) Mean temperature

1700 Hz, 2750 Hz and 3375 Hz, whereas the DMD spectrum of heat release shows only two dominating modes at 1700 Hz and 3375 Hz.

Following the approach outlined in section 3.2, the flame transfer functions corresponding to the first three dominant modes of the pressure, 1700 Hz, 2750 Hz and 3375 Hz were extracted from the hybrid RANS/LES simulation data. The gain of the flame transfer function, which is the ratio of heat release and pressure fluctuations, and phase of the flame transfer function, which is obtained by cross correlation of pressure and heat release fluctuations, for the first three dominant modes is shown in Fig. 4.9. The gain of the FTFs appears to be more distributed for low energy modes and concentrated for the high energy modes. It is expected, since the gain of FTF is the ratio of heat release and pressure fluctuations. Higher heat release and lower pressure fluctuation levels leads to higher FTF gain and vice-versa. The presence of high FTF gain at the pressure node locations, where small amounts of heat addition are much larger than the small pressure fluctuations that exist there, can be explained by the same reason.

The phase difference results show that the temporal coupling between heat release and pressure fluctuations varies across modes. The phase difference plot for the 1700 Hz mode shows a very strong coupling between the heat release and pressure fluctuations compared to other modes. It is evident from Fig. 4.9 that both the FTF gain and phase difference are very distributed, justifying the need for a spatially distributed FTF.

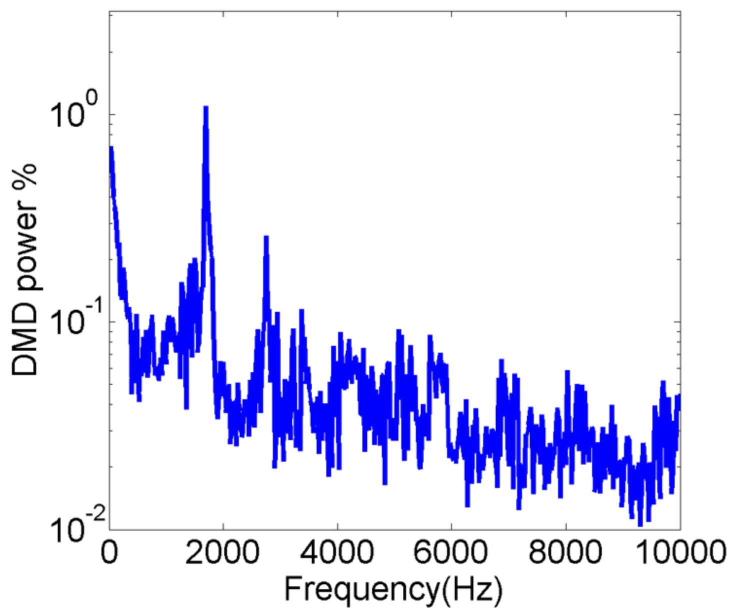

(a)

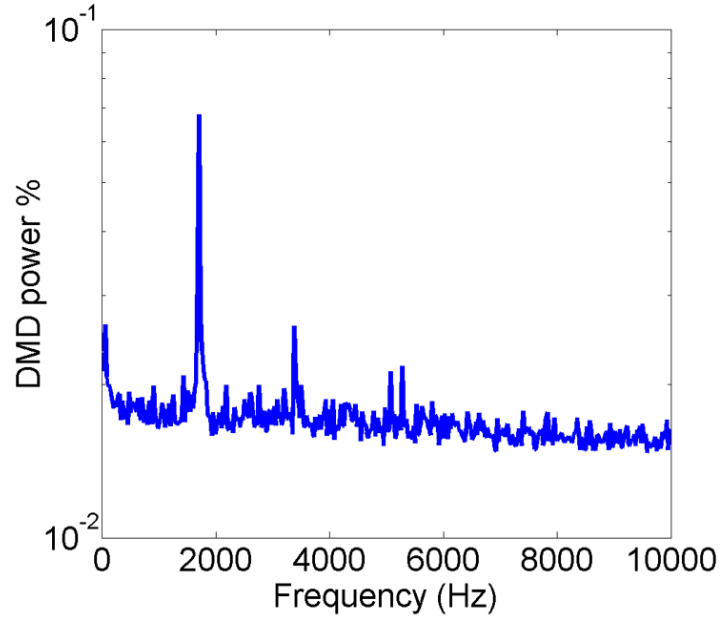

(b)

Fig. 4.8. Dynamic mode decomposition power spectrum of a) pressure fluctuations and b) heat release fluctuations of the CVRC 0.089 m oxidizer post length case

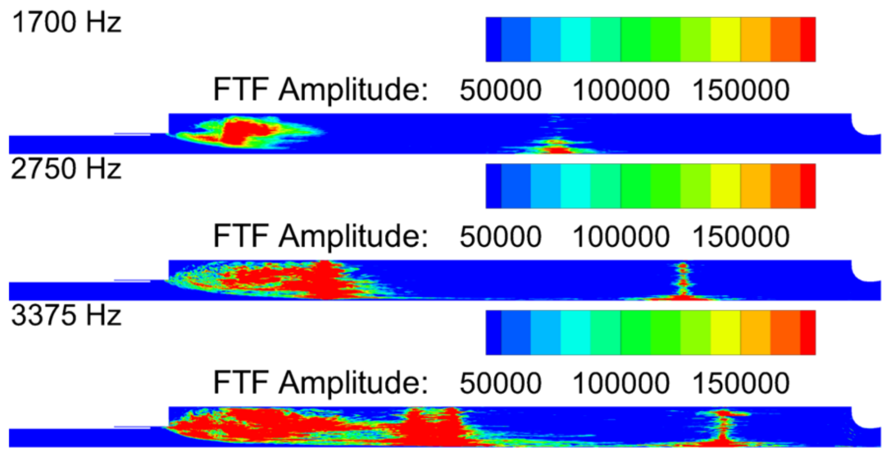

(a)

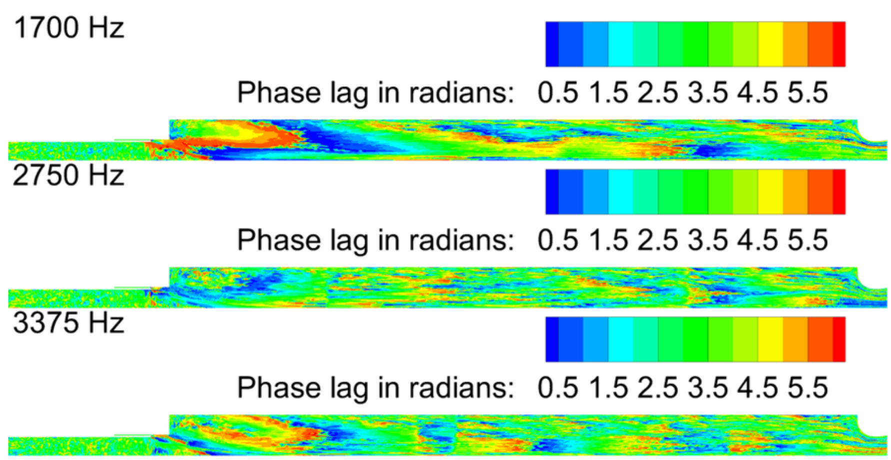

(b)

Fig. 4.9. a) The gain and b) phase of flame transfer function corresponding to the first three dominant modes of the CVRC 0.089 m oxidizer post length case

Once the FTFs were extracted, the NLE- FTF simulation of the CVRC was performed as outlined in section 3.1. To eliminate any mesh size-related uncertainties, the same mesh that was used in the hybrid RANS/LES simulations was used for the NLE simulations. The NLE-FTF simulation was initialized using the time averaged hybrid

RANS/LES solution and the time averaged species production rates of the reference high fidelity simulation were imposed as the species source terms in the NLE simulation. The unsteady NLE simulation with constant species destruction/production rates obtained by time averaging the DES species destruction/production rates was run for around 4ms (without activating the FTF) to calculate the unsteady flow field necessary to activate the FTF. Once sufficient pressure fluctuation data (frequency resolution) were obtained, the data were then passed through the FTF. A series of operations resulted in the heat release fluctuations corresponding to the input pressure fluctuations. The pressure fluctuation data that pass through the FTF to get corresponding heat release fluctuations at every time step were updated at every time step by eliminating the first data point and making space for the new pressure fluctuation data point. The NLE simulation was continued until a limit cycle was reached.

The pressure trace measured 0.368 m downstream of the dump plane in the NLE-FTF simulation is shown in Fig. 4.10a. In the hybrid RANS/LES simulation, pressure oscillations around 10.5% of the mean pressure were observed, whereas in the NLE simulation, pressure oscillations around 16% of mean pressure were observed. A comparison of the PSDs of the NLE and reference hybrid RANS/LES simulation is shown in Fig. 4.10b. As expected, the PSD of NLE simulation showed higher peaks due to higher p' limit cycle amplitudes observed.

A comparison of the time averaged variables between the NLE and DES simulations is shown in Fig. 4.11. The time averaged variables showed that although the mean pressure matched very well between the hybrid RANS/LES and NLE simula-

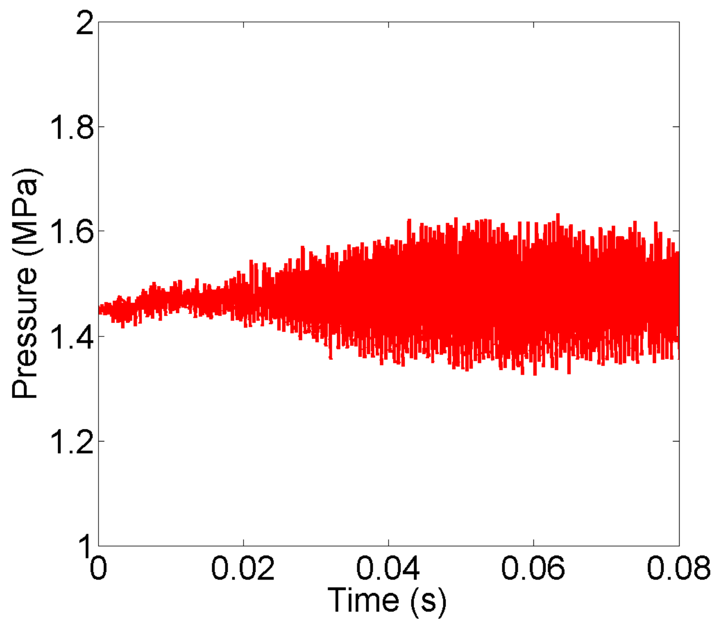

(a)

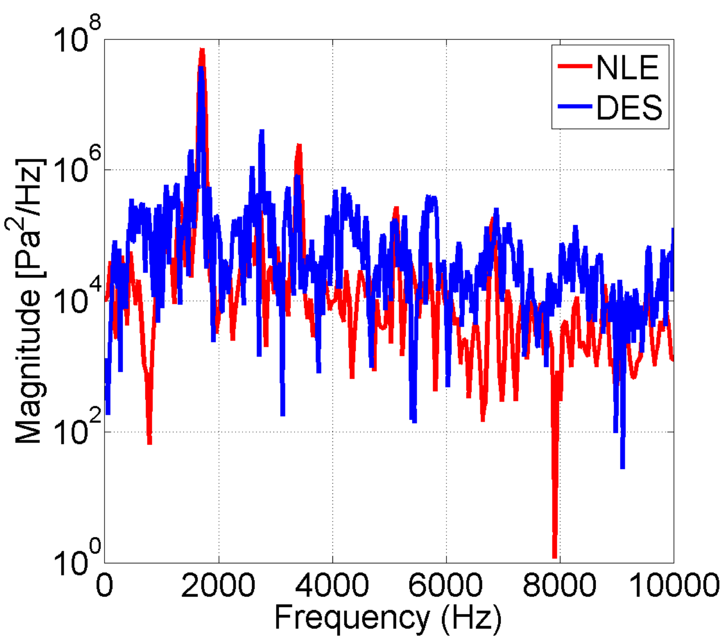

(b)

Fig. 4.10. Pressure trace measured 0.368 m downstream of dump plane in the CVRC 0.089 m oxidizer post length a) NLE simulation with FTF b) Reference DES simulation c) Comparison of PSDs

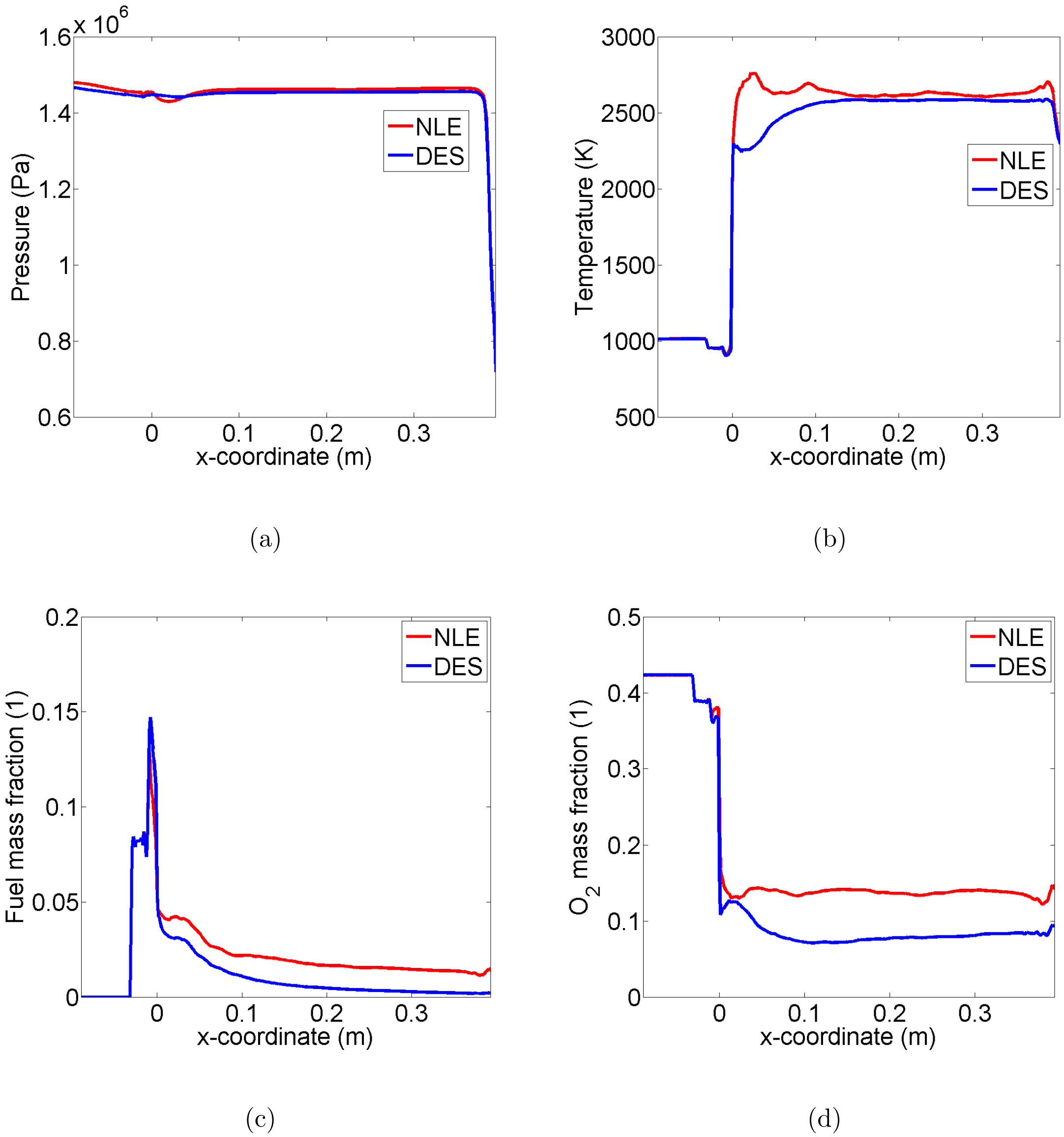

Fig. 4.11. Comparison of time averaged a) Pressure b) Temperature c) CH4 (fuel) mass fraction and d) O2 (oxidizer) mass fraction between the NLE-FTF and hybrid RANS/LES simulation

tions, a very high mean temperature close to the dump plane and higher species mass fractions were observed.

As shown in Fig. 4.12, a closer look at the radial temperature profile revealed that very high temperature was observed especially in the re-circulation zone close to the dump plane.

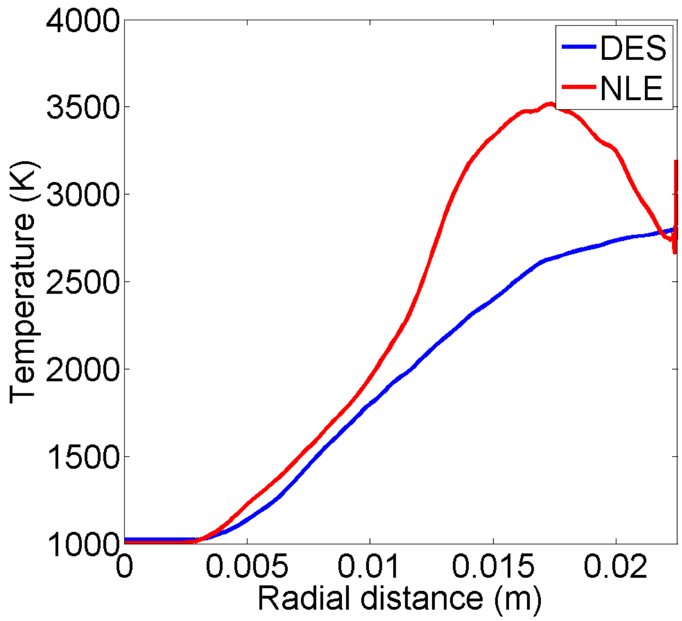

Fig. 4.12. Comparison of the radial distribution of time averaged temperature measured 0.0254 m downstream of the dump plane between NLE-FTF and the hybrid RANS/LES simulation

The unsteady temperature traces measured at locations 0.0254 m downstream of the dump plane and 0.368 m downstream of the dump plane shown in Fig. 4.13 revealed very high temperature fluctuations. The temperature trace at 0.0254 m location showed that temperature near the dump plane reached around 5500K which is non-physical. Although the temperature at the 0.368 m location did not reach 5500 K, it is still far greater than the adiabatic flame temperature. It can be seen from the temperature trace that non-physical temperature was present even before the FTF was activated at 4ms and the temperature appears to have achieved some reasonable values as the time progress and pressure fluctuations increase.

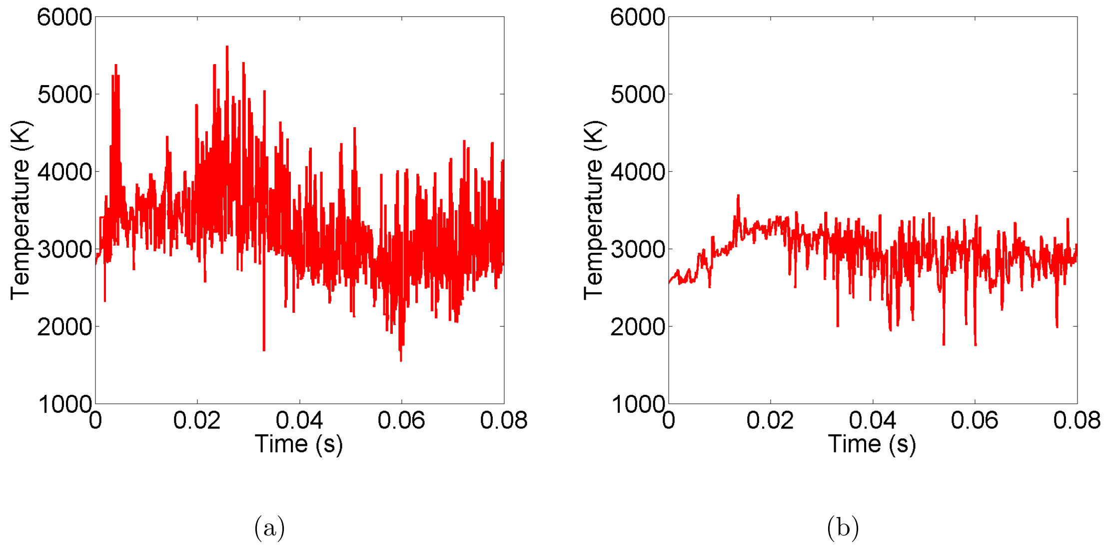

Fig. 4.13. Unsteady temperature trace NLE-FTF simulation measured a) 0.0254 m, and b) 0.368 m downstream of the dump plane

A closer look at the two dimensional contours of the unsteady variables such as temperature, species mass fraction and heat release rate showed that applying constant species destruction rates obtained by time averaging the hybrid RANS/LES species destruction rates resulted in constant addition of heat irrespective of the local cell constituents. In short, heat addition was observed in places where neither fuel nor oxidizer was present. This excessive constant heat addition, especially close to the dump plane, resulted in non-physical temperature. The constant species destruction rates which were imposed in the NLE simulation were obtained by time averaging the species destruction rates of the reference DES simulation which almost reached the limit cycle with 10% pressure fluctuations as soon as the reaction started. However, in the NLE simulation the fluctuations start from almost 0 -1% and grow gradually. Imposing the species destruction rates corresponding to flow with 10% pressure perturbations on a flow field with 1% pressure perturbations resulted in heat addition at the wrong locations. This observation is supported by more reasonable temperature values measured during the time around which higher pressure fluctuations show up as shown in Fig. 4.13.

As a corrective measure, a limit was imposed on the species destruction rates in the NLE simulation, based on the available cell constituents in such a way that only available cell constituents were burnt and the species destruction rates in that location gets adjusted accordingly. This imposed limit made sure that no excessive heat was added in any location where it was not supposed to be added. The NLE simulation without the FTF was then performed for the CVRC 0.089 m oxidizer post length case. The pressure and temperature trace of the CVRC 0.089 m oxidizer post case measured 0.0254 m and 0.368 m downstream of dump plane in the NLE simulation performed without the limit and with limit on species destruction rate are compared in Fig. 4.14 and Fig. 4.15 respectively. Although, the temperature appears to be well within the expected range at both the locations, the pressure dropped considerably.

The time averaged profiles corresponding to the CVRC 0.089 m oxidizer post length case with the limit imposed on species destruction rate is shown in Fig. 4.16. A considerable drop in the all the mean quantities was observed. A considerable amount of fuel and oxidizer were unburnt leading to drop in all mean variables.

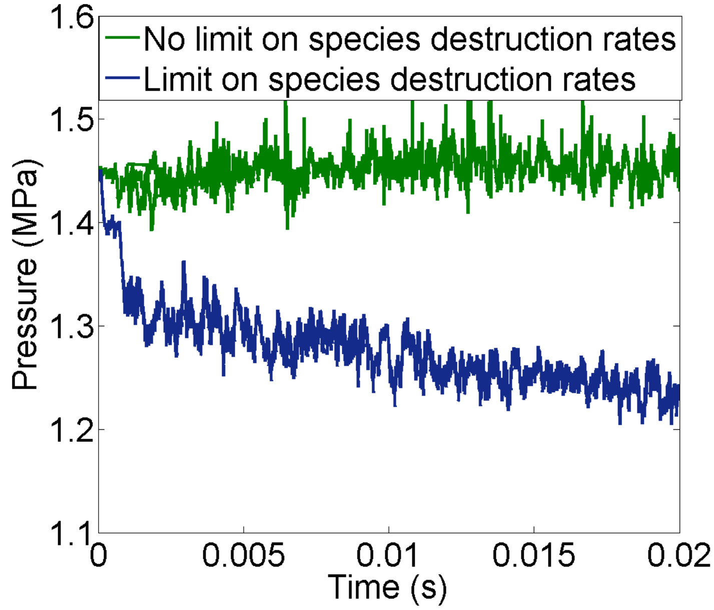

(a)

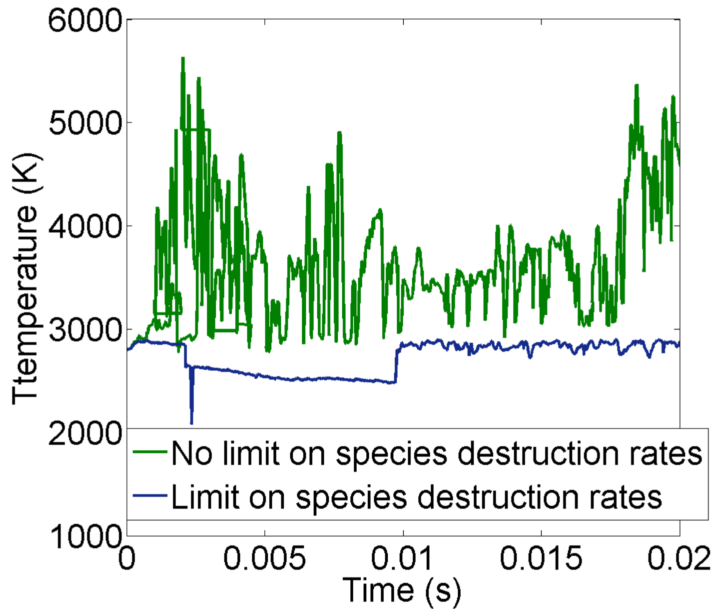

(b)

Fig. 4.14. Comparison of a) pressure, and b) temperature measured 0.0254 m downstream of the plane between the two cases, with and without limit on species

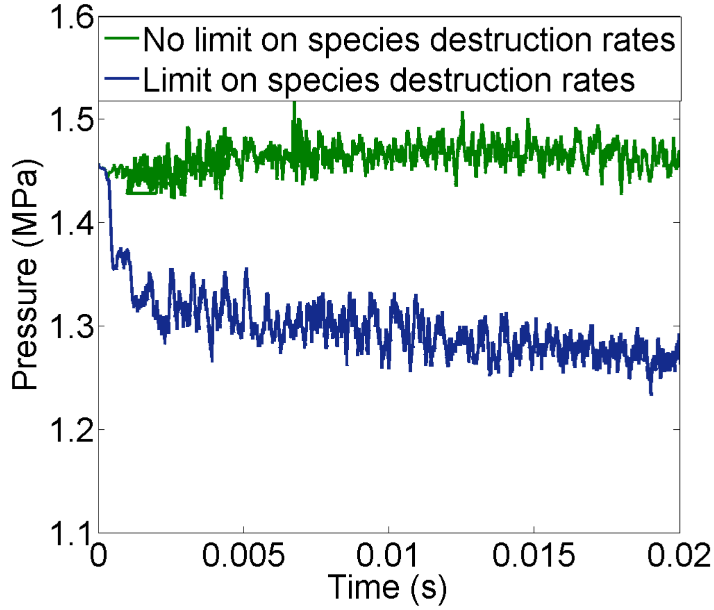

(a)

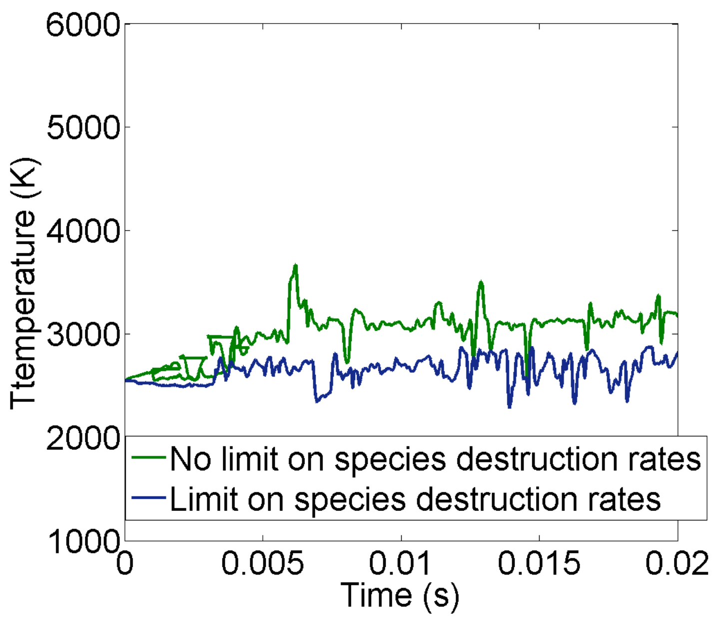

(b)

Fig. 4.15. Comparison of a) pressure, and b) temperature measured 0.368 m downstream of the plane between the two cases, with and without limit on species

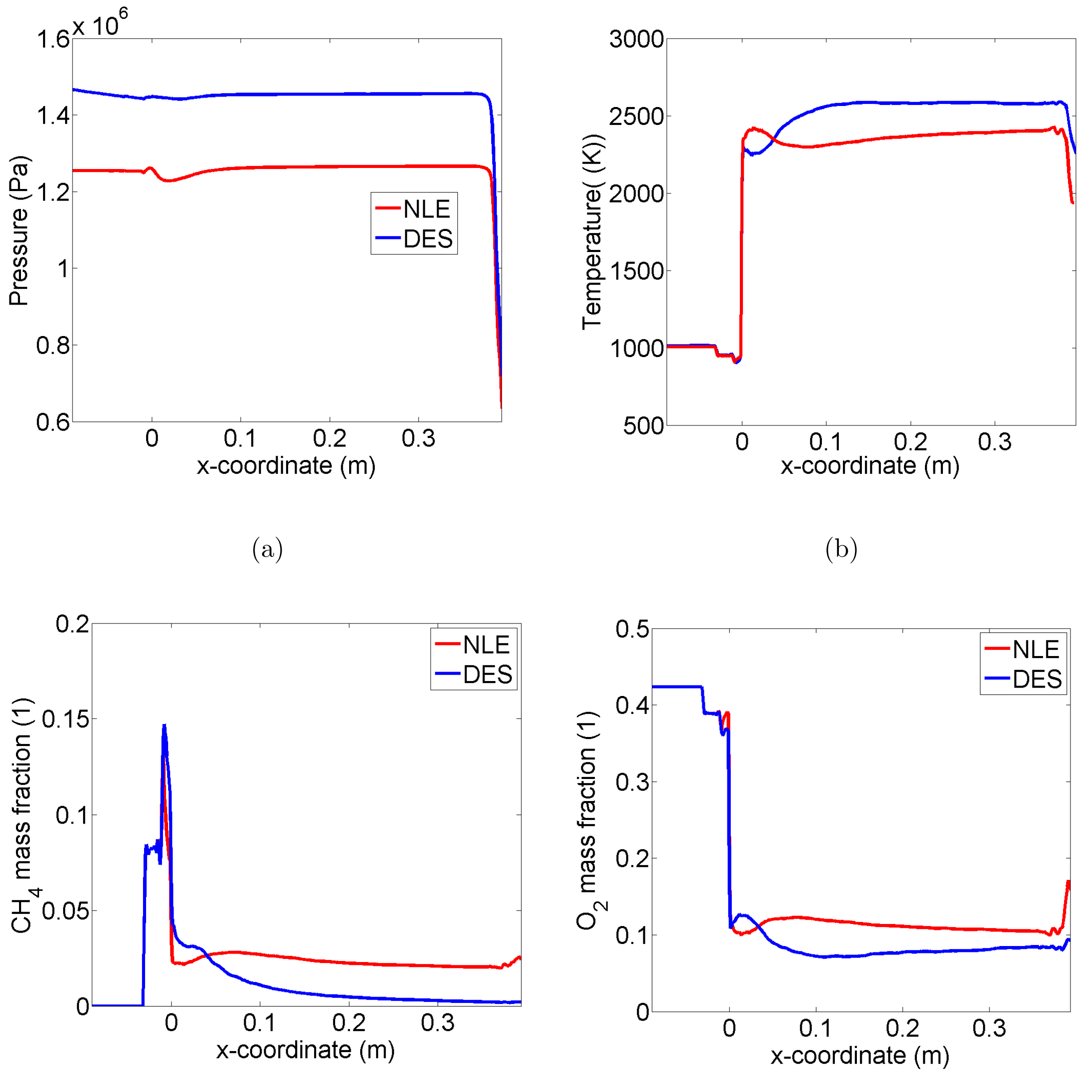

(a) (b)

(c) (d)

Fig. 4.16. Comparison of time averaged a) Pressure b) Temperature c) CH4 (fuel) mass fraction and d) O2 (oxidizer) mass fraction between the NLE-FTF and hybrid RANS/LES simulation

To overcome the issue of the pressure drop that was observed when the limit on species destruction rate was imposed and to use the correct amount of fuel and oxidizer in the NLE simulation, the heat addition approach was modified to account for changes in local cell constituents by implementing a variable gain approach, in which the local species destruction rates were multiplied by a gain defined as the ratio of heat added in the NLE simulation to the mean heat added in the reference hybrid RANS/LES simulation.

$$Gain(t) = \frac{\bar{\dot{q}}_{ref}}{\dot{q}_{NLE}(t)} \tag{4.2}$$

where $\bar{\dot{q}}_{ref}$ is the mean integrated heat release rate of the reference simulation and $\dot{q}_{NLE}(t)$ is the instantaneous integrated heat release rate of the NLE simulation.

$$\dot{\omega}_f(\overrightarrow{\mathbf{x}}, t) = Gain(t) * \bar{\dot{\omega}}_{f,lim}(\overrightarrow{\mathbf{x}}, t) \tag{4.3}$$

where $\dot{\omega}_f(\overrightarrow{\mathbf{x}}, t)$ is the instantaneous local fuel destruction rate of the NLE simulation and $\bar{\dot{\omega}}_{f,lim}(\overrightarrow{\mathbf{x}}, t)$ is the local time averaged fuel destruction rate obtained from hybrid RANS/LES simulation and adjusted for local cell constituents. Using this dynamic gain approach correct mean conditions at every time step of the NLE-FTF simulation and at varying flow fluctuation levels required for using the FTF were obtained.

The FTF was activated once pressure data is obtained and the NLE-FTF simulation was continued thereafter. The pressure trace measured close to the aft end of the combustor, at 0.368 m downstream of the dump plane is compared in Fig. 4.17. The pressure trace in the NLE-FTF simulation shows a steady growth before reaching a limit cycle due to the linear relationship between unsteady heat release and pressure imposed by the FTF. In the NLE-FTF simulation, the heat release rate is maintained constant using the time-averaged species production rates from the high-fidelity simulation. At the beginning of the NLE simulation, when the FTF is turned off, the local change in heat release rate would be only due to the hydrodynamics and/or mass flow fluctuations in the oxidizer and fuel posts but not because of the acoustics. So, the initial pressure fluctuations do not grow (they directly reach a limit cycle due to low-level hydrodynamics and/or mass flow fluctuations that exists in the absence of pressure effects) since there is no coupling between pressure and heat release fluctuations. Once the FTF is turned on, the pressure fluctuations and heat release fluctuations are coupled. However, since the initial pressure fluctuations are only due to hydrodynamics, they will be of a low magnitude and hence the heat release fluctuations corresponding to them will also be low. These low heat release fluctuations will lead to a slight increase in pressure fluctuation level, which then increase the heat release fluctuation level and the process goes on. This growth behavior prevents the NLE simulation to reach the limit cycle immediately. Thus, the NLE-FTF simulation is able to show a growth of pressure fluctuations which was not observed in the hybrid RANS/LES simulations. A comparison of heat release mode shapes during the growth phase of NLE-FTF simulation, corresponding to a pressure peak at the dump plane is shown in Fig. 4.18. It can be observed that the heat release mode shape remains unchanged throughout the growth phase and only the amplitude of heat release increased with the increase in pressure amplitude. This behavior is expected due to the linear nature of the flame transfer function.

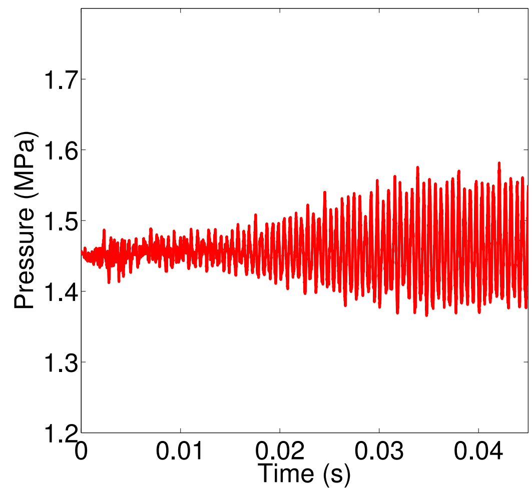

(a)

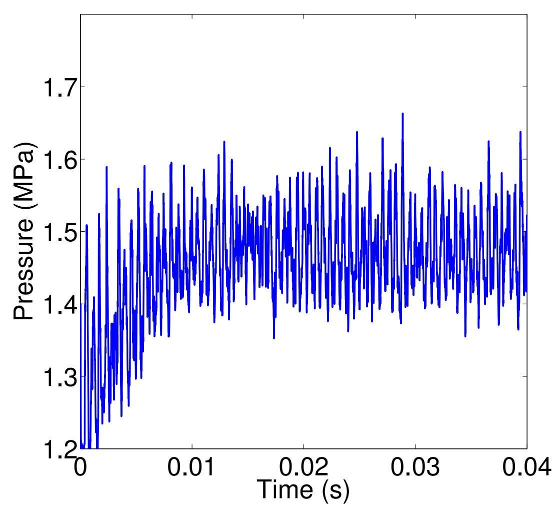

(b)

Fig. 4.17. The pressure trace measured 0.368 m downstream of the dump plane in a) NLE-FTF simulation b) Hybrid RANS/LES simulation

Whereas, in the hybrid RANS/LES simulation, since the pressure and heat release fluctuations are inherently coupled, the ignition event could possibly act as a "bomb setup" [5] [20] and push the system to a high amplitude limit cycle in a very short

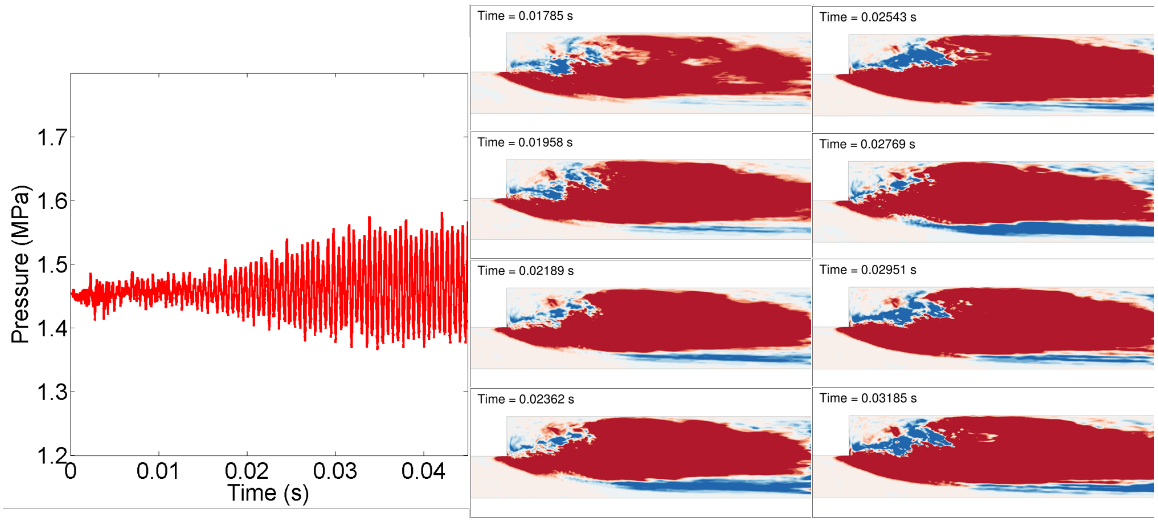

Fig. 4.18. Comparison of the heat release mode shapes during the growth phase of NLE-FTF simulation corresponding to a pressure peak at the dump plane

duration. This is why the hybrid RANS/LES simulation starts to exhibit the high amplitude pressure fluctuations as soon as the ignition occurs. We believe this is largely due to the way the ignition in hybrid RANS/LES is initiated.

Comparison of the pressure-time traces at limit cycle conditions and PSDs between the NLE-FTF and reference high fidelity simulations are shown in Fig. 4.19. The peak-to-peak pressure oscillations in the limit cycle of NLE-FTF simulation were found to be 10.8% of the mean pressure, agreeing well with the reference of 10.5% predicted by the hybrid RANS/LES simulation. However, the NLE-FTF pressure trace appears to be more sinusoidal compared to the hybrid RANS/LES simulation pressure trace which contains much sharper peaks. This difference between the NLE-FTF and the reference simulation is expected since only three FTFs corresponding to

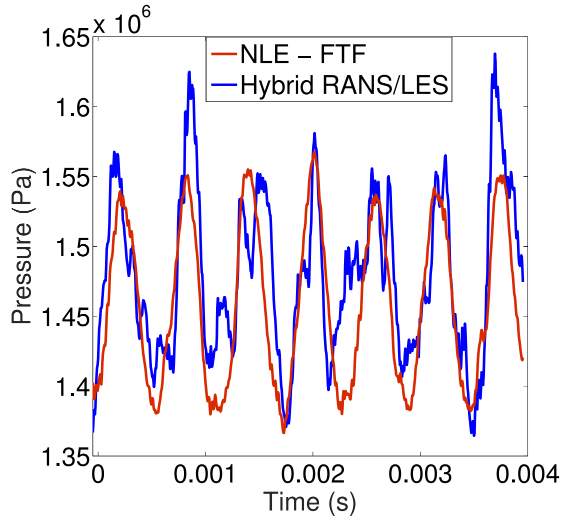

(a)

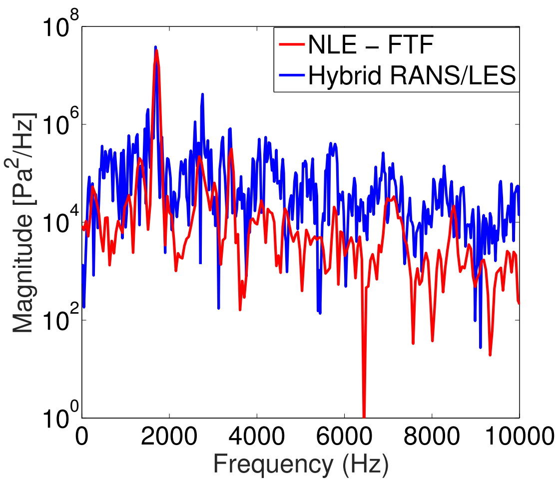

(b)

Fig. 4.19. Comparison of a) limit cycle pressure trace and b) PSDs between the NLE-FTF and hybrid RANS/LES simulations

the first three dominant modes were used. It should be noted that the thermal conductivity and viscosity are not included in the NLE solver. The PSD comparison between the NLE-FTF and high fidelity simulations shows that the dominant 1L mode (1700

Hz) and 2L mode (3375 Hz) are reproduced by the NLE solver to a good extent. Some discrepancy was observed in capturing the 2750 Hz mode. The FTFs included were based on the first three dominant modes observed in the DMD spectrum of the pressure. However, the DMD spectrum of heat release showed only two dominant modes corresponding to the first and third dominant modes of the pressure. The absence of the effects of heat release at frequencies other than the three modes considered could be a reason for the discrepancy observed in the NLE simulation. Also, a comparison of the mean variables as shown in Fig. 4.20, reveal that the NLE-FTF simulation was able to reproduce the mean variables to a good extent. The slight discrepancy in the mean properties is believed to be due to the local flow differences between the NLE-FTF and hybrid RANS/LES simulation.

A typical pressure cycle of the NLE-FTF and hybrid RANS/LES simulation is compared in Fig.4.21. The NLE-FTF simulation is seen to generally match the wave motion in the chamber and oxidizer post as seen from the hybrid RANS/LES. The points of the analyzed cycle are numbered on the pressure trace shown in Fig. 4.19a. The cycle begins with high pressure at the aft end of the combustor in both the sets of results. The correspondence observed at the second point of the cycle between the low pressure region within the oxidizer post suggests the similarities of the physics being modeled. The heat release in the case of NLE-FTF is dependent on the fluctuating pressure, which serves as an input to the FTF. The FTF in addition to the mean species consumption rate, approximates the unsteady heat release in the hybrid RANS/LES and due to the limited number of modes used in its construction, the dif-

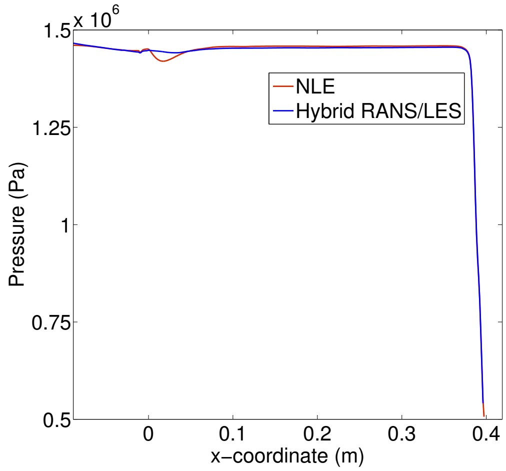

(a)

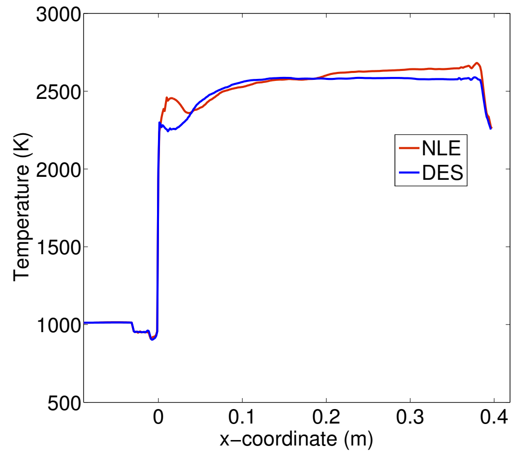

(b)

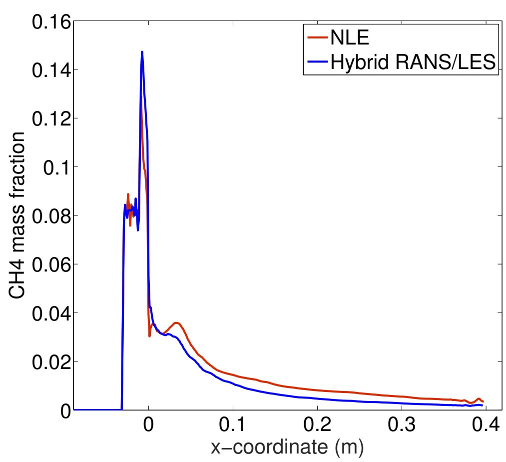

(c)

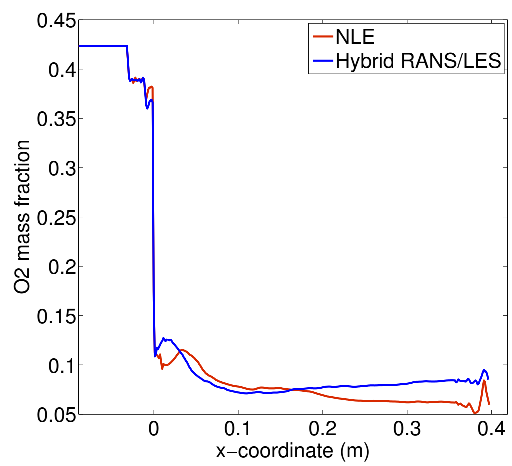

(d)

Fig. 4.20. Comparison of time averaged a) Pressure b) Temperature c) CH4 (fuel) mass fraction and d) O2 (oxidizer) mass fraction between the NLE-FTF and hybrid RANS/LES simulation

ferences in the pressure contours are discernible. The third point of the cycle, which shows the peak pressure at the head end of the combustor shows this difference. Since the heat release at the head end during the limit cycle conditions is the primary driving mechanism, the differences in the rest of the pressure cycle are expected.

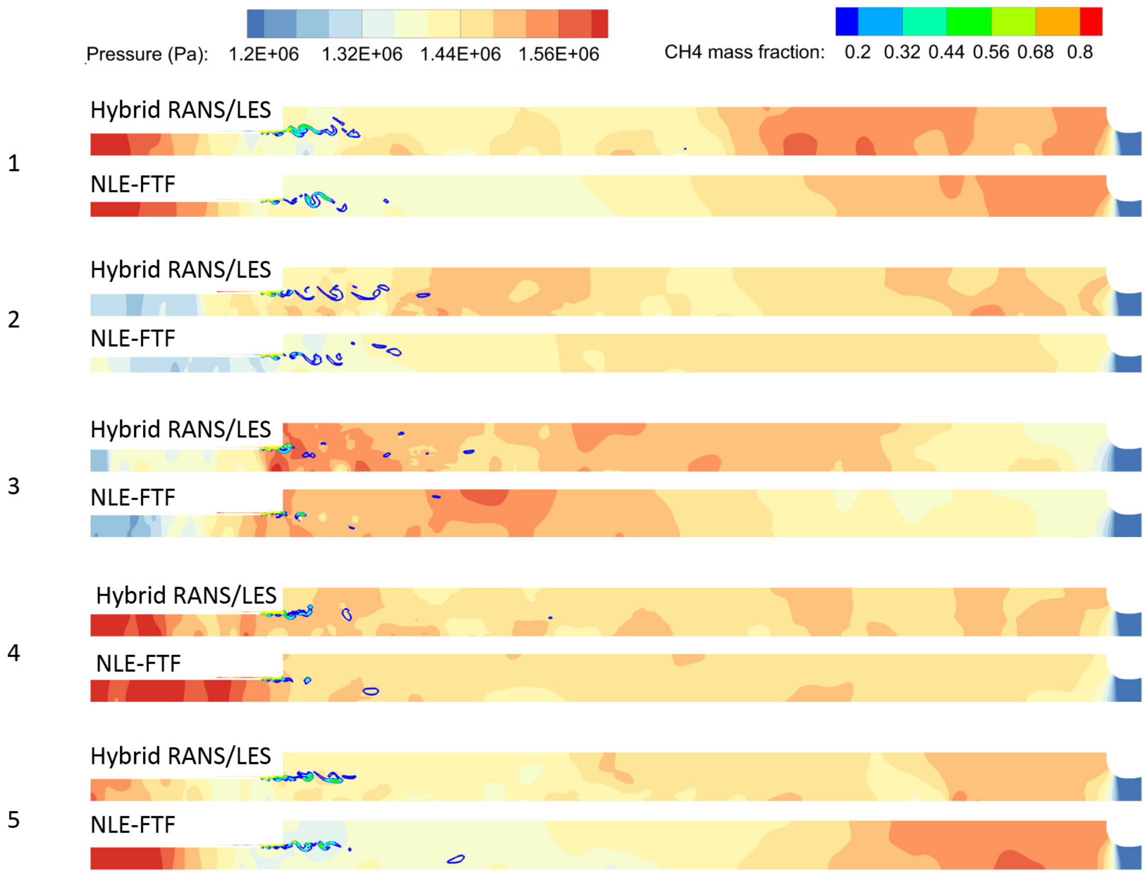

Fig. 4.21. Comparison of pressure and CH4 limit cycles between hybrid RANS/LES and NLE-FTF simulations

The fuel mass fraction cycle obtained is shown in Fig. 4.21. The periodic combustion observed during the limit cycle in the hybrid RANS/LES is mimicked in the NLE-FTF approach. The mean species destruction rates imposed are limited according to the local mixture conditions, which allows the accumulation of the fuel. The

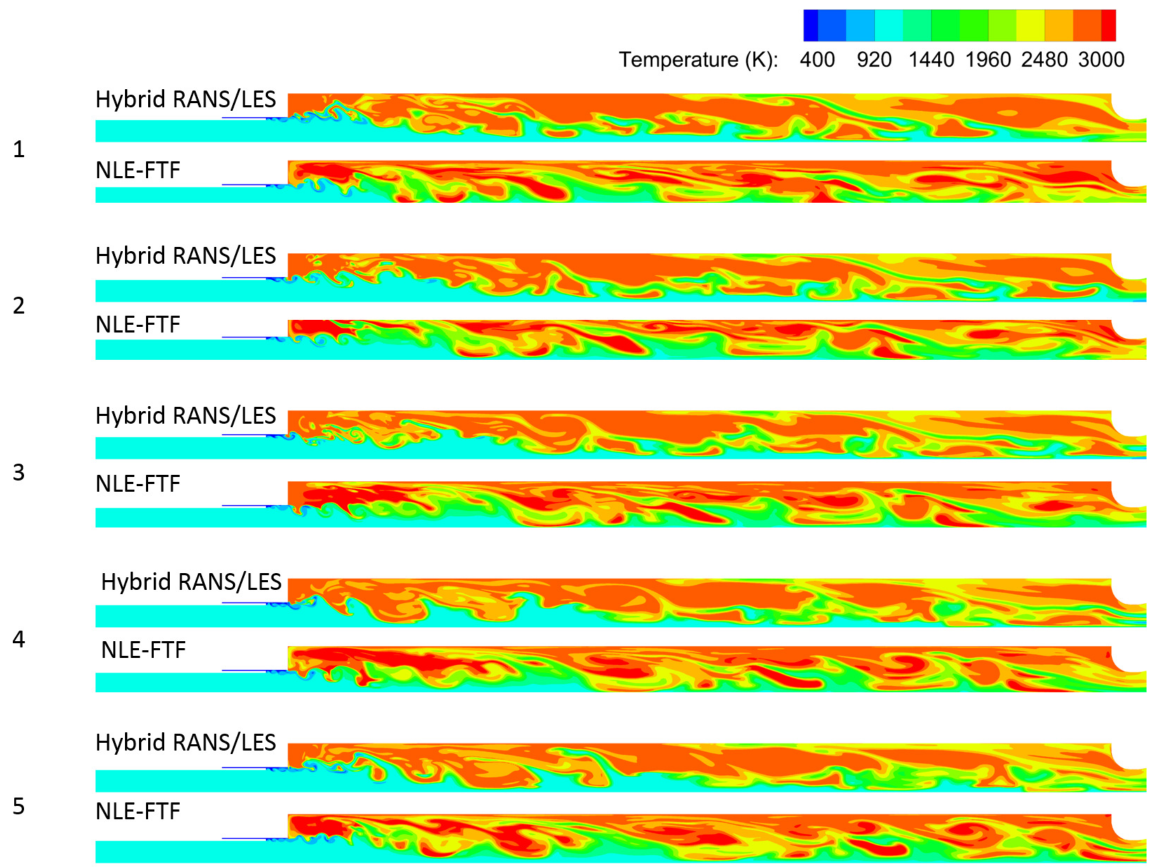

Fig. 4.22. Comparison of axisymmetric two dimensional temperature contours between the NLE - FTF and hybrid RANS/LES simulations for one pressure cycle

FTF based heat release, while accounting for the fluctuating part ensures the total fuel consumption. With this approach, the start of the fuel consumption during the initial two points of the cycle followed by maximum fuel destruction during the third point and beginning of the fuel accumulation for the next cycle can be seen in the last two points of the cycle from both sets of the results.

The corresponding temperature cycle is shown in Fig.4.22. The NLE-FTF simulation has wider range of temperatures compared to the hybrid RANS/LES simulation. This is due to the unsteady heat release, which does not depend on the local cell constituents, instead relying on the unsteady pressure at that location. After reaching the limit cycle condition, the same amount of heat is added and removed during the compression and expansion halves of the cycle, which maintains correct mean temperature and hence the correct mean speed of sound. The frequencies obtained in the NLE-FTF simulation therefore closely match those observed with the hybrid RANS/LES results, as shown in Fig. 4.19b.

As discussed earlier, the NLE-FTF simulation shows the growth of pressure fluctuations before reaching the limit cycle. This behavior of NLE-FTF simulation helps understand how the flow characteristics change with increasing amplitude of pressure fluctuations. A comparison of pressure and fuel cycles at the beginning of growth period and during the limit cycle of NLE-FTF simulation is shown in Fig. 4.23. From the figure, it can be seen that, a major difference between the two regimes appear to be the amount of fuel accumulated near the dump plane as the returned pressure wave from nozzle reaches the dump plane. At the beginning of the growth phase, since amplitude of pressure fluctuations is low, the amount of fuel accumulation upstream the dump plane is low. So, the flame is still attached and continuous. In contrast, during the limit cycle, the high amplitude pressure fluctuations lead to considerable amount of fuel accumulation upstream of the dump plane and prevents the fuel from entering the combustor. This may lead to a detached and discontinuous flame and equivalence ratio fluctuations. Hence, at high levels of instability it is difficult to isolate the mechanisms leading to instability. The flow behavior observed in the NLE-FTF simulation at low and high instability levels is in good agreement with the historical studies on effect of vortex shedding on combustion instability [25] [16] [17].

The cycle analysis and PSD amplitude comparison shows that the NLE-FTF simulation is able to reproduce the major flow characteristics. From the perspective of the limit cycle comparison, the NLE-FTF simulation was able to reproduce the high fidelity solution to a good extent. It suggests that the proposed approaches of the spatially resolved FTFs extracted from the high fidelity hybrid RANS/LES simulation together with a nonlinear Euler solver can reproduce the behavior of a rocket combustor to a good extent both in terms of mean variables and limit cycle statistics. Although the results obtained motivate the extension of this approach to a multi-element system, the next imperative is to understand the effects of the model control parameters on its predictive capability.

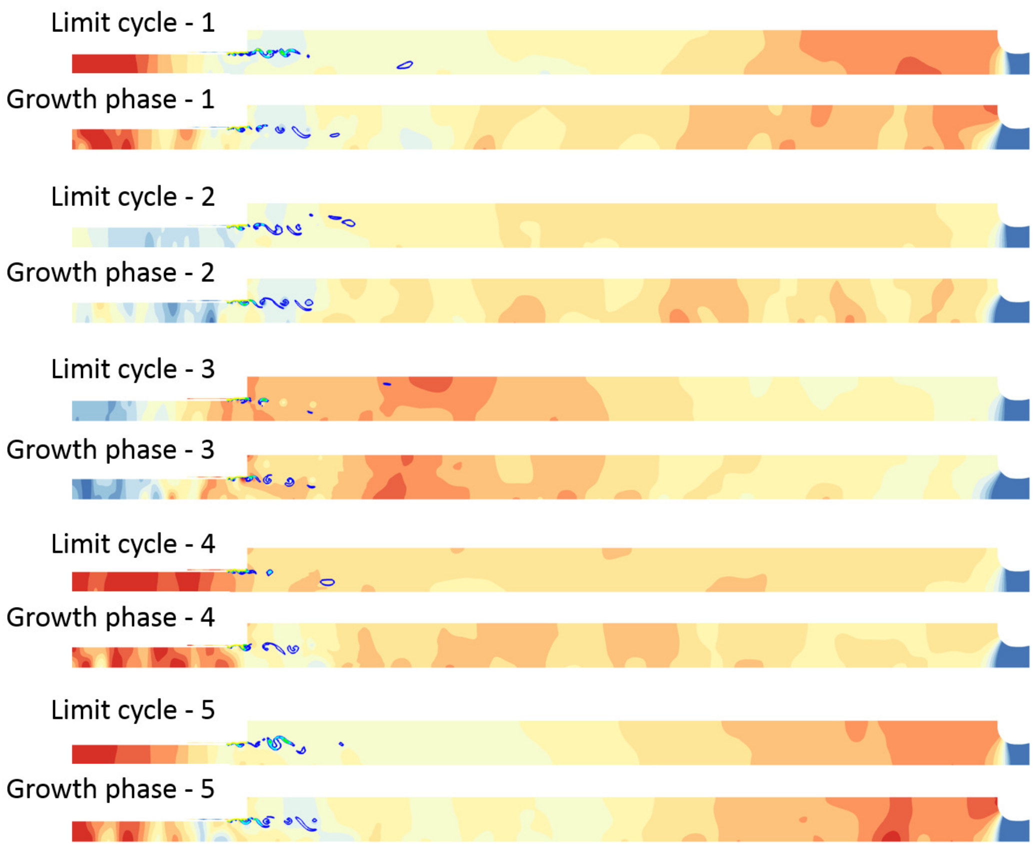

Fig. 4.23. Comparison of pressure and fuel mass fraction contours for one pressure cycle between the growth phase and limit cycle of NLE-FTF simulation

5. SENSITIVITY ANALYSIS OF THE REDUCED FIDELITY MODEL

In this chapter, the sensitivity analysis of the reduced fidelity model is presented. The sensitivity of the model to the number of modes in the FTF, the number of sampling points used in the Fourier transform of unsteady heat release calculation and the mesh size is discussed. The issues observed due to the presence of pressure node in the heat release region are discussed in detail. The NLE-FTF simulation was able to reproduce the high fidelity simulation to a good extent under the constraints of good spatial resolution and an FTF that includes modes at least one higher dominant frequency than the frequencies of interest. Further, analysis of NLE simulations with reference point based two-dimensional FTF and one-dimensional local FTF is also presented. The results obtained indicate that the NLE-FTF simulation was able to reproduce the reference high-fidelity simulation to a better extent when two-dimensional local FTFs are used instead of reference point based two-dimensional FTF and one-dimensional local FTF. The results of the hybrid RANS/LES-FTF simulation of the CVRC are also presented.

The CVRC results presented in section 4.3 were obtained using the FTFs corresponding to first three dominant modes observed in the DMD power spectrum of pressure, the same mesh as reference hybrid RANS/LES simulation and 1024 sampling points for Fourier transform calculation of the unsteady heat release. The control parameters such as the number of modes in the FTF, the number of sample points used for the Fourier transform and the mesh size may influence the prediction capability of NLE - FTF model to a certain extent. To establish the utility and generality of the model, we characterize the effects of these control parameters on its predictive capability. Hence a sensitivity analysis of the proposed NLE - FTF reduced fidelity model was performed using the CVRC 0.089 m post length case. The number of modes considered for FTF extraction to use in the NLE - FTF simulation were varied from one to five; the number of sampling points for the unsteady heat release calculation was varied from 128 to 1024; and the mesh size was varied from 20000 to 100000 nodes.

5.1 Number of modes in the FTF

Five cases were studied by varying the number of modes included in the flame transfer function used in the reduced fidelity simulation. In case 1, only the first longitudinal mode of the CVRC, 1700 Hz mode, was included in the FTF. This mode was apparent in both pressure and heat release spectra. In case 2, the first two longitudinal modes of the CVRC, 1700 Hz and 3400 Hz modes were included in the FTF. Again, both these modes were apparent in pressure and heat release spectra. In case 3, the first three dominant modes of the DMD power spectrum of pressure, 1700 Hz, 2750 Hz and 3400 Hz modes were included in the FTF. In case 4, the FTFs corresponding to the first four dominant modes of the DMD power spectrum of heat release, 1700 Hz, 3400 Hz, 5075 Hz and 5275 Hz were included in the FTF. In case 5, the FTFs corresponding to the first five dominant modes observed in the DMD power spectrum of the pressure and heat release, 1700 Hz, 2750 Hz, 3400 Hz, 5075 Hz and 5275 Hz were considered. To avoid any inconsistencies due to mesh size, all the cases were run using the same mesh used for reference hybrid RANS/NLE simulation.

First, the results of NLE-FTF simulation are compared to the results of hybrid RANS/LES simulation from which the FTFs were extracted. A comparison of the limit cycle pressure trace between the hybrid RANS/LES simulation and reduced fidelity NLE simulations with varying number of modes in the FTF is shown in Fig. 5.1. From the plot, it can be seen that the limit cycle pressure traces of all the NLE-FTF simulations except the 1-mode and 5-mode NLE - FTF simulation are in close agreement with each other and agree with the reference high fidelity simulation data to a good extent. The average peak-to-peak pressure oscillations in the reference high fidelity simulation measured over the entire limit cycle are 10.5% of the mean pressure. In the reduced fidelity simulation, the average peak to peak pressure oscillations of the 1-mode, 2-mode, 3-mode, 4-mode FTF and 5-mode FTF simulations are 14.0%, 13.5%, 10.8%, 12.0%, and 14.5% respectively. The limit cycle amplitudes observed in the experiment, hybrid RANS/LES simulation and the reduced fidelity simulations are summarized in Table. 5.1 [98].

From the results, it can be seen that agreement between the NLE-FTF and reference simulation improves as the number of modes in the FTF are increased from 1 to 3. However, the NLE-FTF simulations with the 4-mode and 5-mode FTF showed

Table 5.1.
The peak-to-peak amplitude of limit cycle oscillations

Case	Modes included in the FTF	Peak to peak limit cycle amplitude (% of mean pressure)
Experiment		8.5 %
Hybrid RANS/LES simulation		10.5 %
1 mode FTF simulation	1700 Hz	14.0 %
2 modes FTF simulation	1700 Hz & 3400 Hz	13.5 %
3 modes FTF simulation	1700 Hz, 2750 Hz, & 3400 Hz	10.8 %
4 modes FTF simulation	1700 Hz, 3400 Hz, 5075 Hz, & 5275 Hz	12.0 %
5 modes FTF simulation	1700 Hz, 2750 Hz, 3400 Hz, 5075 Hz, & 5275 Hz	14.5 %

slightly higher level of fluctuations than the 3-mode FTF simulation. We conjecture that the discrepancy in the limit cycle amplitudes of the 4-mode and 5-mode FTF simulations is due to the presence of a pressure node in the heat release zone for these higher modes. Among the five cases, the peak to peak pressure oscillations in the limit cycle of NLE-FTF simulation with the 3-mode FTF agreed best with the hybrid RANS/LES simulation.

As is evident from Fig. 5.1, the hybrid RANS/LES simulation exhibited much sharper peaks compared to the NLE-FTF simulation. The NLE-FTF simulation with the least number of modes in the FTF exhibited more sinusoidal behavior (broad peaks) than others. This behavior may be due to the approximation of heat release oscillations as the sum of limited number of sine waves. It can be observed from the plots that the pressure peaks are becoming much sharper as the number of modes in the FTF are increasing. A near-exact match of wave shape may be possible if even more modes are included in the FTF formulation. However, this is prevented by the numerical issues that arise in the high frequency modes due to the presence of pressure node in the heat release region.

A comparison of PSDs between the hybrid RANS/LES simulation and the NLE-FTF simulations is shown in Fig. 5.2. From the plot, it can be seen that the NLE-FTF simulations mostly reproduced the modes that were included in the FTF of that particular simulation. The 1-mode FTF simulation reproduced only the first longitudinal mode, which was overestimated. No other dominant peaks corresponding to the higher longitudinal modes were observed. The 2-mode FTF simulation reproduced the first

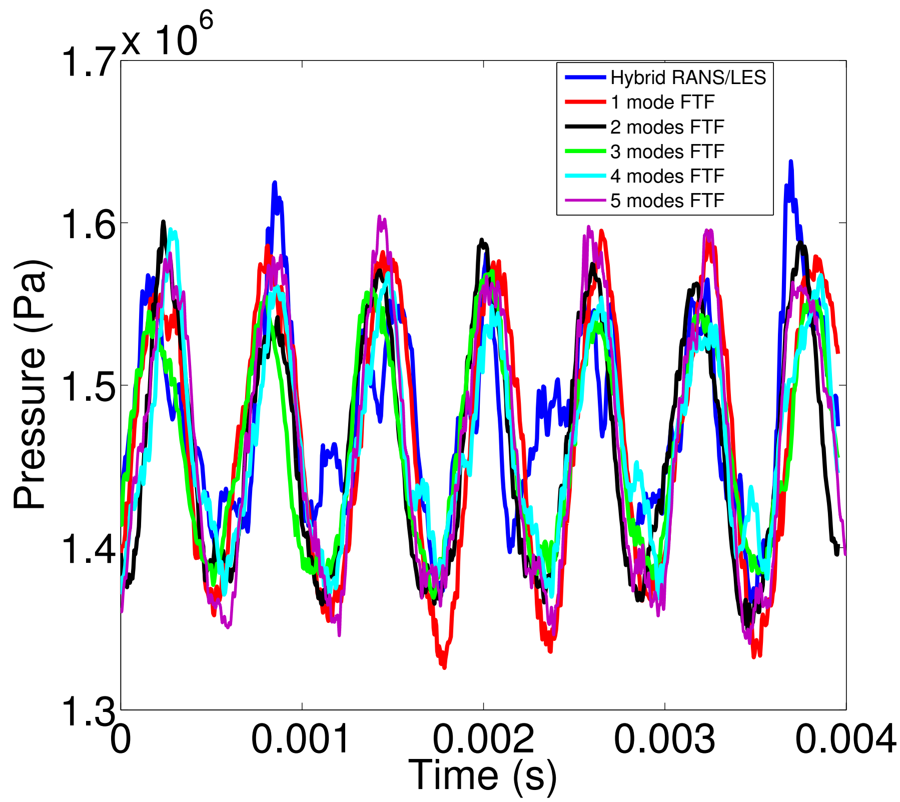

Fig. 5.1. Comparison of limit cycle pressure trace between the NLE-FTF simulations with varying number of modes and the hybrid RANS/LES simulation

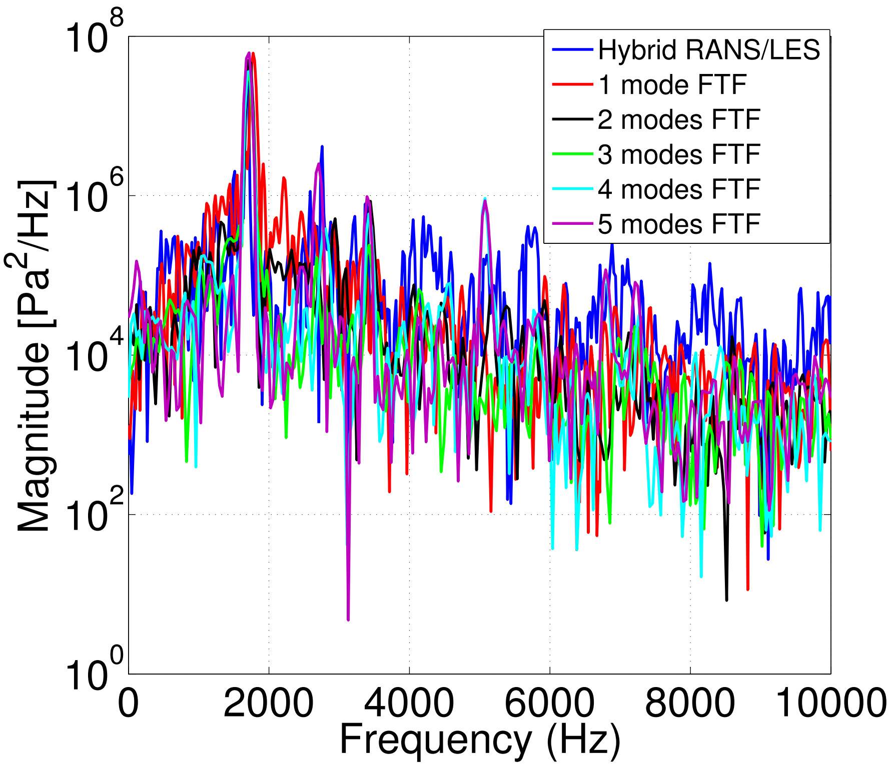

Fig. 5.2. Comparison of PSDs between the NLE-FTF simulations with varying number of modes and the hybrid RANS/LES simulation

longitudinal mode to a good extent and slightly under-estimated the second longitudinal mode. Similar to the 1-mode FTF simulation, no other peaks corresponding to the higher longitudinal modes were observed. The 3-mode FTF simulation reproduced the first longitudinal mode to a good extent, but under-estimated both the 2750 Hz mode and second longitudinal mode. The 4-mode FTF simulation reproduced the first and second longitudinal modes to a good extent but overestimated the 3L mode. Similarly, the 5-mode FTF simulation reproduced the first and second longitudinal modes to a good extent but overestimated the 3L mode. In addition, the 5-mode FTF simulation also reproduced the 2750 Hz mode to a good extent. Although the 4- and 5-mode FTF simulations have slightly overestimated the limit cycle amplitudes, the overshoot appears to be mainly due to incorrect estimation of the 3L mode. Both 4-, and 5-mode FTF simulations have reproduced the 1L, and 2L modes more accurately than other FTF simulations. To get better insights, the limit cycle pressure fluctuations observed in the NLE-FTF simulations were band-passed around the dominant frequencies (with 5% filter width on either side of the dominant frequency) and the observed peak-to-peak amplitudes are summarized in Table. 5.3. The band-passed results confirm the trend observed in the PSDs. Although the PSD comparison showed that the peaks of the 1L mode matched well between the NLE-FTF and hybrid RANS/LES simulation, the band-passed data revealed that the peak-to-peak amplitudes of the 1L mode observed in the 3-, 4-, and 5-mode NLE-FTF simulations is higher than the hybrid RANS/LES simulation by 1%. This indicates that the PSD peak corresponding to 1L mode is slightly broader in the NLE-FTF simulations when compared to the hybrid RANS/LES simulation. The band-passed results confirm that the discrepancy observed in the limit cycle amplitudes of 4- and 5-mode FTF simulations is due to the overestimation of 3L mode.

As mentioned earlier, the presence of pressure node of high frequency mode in the heat release region is believed to be partly responsible for this overestimation of the 3L mode by the 4-, and 5-mode FTF simulations. The pressure and the heat release mode shapes corresponding to the 5075 Hz mode of the 4 modes FTF simulation are shown in Fig.5.3. The mode shapes reveal the presence of pressure node in the region where the heat release is substantial. The FTF, being the ratio of heat release fluctuations and pressure fluctuations, can have a very large value at the pressure node as a consequence. The gain of the FTF of 5075 Hz is shown in Fig.5.4a. From the plot, it can be seen that the gain of the FTF is very high at the location of pressure node, which probably leads to non-physical heat addition/removal in the NLE-FTF simulation.

To address this issue, the pressure mode shape of the 5075 Hz mode was slightly modified by spreading the node out so that the high gain regions in the flame transfer function are eliminated as shown in Fig.5.4b. It can be seen from the FTF plot that the correction eliminated only the hot spots near the node, and the magnitude of FTF was unaltered at other locations. A sample 3L pressure mode shape and the pressure mode shape with spread out nodes is shown in Fig. 5.5. This correction is believed to have led to overestimation of 3L mode by the 4-, and 5- mode FTF simulations. A correction of this sort is likely necessary for any spatially-resolved FTF simulations

Table 5.2.
The peak-to-peak amplitude of band-passed limit cycle oscillations

Case	Peak-to-peak amplitude $= 2\sqrt{2}p'_{rms}$ (% of mean pressure)			
	1700 Hz	2750 Hz	3400 Hz	5075 Hz
Hybrid RANS/LES simulation	8.0%	2.5%	1.4%	0.9%
1 mode FTF simulation	10.5%	0.9%	0.8%	0.3%
2 modes FTF simulation	10.0%	1.1%	1.4%	0.4%
3 modes FTF simulation	8.9%	1.0%	1.0%	0.3%
4 modes FTF simulation	8.7%	1.0%	1.2%	1.9%
5 modes FTF simulation	9.0%	1.9%	1.3%	1.9%

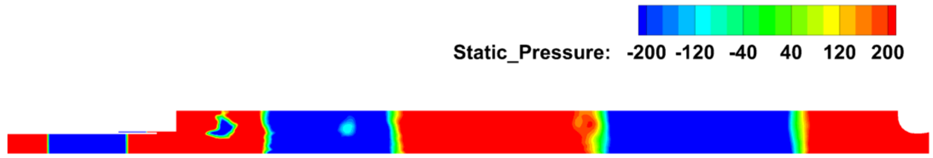

(a)

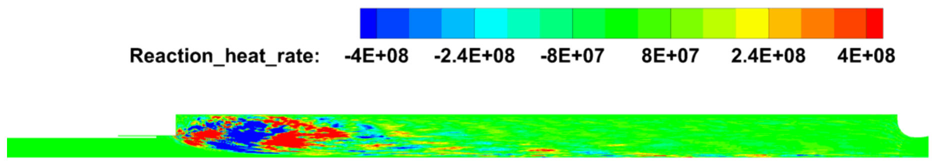

(b)

Fig. 5.3. The a) pressure mode shape and b) heat release mode shape corresponding to the 5075 Hz mode of the CVRC

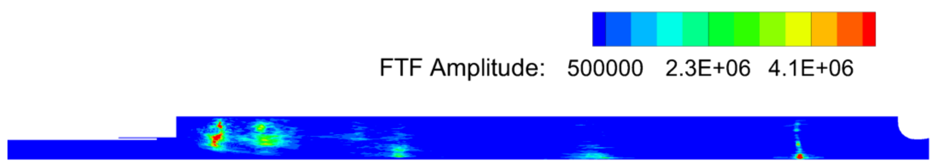

(a)

(b)

Fig. 5.4. The gain of flame transfer function of 5075 Hz mode a) before and b) after correction

with high frequency modes (which may have pressure nodes in the heat release zone) and needs to be investigated further. Based on the results of all NLE-FTF simulations, it appears that we may have to consider $n+1$ modes FTF for accurate prediction of n dominant mode system, where n is the number of dominant modes expected in the

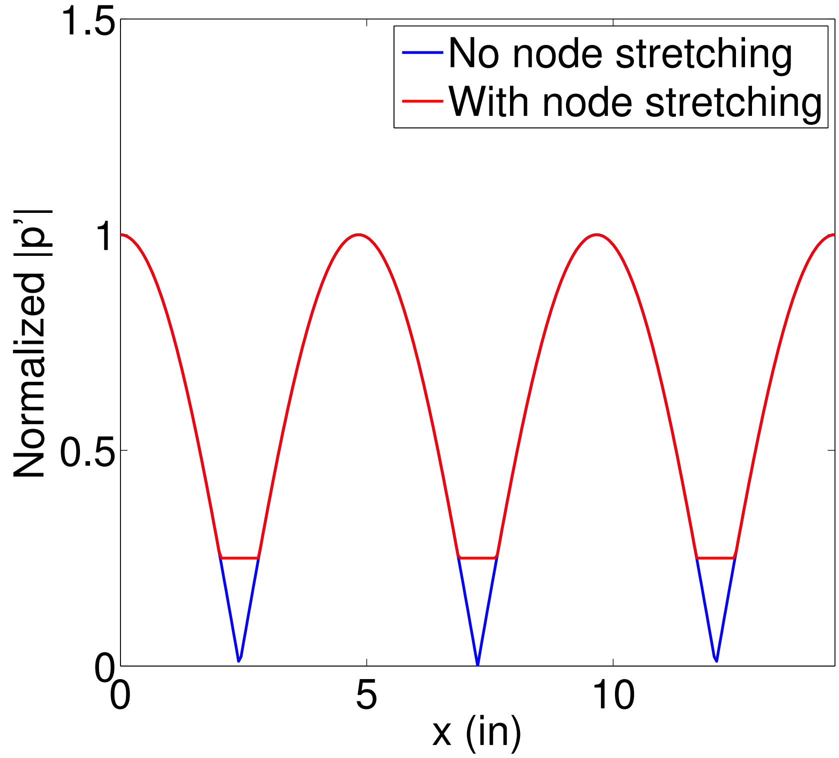

Fig. 5.5. The sample pressure mode shapes of a 3L (third longitudinal) mode showing the node stretching

system. For example, if a system exhibits first harmonic at 2000 Hz and if we would like to predict the behavior of system till the third harmonic, 6000 Hz, then it may be necessary to include modes up to 8000 Hz in the FTF formulation.

A comparison of the pressure mode shapes between the hybrid RANS/LES simulation and the NLE-FTF simulations is shown in Fig. 5.6 and Fig. 5.7. All the NLE-FTF simulations with varying number of modes in the FTF reproduced the mode shape of first longitudinal mode accurately. The 1-mode FTF simulation failed to reproduce the mode shape of second longitudinal mode. It was expected since only the information related to the first longitudinal mode was included in the FTF. The

2-, 3-, 4- and 5-mode FTF simulations reproduced the mode shape of the second longitudinal mode well. From the results, it is evident that if sufficient number of modes are included in the FTF, the NLE-FTF approach can predict accurate limit cycle behavior, mean flow conditions and mode shapes.

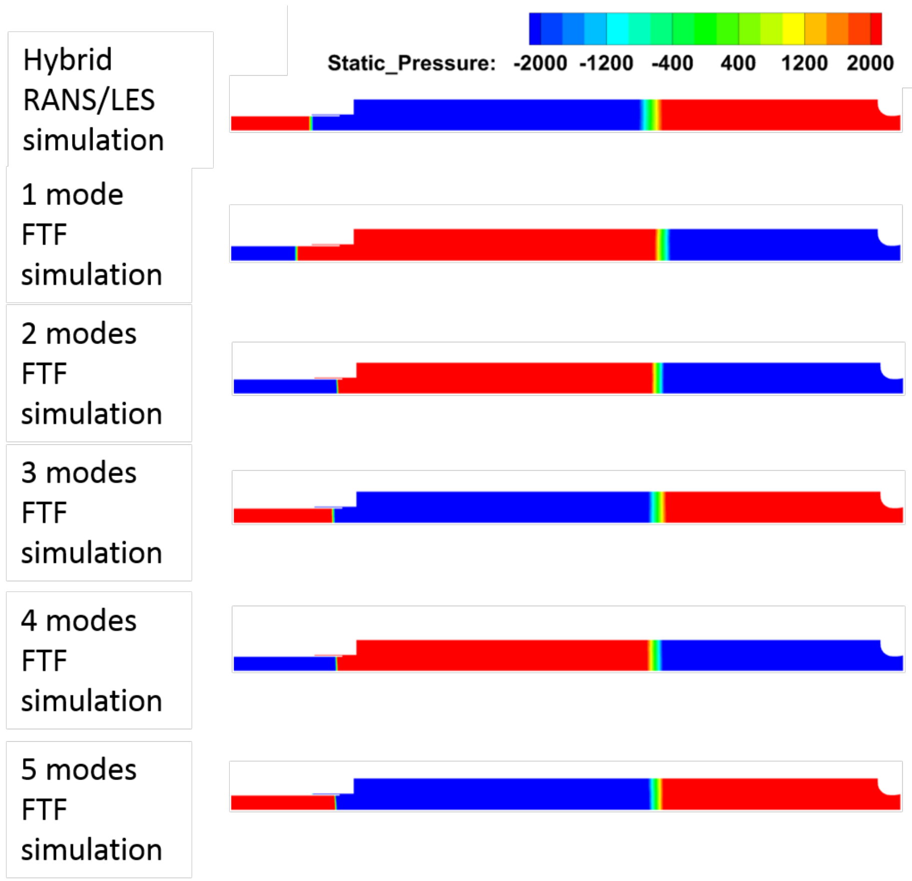

Fig. 5.6. Comparison of the mode shapes of first longitudinal mode between Hybrid RANS/LES simulation and NLE - FTF simulation

One of the interesting features of the reduced fidelity NLE-FTF approach is that it is capable of capturing growth rates in addition to the limit cycle behavior, mean flow conditions and mode shapes. The flow fluctuations in the NLE-FTF simulation start at very low level and grow until they reach the limit cycle prescribed by the FTF

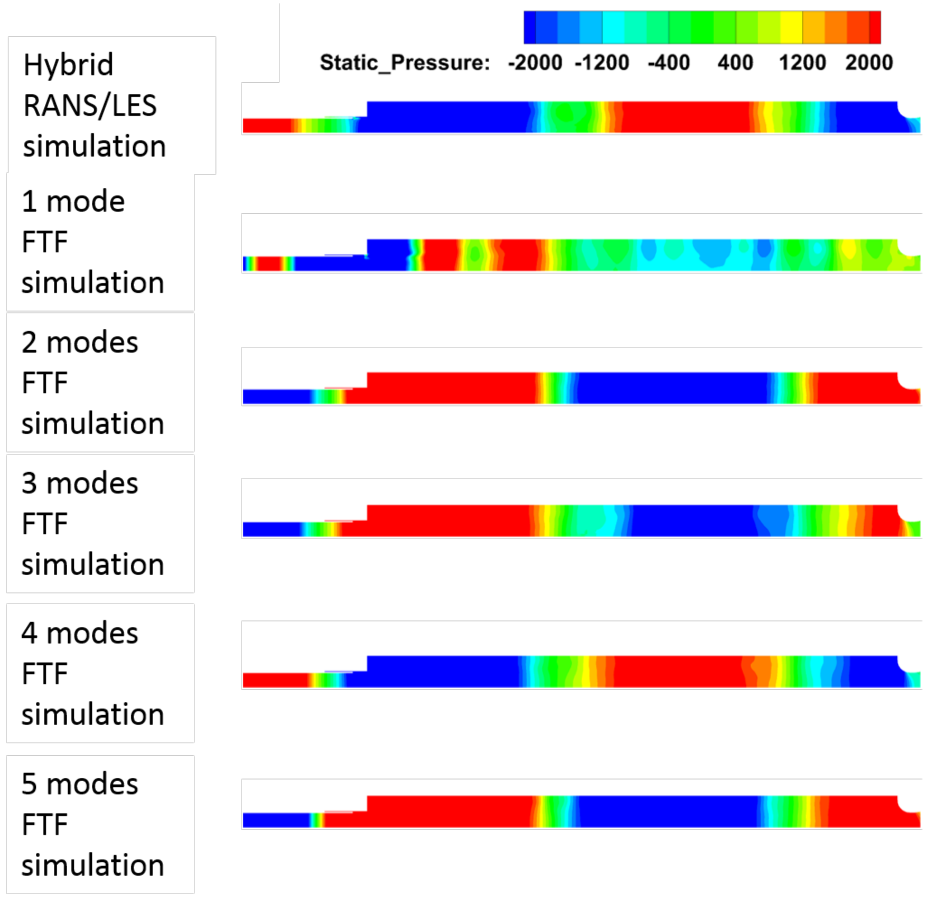

Fig. 5.7. Comparison of the mode shapes of second longitudinal between Hybrid RANS/LES simulation and NLE - FTF simulation

extracted from the high-fidelity simulation. During this period of growth, for a certain period of time when the flow oscillations are small, they grow at an exponential rate, termed as linear growth. As the fluctuation level increases, the nonlinearity of the system starts to dominate, and the growth of flow fluctuations deviates from being exponential and may reach a limit cycle or exhibit transient behavior. The linear growth rate has been a primary interest of reduced fidelity solvers that use wave equation or linearized Euler equations [34]. It should be noted that the experiment also exhibits a period of linear growth.

The growth rates of the first longitudinal mode of the 2-, 3-, 4-, and 5-mode FTF simulations were measured using the band passed pressure signal and fitting an exponential curve to the peaks of pressure trace. The growth rates reported in this study were measured during the period of growth where the growth is linear or best represented by the exponential curve. The exponential curve fit was not applied to the entire growth period since the growth might not be linear throughout the growth period. The 1-mode FTF simulation is not included in the comparison since it overestimated the first longitudinal mode. A comparison of the growth rates between the NLE-FTF simulation and experiment is shown in Fig. 5.8. Since the hybrid RANS/LES simulation did not exhibit growth of modes to limit cycle, the experimental data were used here for the comparison with the NLE - FTF simulations. In the experiments, the growth rate of the first longitudinal mode was found to be approximately 76 1/s. In the 2-,3-, 4-, and 5-mode FTF simulations the growth rate of the first longitudinal mode was found to be 96 1/s, 116 1/s, 98 1/s, and 95 1/s respectively, in reasonable agreement with each other and the experiment. From the figure, it can also be observed that the limit cycle amplitude of pressure fluctuations in the experiment is considerable smaller than that observed in the NLE-FTF simulation. It is expected because the reference experiment exhibited two dominated modes of equal strength as shown in Fig. 2.3.

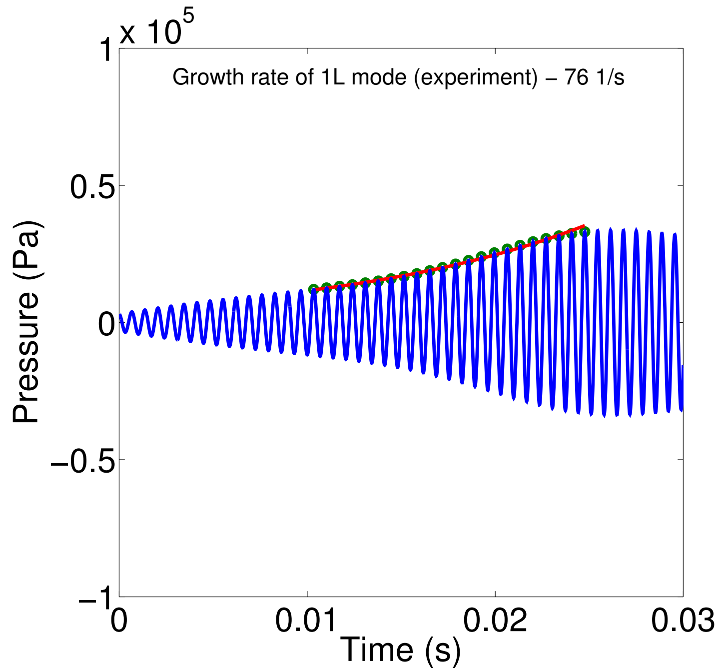

(a)

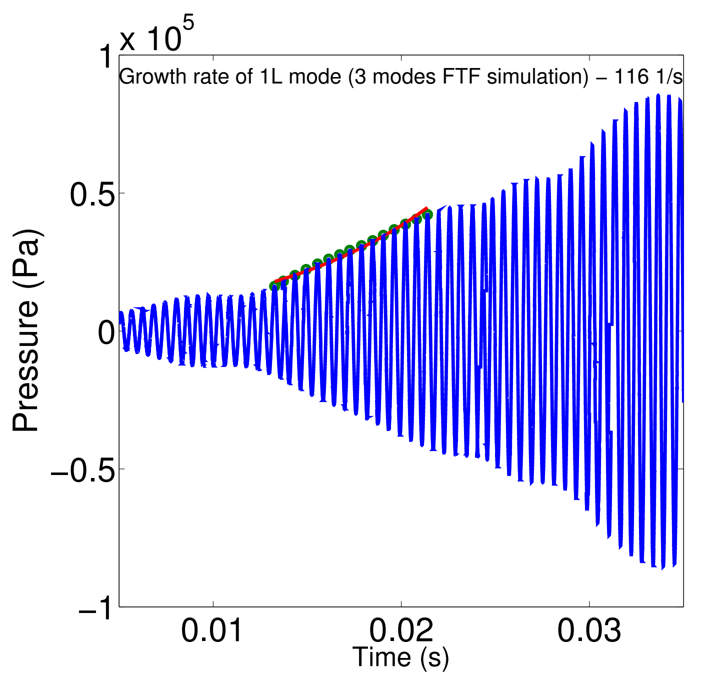

(b)

Fig. 5.8. Growth rate plots of the first longitudinal mode of a) CVRC 0.089 m experiment, and b) 3 modes FTF simulation, (The red line shows the exponential curve fit to the band passed pressure trace - this is the period of linear growth)

A comparison of the growth rates of the second longitudinal mode between the experiment and 5-mode FTF simulation is shown in Fig. 5.9. The growth rate of the second longitudinal mode in the experiment, 4-mode FTF, and 5-mode FTF simulation was found to be 300 1/s, 270 1/s, and 330 1/s respectively. The 1-, 2- and 3-mode FTF results are not included in the growth comparison of the second longitudinal mode since they either over or under-estimated the second longitudinal mode. The growth rates corresponding to various FTF simulations is shown in Table. 5.3. From the results obtained, it is clear that the NLE-FTF simulations estimated very reasonable growth rates when compared to the experimental growth rates. This potential ability of the FTF-NLE model to accurately grow to the limit cycle prescribed by the extracted FTF at limit cycle conditions is remarkable and needs to be further investigated. For instance, nonlinearities of heat release field at the conditions of this study may be sufficiently weak such that linear growth to the limit cycle is a good approximation (acoustic nonlinearities are accounted for by the NLE framework). The use of amplitude dependent FTFs, or flame describing functions, are probably needed for cases where there are strong nonlinear effects of amplitude on the heat release.

A comparison of the phase-plane plots between the hybrid RANS/LES simulation and the NLE-FTF simulation is shown in Fig. 5.10. The phase-plane plots confirm the observations from the limit cycle pressure trace comparisons and cycle analysis presented earlier that the NLE-FTF simulations were only able to reproduce the major characteristics of the flow that are represented by the FTFs included. The chaotic phase portrait of the hybrid RANS/LES simulation indicates that there are numer-

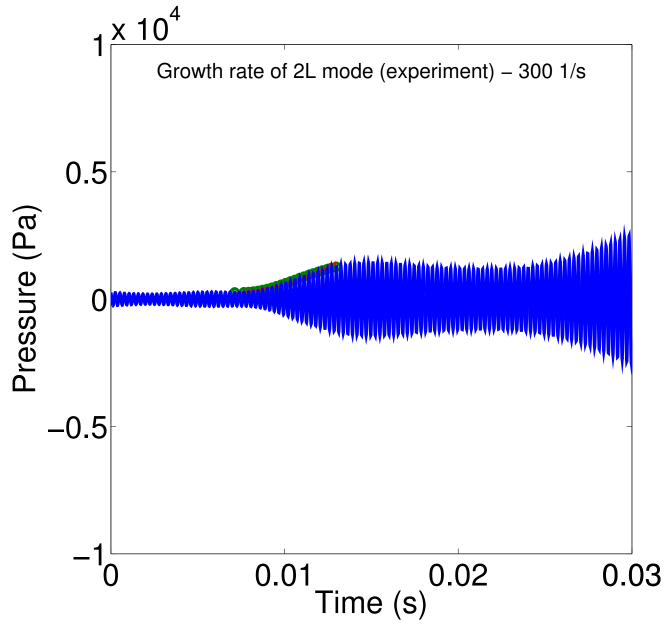

(a)

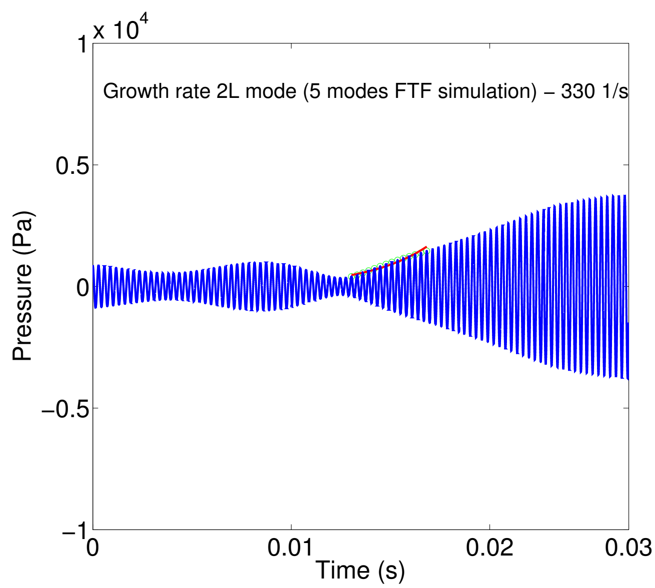

(b)

Fig. 5.9. Growth rate plots of the second longitudinal mode of a) CVRC 0.089 m experiment, and b) 5 modes FTF simulation and (The red line shows the exponential curve fit to the band passed pressure trace - this is the period of linear growth)

Table 5.3.
The growth rate observed in NLE-FTF simulations

Case	Modes included in the FTF	Growth rate (1/s)	
		1L mode	2L mode
Experiment		76	300
Hybrid RANS/LES simulation		-	-
1 mode FTF simulation	1700 Hz	-	-
2 modes FTF simulation	1700 Hz & 3400 Hz	96	-
3 modes FTF simulation	1700 Hz, 2750 Hz, & 3400 Hz	116	-
4 modes FTF simulation	1700 Hz, 3400 Hz, 5075 Hz, & 5275 Hz	98	270
5 modes FTF simulation	1700 Hz, 2750 Hz, 3400 Hz, 5075 Hz, & 5275 Hz	95	330

ous high frequency modes present in the system, whereas the more organized phase portrait of NLE-FTF simulations indicate that there are limited number of modes in the system. This the reason why the hybrid RANS/LES simulation exhibited much sharper pressure peaks whereas the NLE-FTF simulation pressure traces were more sinusoidal.

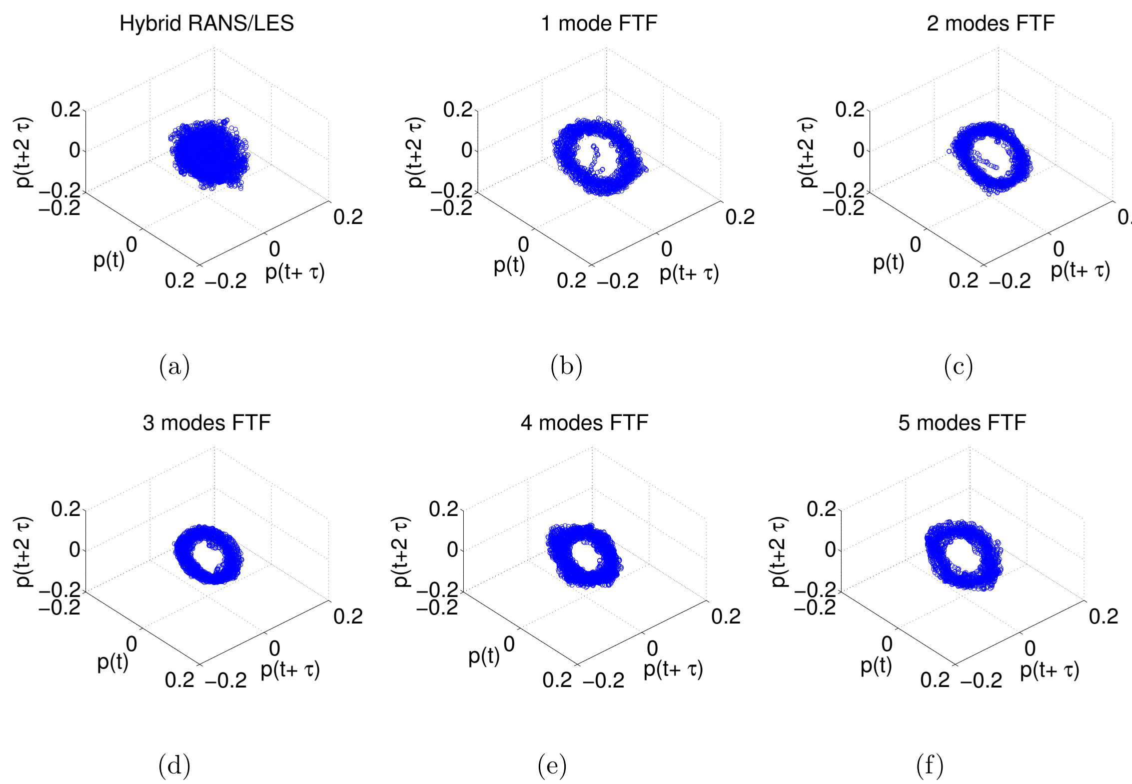

Fig. 5.10. Comparison of phase plane portraits between the hybrid RANS/LES simulation and NLE-FTF simulations

A comparison of the Rayleigh index, defined as,

$$R(\overrightarrow{\mathbf{x}}) = \frac{1}{t_2 - t_1} \int_{t_1}^{t_2} p'(\overrightarrow{\mathbf{x}}, t)\dot{q}'''(\overrightarrow{\mathbf{x}}, t)dt, \tag{5.1}$$

between the NLE-FTF simulations and the hybrid RANS/LES simulation is shown in Fig. 5.11. Rayleigh index reveals the extent of coupling between the pressure and heat release fluctuations. From the Rayleigh index of hybrid RANS/LES simulation we can see that the pressure and heat release are coupled in phase in the shear layer and out of phase in the recirculation zone. The Rayleigh index of all the NLE-FTF simulations show that the coupling between heat release and pressure fluctuations in the shear layer region and recirculation zone is accurately reproduced. However, the magnitude of Rayleigh index is slightly high in case of 1-, 2-, and 5- mode FTF simulations. This is because of the slightly higher limit cycle pressure oscillations and subsequent higher heat release fluctuations observed in the NLE-FTF simulations.

5.2 Number of sample points used in unsteady heat release calculation

In addition to varying the number of modes in the FTF, a sensitivity analysis is also performed by varying the number of sampling points of pressure used in Fourier transform to obtain the unsteady heat release. By varying the number of sample points, we effectively varied the rate at which pressure data is collected in the NLE-FTF simulation to calculate the unsteady heat release. The rate at which pressure data were collected determines the highest frequency resolved. Four cases were simulated with number of sampling points set to 128, 256, 512 and 1024 points. For this analysis, all the simulations were run using the 3-mode FTF, since that simulation showed better agreement with the hybrid RANS/LES simulation in terms of the limit cycle amplitude. It was found that the NLE-FTF simulation with 128 and 256 sampling points exhibited pressure fluctuations with peak-to-peak amplitudes measured around 14% of the mean pressure. Whereas, the NLE-FTF simulation with 512 and

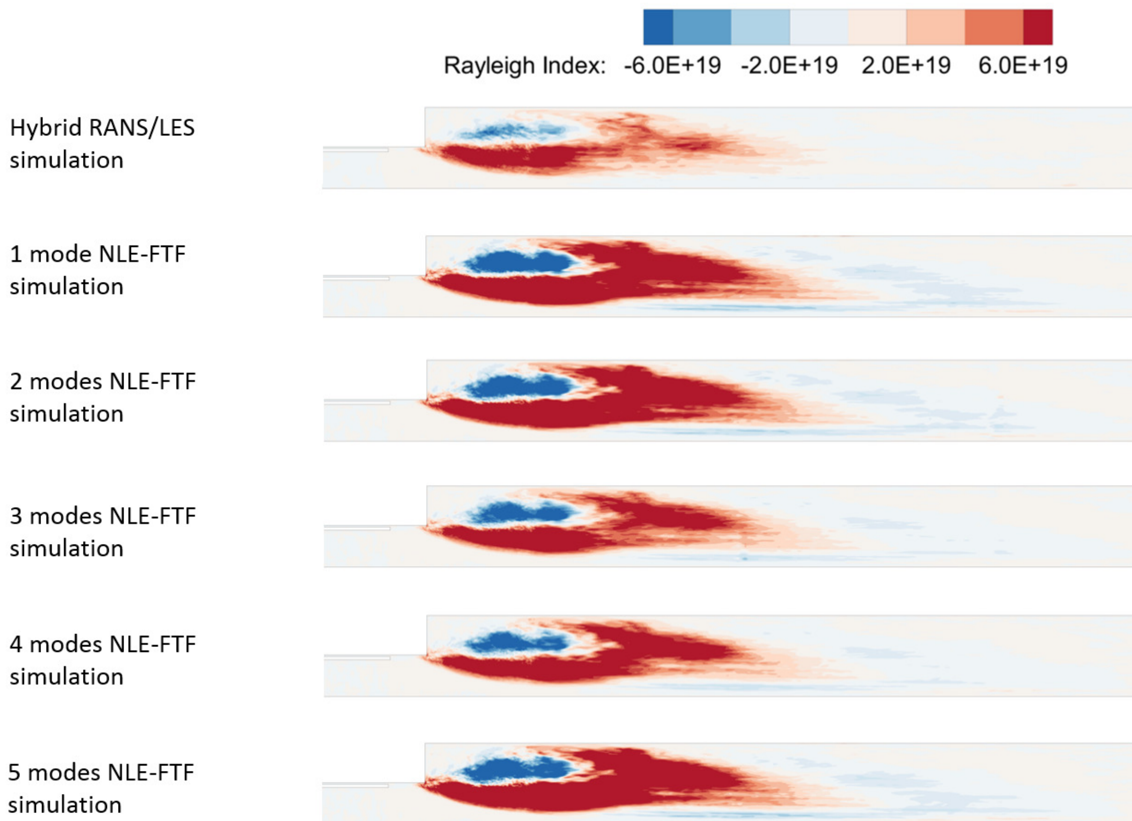

Fig. 5.11. Comparison of Rayleigh index ($Pa.W/m^3$)) between the NLE-FTF simulations and hybrid RANS/LES simulation

1024 sampling points exhibited pressure fluctuations with peak to peak amplitudes measuring around 13% and 10.8% of the mean pressure respectively. A comparison of PSDs between the FTF-NLE simulations with varying number of sampling points and hybrid RANS/LES simulations is shown in Fig. 5.12. It can be observed from the PSDs comparison plot that as the number of sampling points were increased the prediction capability of the NLE- FTF simulations seemingly improved. The NLE-FTF simulations with a smaller number of sampling points overestimated the first two longitudinal modes. It is noteworthy that the difference in the limit cycle amplitudes between the hybrid RANS/LES simulations and the NLE-FTF simulation is within 2%.

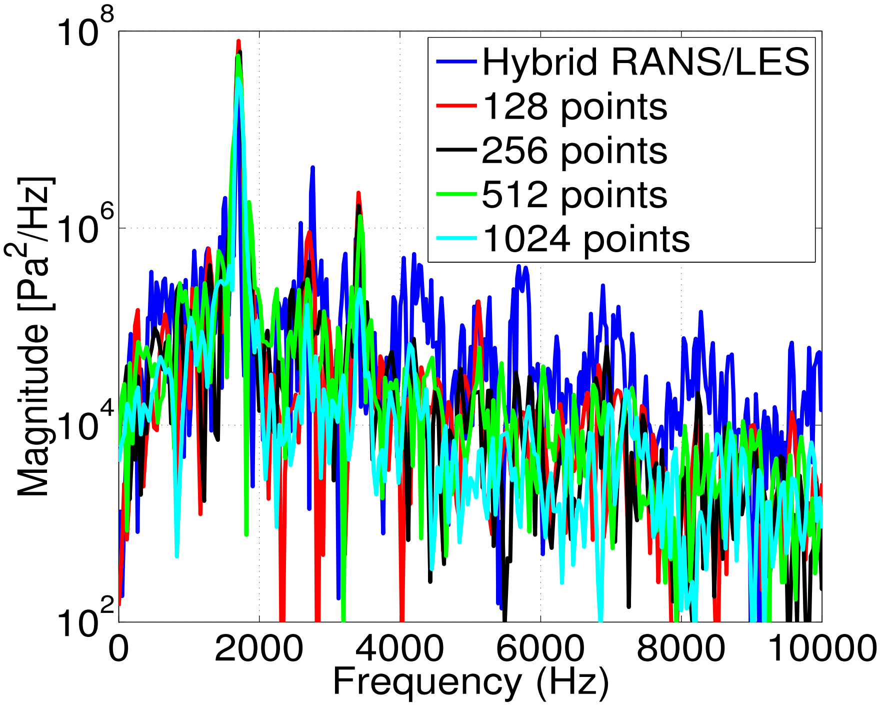

Fig. 5.12. Comparison of PSDs between NLE-FTF simulations with varying number of sampling points and hybrid RANS/LES simulation

5.3 Mesh size

Mesh sensitivity analysis was performed by varying the mesh size from 20,000 nodes to 100,000 nodes. This analysis was performed using the 3-mode FTF, similar to the sampling points analysis. Three simulations were performed by setting mesh size to 20,000, 50,000 and 100,000 nodes corresponding to the coarse, intermediate and fine mesh sizes respectively. The peak to peak limit cycle amplitudes of pressure fluctuations were found to be 4%, 8% and 11% of the mean pressure in the coarse, intermediate and fine mesh respectively. This deviation of results at lower mesh size is expected due to excessive numerical damping in coarse mesh. A comparison of the PSDs between the hybrid RANS/LES simulation and the NLE-FTF simulation at various mesh sizes is shown in Fig. 5.13. From the plot, it can be seen that very low energy dominant modes were observed in the case of coarse mesh and the energy of dominant modes converge to the hybrid RANS/LES simulation as the mesh size was increased. Also, it was observed that as the mesh size was increased from coarse to fine, the limit cycle amplitudes of pressure fluctuations converged to the hybrid RANS/LES simulation results. The fine mesh, which was used for hybrid RANS/LES simulation was used for all the NLE-FTF simulations.

5.4 Two dimensional reference point based FTF

Most previous applications of the FTF uses a reference signal, e.g. velocity fluctuations at the combustor inlet, as input. To understand the importance of accounting for local coupling between heat release and pressure fluctuations, further analysis was performed using two dimensional point based distributed FTF. In two dimensional point based distributed FTF, instead of calculating the gain and phase of the FTF using local heat release and pressure information, the gain and phase of the FTF were calculated using a reference pressure signal located upstream of the dump plane. For this study, the pressure signal 0.0127 m upstream of the dump plane was used as

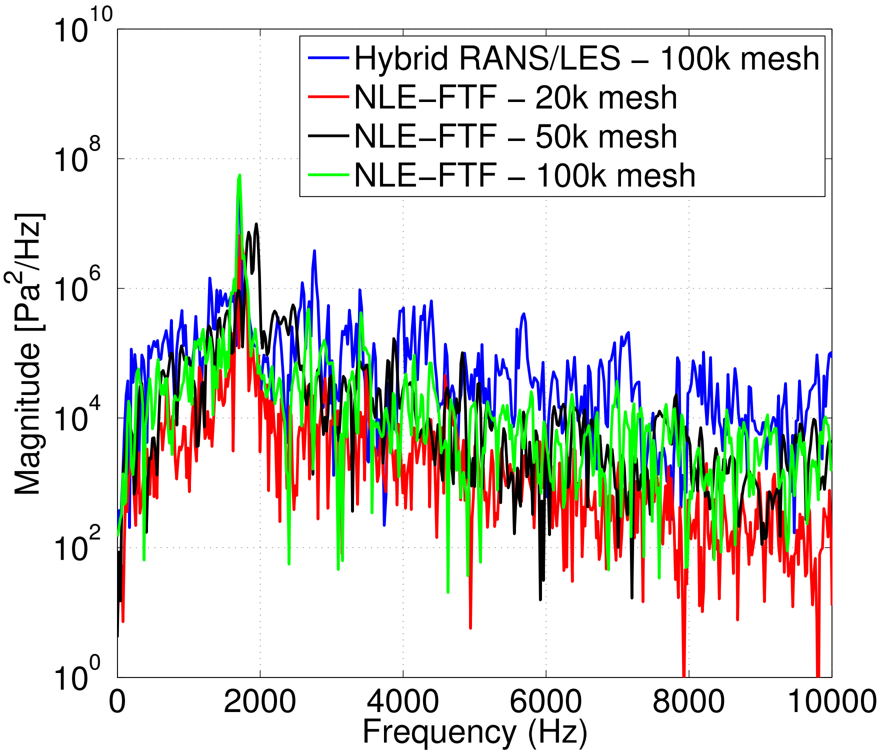

Fig. 5.13. Comparison of PSDs between NLE-FTF simulations with varying mesh size and hybrid RANS/LES simulation

the reference and only the first three dominant modes, 1700Hz, 2750Hz, and 3400 Hz were considered in the extraction of FTF. The gain and phase of the two dimensional point based distributed FTF is shown in Fig. 5.14.

One advantage of using FTFs based on the reference signal is that it eliminates the issues related to the presence of pressure nodes in the heat release zone, which were observed in two dimensional spatially resolved FTFs with 4 and 5 modes. However, the dependency of the heat release fluctuations of the entire combustor on the pressure signal at one particular location makes the approach vulnerable. The obtained FTFs were integrated with the NLE solver in the same way as outlined in section 3.1. The

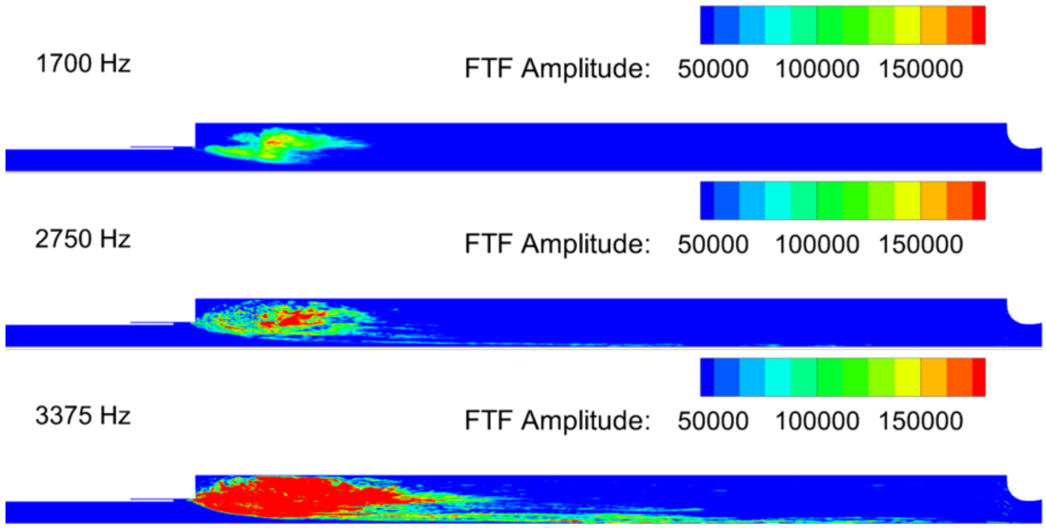

(a)

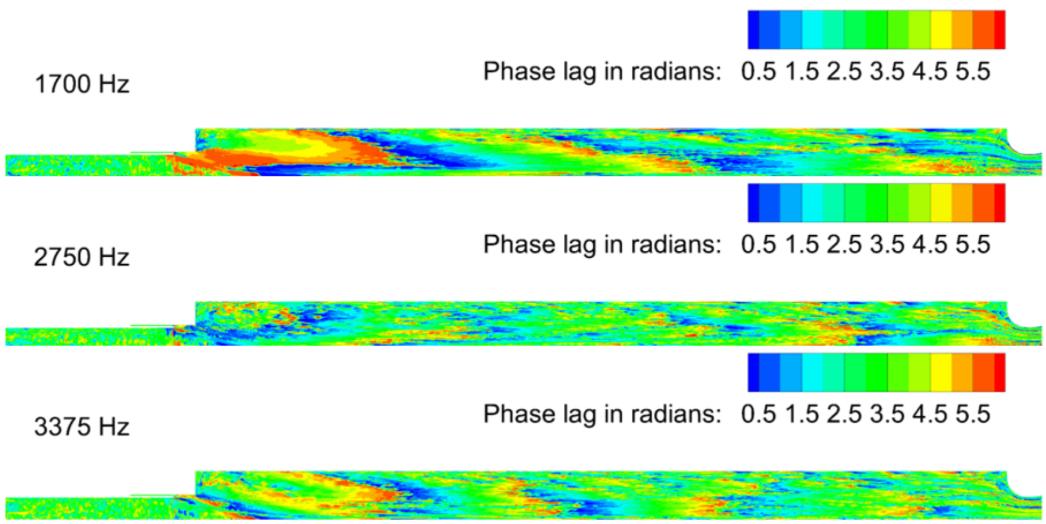

(b)

Fig. 5.14. The gain and phase of the first three modes of two dimensional reference point based FTF

pressure trace measured in the NLE-FTF simulation 0.368 m downstream of the dump plane is shown in Fig. 5.15.

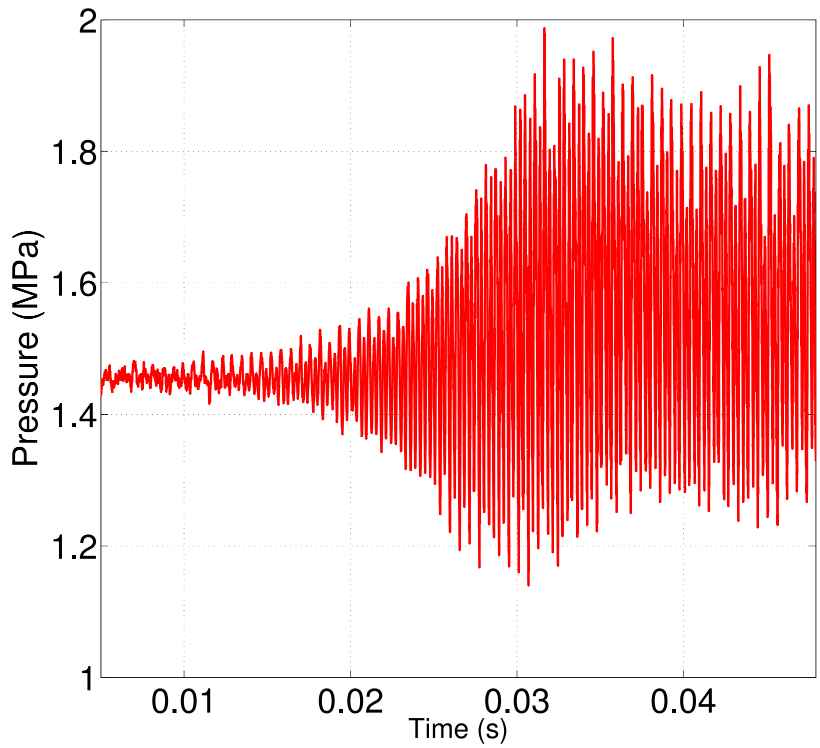

Fig. 5.15. The pressure signal measured 0.368 m downstream of the dump plane in NLE-FTF simulation with two- dimensional reference point based FTF

From the plot, it can be observed that the pressure fluctuations grew exponentially up to 40% of the mean pressure before the system reached a limit cycle with pressure fluctuations that are 30% of the mean pressure, far off the expected results. In contrast, the NLE-FTF simulation performed using two-dimensional spatially resolved FTF reached a limit cycle with pressure fluctuations 10.8% of the mean pressure, as shown in Fig. 4.19a, close to the p' predicted by reference hybrid RANS/LES simulation. A comparison of the limit cycle amplitudes and PSDs between the two dimensional point based FTF and reference hybrid RANS/LES simulation is shown in Fig. 5.16. The PSD and pressure trace comparison show that the NLE-FTF simulation with two dimensional point based FTF has resulted in a completely different system in comparison to the reference hybrid RANS/LES simulation. The instantaneous high heat release events in the rocket combustor may affect the local coupling between pressure and heat release fluctuations. Hence, the use of a reference pressure signal may not be able to accurately capture the coupling between pressure and heat release fluctuations, leading to results that are far off from the reference simulation. Hence, it is preferable to use spatially resolved FTFs based on local heat release and pressure for prediction of combustion instabilities in rocket combustors.

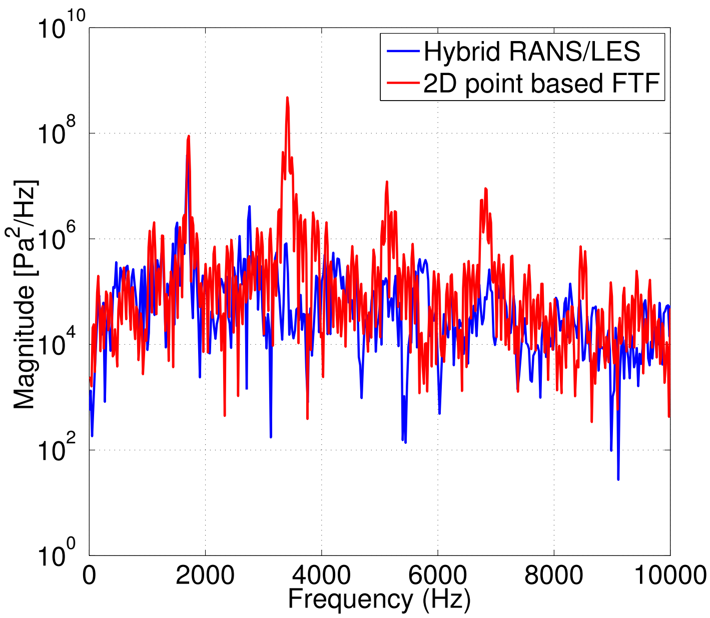

(a)

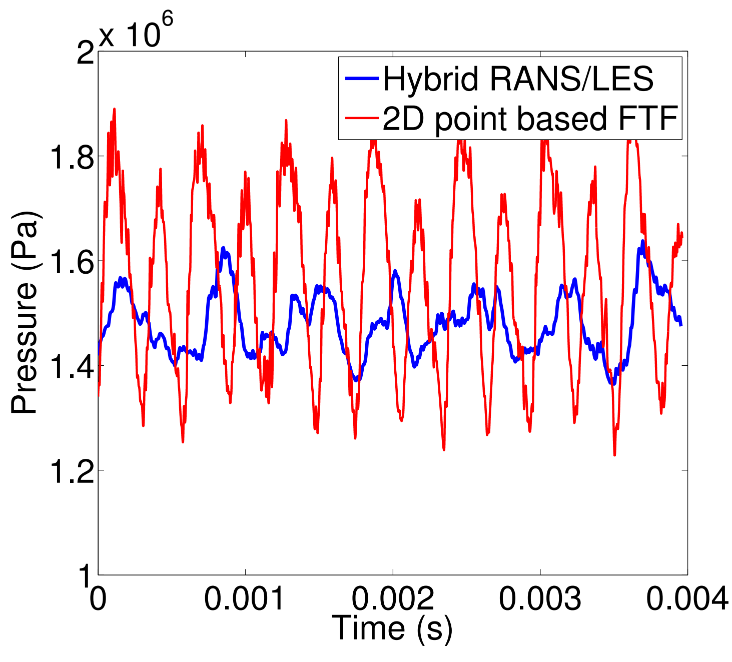

(b)

Fig. 5.16. Comparison of a) PSDs and b) pressure trace between the hybrid RANS/LES simulation and the NLE-FTF simulation with two-dimensional reference point based FTF

5.5 One dimensional spatially resolved local FTF

To understand the importance of accounting for two-dimensional effects, further analysis was performed using a one dimensional spatially distributed FTF. The one dimensional spatially distributed FTF was obtained by using spatially averaged (in radial direction) DMD modes of pressure and heat release. The gain and phase of the FTF were then calculated using local pressure and heat release fluctuations. For this study, the 3-mode FTF with the first three dominant modes, 1700 Hz, 2750 Hz and 3400 Hz was considered. The gain and phase of the one dimensional spatially distributed FTF is shown in Fig. 5.17. It can be seen that there is no variation of the gain and phase of the FTF in the radial direction for the one-dimensional FTFs. For this study, two dimensional axisymmetric NLE simulation was performed together with the one dimensional FTF.

A comparison of the pressure traces and PSDs between the hybrid RANS/LES simulation, the NLE-FTF simulation with two dimensional spatially resolved FTF (henceforth referred as 2D FTF simulation), and the NLE-FTF simulation with one dimensional spatially resolved FTF (henceforth referred as 1D FTF simulation) is shown in Fig. 5.18. In 1D FTF simulation, the limit cycle has peak-to-peak pressure fluctuations 14% of the mean pressure, 3% higher than those observed in the 2D FTF simulation. The PSDs show that the 1D FTF simulation has overestimated both the 1L and 2L modes. Also, the growth rate measured in the 1D FTF simulation is 39 1/s, much lower than the growth rate observed in the 2D local FTF simulations.

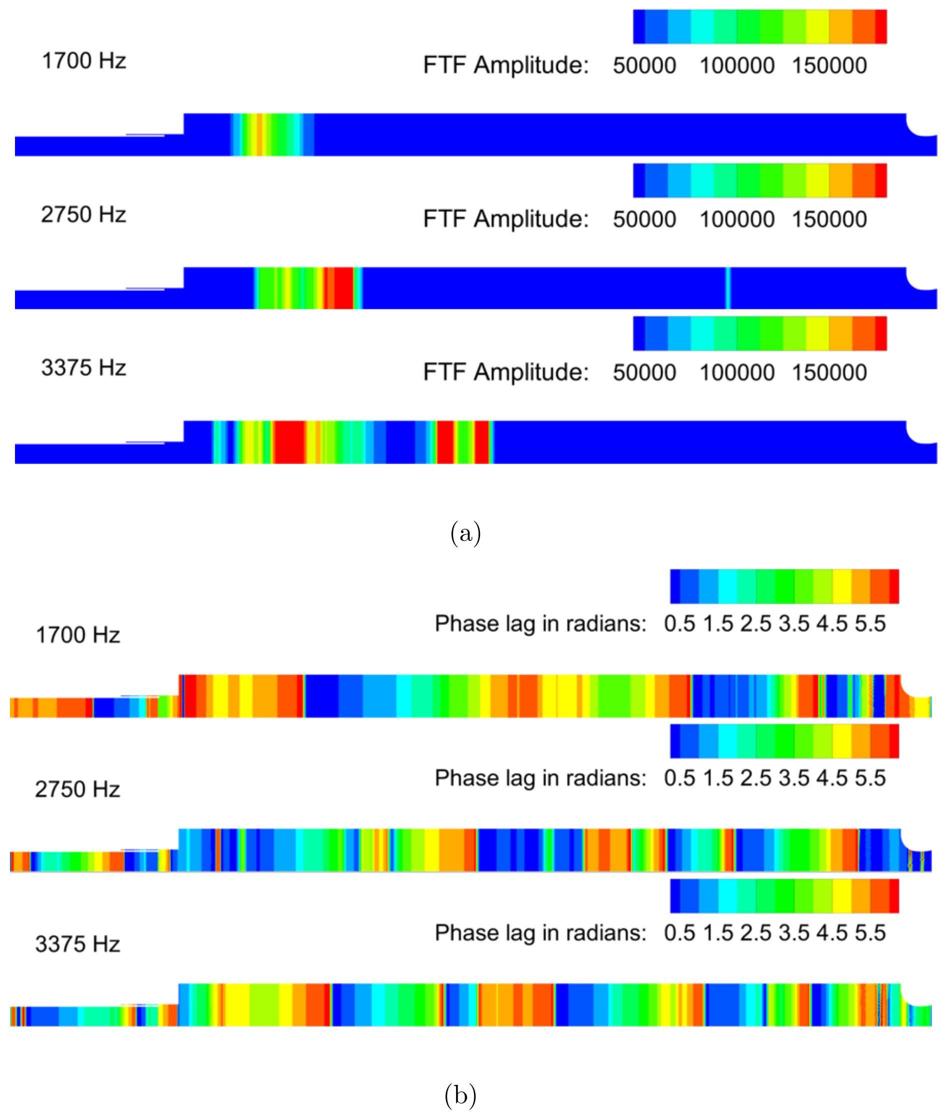

Fig. 5.17. The gain and phase of the first three modes of one-dimensional spatially resolved local FTF

Although no significant difference in the limit cycle amplitudes was observed between the 2D FTF and 1D FTF simulations, in both the simulations local gain and phase were used to calculate the corresponding heat release fluctuations and the simulations were performed using 2D NLE solver. Since the computational cost is same for both the 1D FTF and 2D FTF simulations and better agreement with the high-

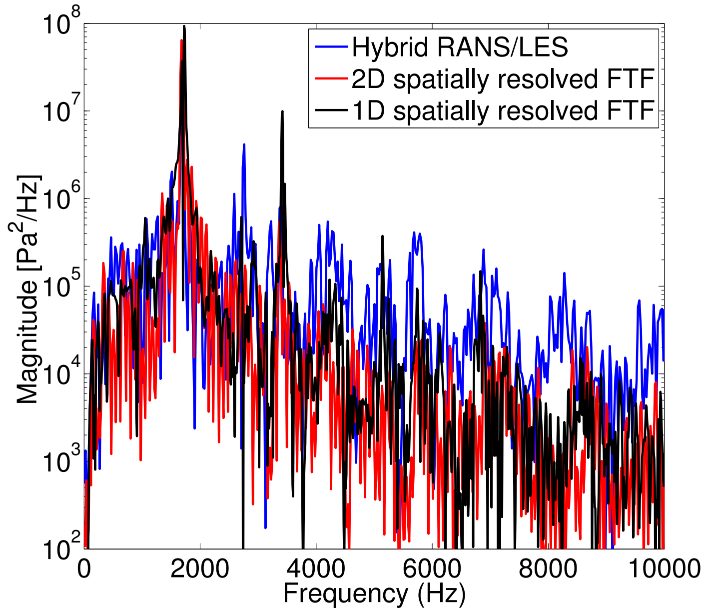

(a)

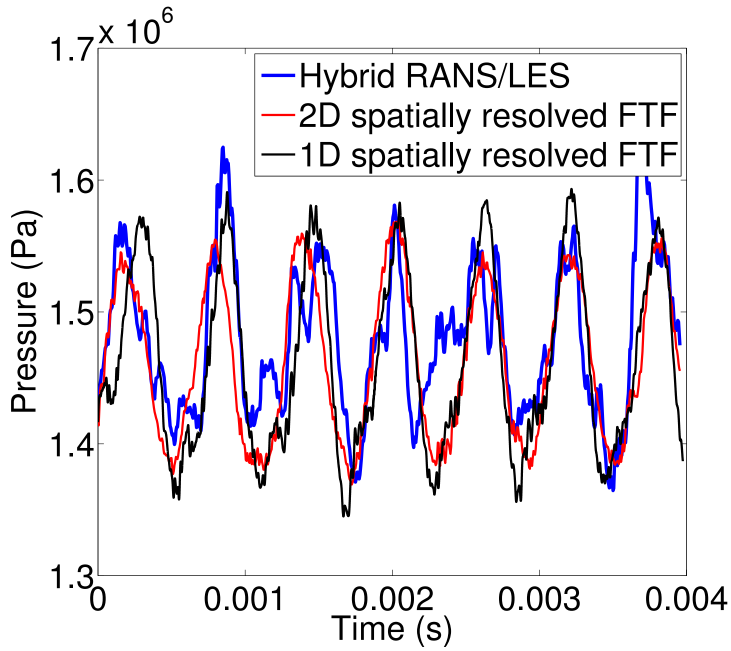

(b)

Fig. 5.18. A comparison of the a) PSDs and b) limit cycle pressure trace between the hybrid RANS/NLE simulation, the NLE-FTF simulation with two-dimensional spatially resolved local FTF, and the NLE-FTF simulation with one-dimensional spatially resolved local FTF

fidelity simulations was observed in case of 2D FTF simulations, it is preferable to use 2D FTF simulations for prediction of combustion instabilities in rocket combustors. The results obtained indicate that two dimensional spatially distributed local FTF simulations reproduced the combustion instabilities more accurately than the one dimensional FTF simulations and two dimensional point based FTF simulations.

5.6 Hybrid RANS/LES simulation with FTF

To evaluate the effects of viscosity, thermal conductivity and species diffusion on the results obtained, a hybrid RANS/LES simulation with 3-mode FTF was performed. This simulation was performed as outlined in section 3.1, in the same way as NLE-FTF simulation. A comparison of the pressure trace between the hybrid RANS/LES-FTF and NLE-FTF simulations with 3-mode FTF is shown in Fig. 5.19.

It was observed that the hybrid RANS/LES simulation exhibited limit cycle with peak-to-peak pressure fluctuations 2.5% of the mean pressure whereas the NLE-FTF simulation exhibited limit cycle with peak-to-peak pressure fluctuations 10.8% of the mean pressure. The hybrid RANS/LES-FTF simulation did not continue to grow to a high amplitude limit cycle unlike the NLE-FTF simulation. The comparison of pressure traces revealed that both the hybrid RANS/LES-FTF and NLE-FTF exhibited similar peak-to-peak amplitude for a certain duration (6ms-18ms), after which the NLE simulation grew to a limit cycle whereas the hybrid RANS/LES simulation continued to exhibit low amplitude limit cycle. A comparison of the PSDs for that duration (6ms-18ms), shown in Fig. 5.20 confirmed that both the simulations have

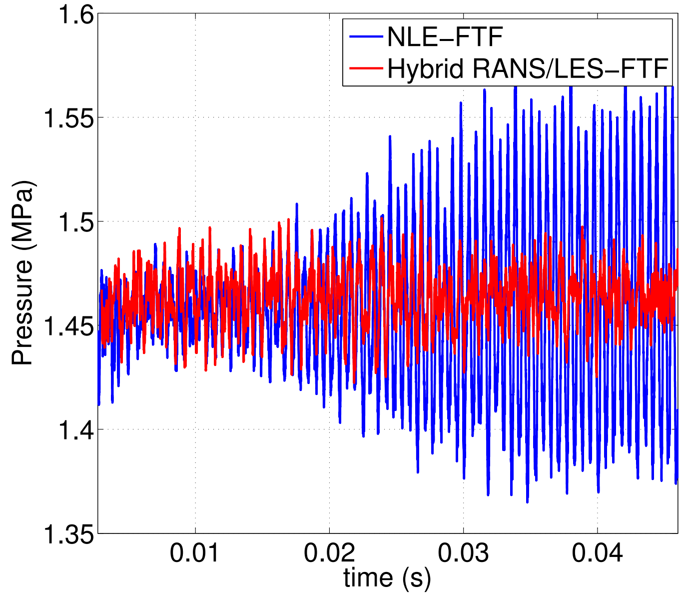

Fig. 5.19. Comparison of pressure traces between the NLE-FTF and hybrid RANS/LES-FTF simulation with 3-mode FTF

similar frequencies and magnitudes corresponding to the dominant modes (1700 Hz and 2750 Hz). These results indicate that the FTF imposed did not result in accurate gain that was necessary for the pressure fluctuations to grow in the hybrid RANS/LES-FTF simulation, whereas in the NLE-FTF simulation the gain imposed by the FTF was sufficient to make the pressure fluctuations to grow to a high amplitude limit cycle. The inclusion of viscosity, thermal conductivity and species diffusion effects appears to damp the pressure fluctuations to a certain extent and hence a higher gain of FTF might be necessary for the pressure fluctuations to grow. So, it might be necessary to use amplitude dependent FTF (FDF) to capture the growth of pressure fluctuations in the hybrid RANS/LES-FTF simulation. Further investi-

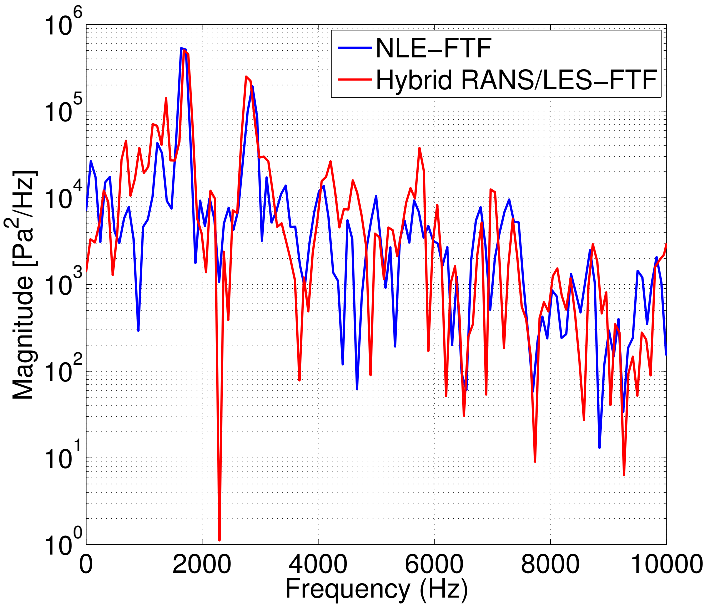

Fig. 5.20. Comparison of PSDs between the NLE-FTF and hybrid RANS/LES-FTF simulation with 3-mode FTF when both the simulations have exhibited similar p'

gation into the hybrid RANS/LES-FTF simulation is necessary to better understand the effects of viscosity, thermal conductivity and species diffusion.

6. SUMMARY AND CONCLUSIONS

In this chapter, the summary of the work done, and conclusions are presented. Further the recommendations for future work and the contribution of this thesis towards scientific community is also presented.

6.1 Summary

The work presented here centered on an exploration of the use of flame transfer functions together with the nonlinear Euler equations to reproduce the combustion instabilities in a model rocket combustor. The approach followed to extract the flame transfer functions and to integrate the flame transfer functions with nonlinear Euler equations was presented. The proposed approach was successfully verified using a horizontal Rijke tube test case and the results were presented. Further, the proposed approach was applied to the CVRC 0.089 m oxidizer post length cases and the results obtained were presented along the issues identified. The sensitivity of the reduced fidelity model to control parameters was studied and the results were presented.

In this thesis, the NLE solver was used as a reduced fidelity solver that uses two-dimensional spatially resolved local FTF as the combustion response function. The NLE solver is at the bottom of the list in terms of computational power requirements among the solvers that can solve for the mean flow and allow multi-dimensional modeling. Unlike acoustic solvers, NLE solver accounts for flow mixing (through numerical viscosity) that characterize the non-premixed flows and captures the steep fronted waves in addition to accounting for compressibility effects. Through this solver complicated geometries can be modeled and realistic boundaries (same boundary conditions as the high-fidelity simulations) can be simulated. The NLE solver also allows for modeling of transverse instability waves and rectangular chambers. However, the impact of the absent viscous terms on the performance of this model may need to be evaluated. The choice of a spatially resolved local FTF was made based on the fact that the flame in non-premixed combustor extends far into the chamber unlike the premixed flames which are compact. Also, in the system considered, the rocket combustors, in addition to high energy levels, the flame is erratic, detached and intermittent. This behavior of the flame can affect the local coupling between the heat release and pressure fluctuations and hence, a spatially distributed local FTF was used in this thesis.

The reference experiment used in this thesis, Continuously Variable Resonance Combustor (CVRC) is a single element model rocket combustor developed at Purdue University to study longitudinal combustion instabilities. This system is equipped with a movable oxidizer post whose length can be varied from 0.089 m to 0.1905 m either continuously during a test or fixed for a particular test. The stability behavior of the CVRC ranged from 8% to 40% when the oxidizer post length was changed from 0.089 m to 70.1905 m. Numerous tests of the CVRC revealed that this system exhibited a consistent and repeatable behavior of pressure oscillations that are 8% of the mean pressure when the oxidizer post length was fixed at 0.089 m. Hence this case of CVRC with 0.089 m oxidizer post length was chosen as the reference case. The high fidelity simulation of the same case, a two-dimensional axisymmetric hybrid RANS/LES simulation, was performed using an in-house solver GEMS. This simulation was performed using a mesh consisting of 100k nodes and a single step global chemistry. The high-fidelity simulation predicted limit cycle pressure oscillations on the order of 10.5% of the mean pressure. This high-fidelity reference simulation was used as the source to extract the data necessary to perform a reduced fidelity NLE-FTF simulation. Further, the Dynamic Mode Decomposition (DMD) was used in this thesis to extract the flame transfer functions. DMD was preferred for the work presented in thesis due to its capability to decompose the data based on the frequency content.

Flame transfer functions were extracted from the high fidelity simulations by applying DMD to the pressure and heat release fluctuations in the time domain to isolate frequency content. This is the first step in integrating the FTF and NLE solver. In the next step, the time averaged species destruction rates from the high fidelity simulation were imported to the NLE solver. In the NLE solver, the source term was split into the mean and fluctuating part. The mean source terms comprise of the time averaged species destruction rates from the hybrid RANS/LES simulation. In the final step, the FTF obtained in the first step was integrated with the NLE solver as the fluctuating source term of energy equation. The imported FTFs make use of the evolving pressure data of the NLE solver and calculate appropriate unsteady heat release.

The proposed approach was verified using a Rijke tube test case. The test case is a tube of length 0.5 m with a heat addition zone 0.125 m from the inlet of the tube. Crocco's n-τ model was used to generate the unsteady heat release fluctuations. This model allowed for accurate verification of the numerical aspects of the proposed approaches of FTF extraction and its integration with NLE solver. The results obtained revealed that the amplitude of the FTF extracted is equal to n imposed and the phase of the FTF is equal to the τ imposed. The obtained FTFs when integrated with the NLE solver were able to reproduce the mean variables and limit cycle statistics to a good extent verifying the proposed approaches.

Upon successful verification, the proposed approach was applied to the CVRC. During the initial runs, although the NLE-FTF simulation reached a limit cycle, non-physical temperature was observed close to the dump plane due to constant addition of mean heat without considering the local cell constituents. However, imposing a restriction on the mean heat based on the local cell constituents lead to pressure and temperature drop. This issue was corrected by following a variable gain approach which maintains correct amount of heat in the system while considering the local cell constituents. Through the variable gain approach, accurate mean conditions in the chamber were maintained and the NLE-FTF simulation was able to reproduce the limit cycle to a good extent. The pressure cycle analysis revealed that the NLE-FTF simulation was able to predict global pressure trends however it couldn't capture all the details of hybrid RANS/LES simulation. The fuel cycle analysis revealed that the NLE-FTF simulation was able to capture the fuel accumulation near the dump plane during the compression cycle and its destruction during the expansion cycle. However, the temperature cycle analysis revealed that the NLE-FTF simulation showed broader temperature range as expected because the unsteady heat release does not consider the local cell constituents.

The sensitivity of the model to the number of modes in the FTF, the number of sampling points used in the Fourier transform of unsteady heat release fluctuation and the mesh size was studied. For high frequency modes where there was significant heat addition at a pressure node, this approach resulted in numerical instability since the FTF was defined as the ratio of heat release fluctuations to pressure fluctuations. To eliminate this issue, the pressure modes were stretched at the location of pressure node. This resulted in a slight increase in the limit cycle amplitude of the NLE-FTF simulations. As the number of modes included in the FTF were increased, the limit cycle amplitudes of the NLE-FTF simulation approached the reference high-fidelity simulation. However, the 4- and 5- mode simulations showed slightly higher limit cycle amplitudes due to the aforementioned node issues. The NLE-FTF simulation was able to reproduce the high fidelity simulation to a good extent under the constraints of good spatial resolution and an FTF that includes all dominant modes up to at least one higher dominant frequency than the frequencies of interest. In addition to the limit cycle amplitudes, the NLE-FTF simulations were also able to reproduce the mode shapes and linear growth rates observed in the experiment. Further analysis using a point based two-dimensional FTF resulted in higher limit cycle amplitudes revealing that it is necessary to account for local coupling between the heat release and pressure fluctuations. Also, the simulation with one-dimensional local FTF resulted in higher limit cycle amplitudes and lower growth rates indicating that the two dimensional effects are important. Hybrid RANS/LES-FTF simulation of the CVRC revealed that it might be necessary to use Flame Describing Function (FDF) to capture the growth of pressure fluctuations to limit cycle when Navier-Stokes solver is used.

6.2 Conclusion

A reduced fidelity model that solves the nonlinear Euler equations together with a two-dimensional spatially distributed multi-mode flame transfer functions obtained from high-fidelity hybrid RANS/LES simulation was used to predict combustion instabilities in a model rocket combustor exhibiting self-excited instabilities. The methodology for extraction of the flame transfer functions from high-fidelity simulations and their integration with nonlinear Euler equations is detailed. Spatially distributed flame transfer functions corresponding to the strongest modes apparent in the pressure and/or heat release spectra were extracted from the high-fidelity simulation using DMD. The unsteady heat release was added as a source term in the nonlinear Euler solver. The approach was successfully verified using a Rijke tube test case, and then applied to the CVRC to assess the capability of the reduced fidelity model to reproduce the high fidelity simulation behavior. The mean pressure and the limit cycle amplitude of pressure fluctuations predicted by the reduced fidelity model were in close agreement with the reference high fidelity simulation. The cycle analysis revealed that the reduced fidelity model captured the global pressure trends and periodic combustion behavior.

To better understand the effects of control parameters of the reduced fidelity model, a sensitivity analysis was performed by varying the number of modes in the flame transfer function, the number of sampling points used to calculate the unsteady heat release, and the mesh size. The sensitivity analysis showed that the reduced fidelity model could reproduce the limit cycle amplitude predicted by the high fidelity simulation very closely, with deviations within 2% of the mean pressure, when good spatial constrain was applied together with a flame transfer function that contains unsteady heat release information at frequencies at least one mode higher than the frequencies of interest. The reduced fidelity model was also able to reproduce the mode shapes. The reduced fidelity model also showed linear growth prior to the limit cycle, with predicted growth rates in good agreement with experimental growth rates. However, this somewhat surprising result should be further investigated. Analysis of two-dimensional effects and coupling between the local pressure and heat release fluctuations showed that it may be necessary to use two-dimensional spatially distributed local FTFs for accurate prediction of combustion instabilities in high energy devices such as rocket combustors. To understand the importance of viscosity, thermal conductivity and species diffusion, which were neglected in the NLE-FTF simulation, a hybrid RANS/LES-FTF simulation was performed. The results revealed that it might be necessary to use the FDF to capture the growth of pressure fluctuations to high amplitude limit cycle in the hybrid RANS/LES-FTF simulation. Using FTF together with hybrid RANS/LES resulted in low amplitude limit cycle. Further investigation is necessary to better understand the effects of the viscosity, thermal conductivity and species diffusion.

The results suggest the reduced fidelity model, nonlinear Euler solver together with spatially distributed local FTF, may be able to predict the behavior of weakly nonlinear combustion instabilities. For more nonlinear behavior, amplitude-dependent flame describing functions may be necessary. Important next steps in proving the generality and utility of this approach include its application to transverse instabilities, and a combustor with multiple elements.

6.3 Future Work

The work done through this thesis is only the first step towards developing reduced fidelity tool for combustion instability prediction. In this thesis, only the capability of the proposed model to reproduce the high-fidelity simulation was evaluated. Further steps towards the final goal include evaluation of the capability of the proposed model to reproduce the multi-element transverse instability chamber, to predict an unknown longitudinal instability chamber and finally to predict an unknown multi-element transverse instability chamber. Also, instead of using 2D axisymmetric hybrid RANS/LES simulation as the reference high fidelity simulation, a 3D DES simulation should be used since the physics of turbulent flows may not be accurately captured by the 2D axisymmetric simulation. The advantage of the proposed approach over flamelet model based simulations needs to be evaluated.

To evaluate the capability of the reduced fidelity model to reproduce the multi-element transverse instability chamber, first the multi-element system that exhibits pressure oscillations around 10% of the mean pressure needs to be identified. Then, similar to the CVRC case, reduced fidelity simulation should be performed by extracting the flame transfer functions from high-fidelity simulations and integrating them with the nonlinear solver. However, the node issue observed in the CVRC reduced fidelity simulations with high frequency modes, may cause issues in the multi-element reduced fidelity simulation even with the first few dominant modes. In case of multi-element simulation, the heat release is spread across the chamber and there is a greater possibility to have non-collocated pressure and heat release nodes. Similar to the CVRC simulation, mode stretching near the nodes can be applied as an initial correction step to check the effect of the correction. However, a detailed study needs to be performed to evaluate the effect of extent of mode stretching. Another approach to solve this issue is to formulate the FTF based on two independent variables so that in the vicinity of the node of one variable, FTF can be defined based on the other variable. However, it would require utmost care in identifying and extracting the FTFs from the independent variables. If the variables are dependent, then there is a chance the effects of variables on the FTF may be double counted. While performing this work, it would be interesting to evaluate the effect of the input FTF, i.e., the behavior of the reduced fidelity model when FTFs corresponding to 1-, 2-, and 3-injector element sets were used as the FTFs for all other elements. This will help obtain information on the minimum number of injector elements that needs to be modeled in the high fidelity simulation.

Further, the capability of the reduced fidelity model to predict the behavior of an unknown single element longitudinal chamber must be evaluated. To do this, the FTFs corresponding to a wide range of frequencies must be extracted. For this study, the CVRC 0.089 m oxidizer post length case can be treated as an unknown system. To extract the FTFs at different frequencies, high-fidelity simulations can be performed by adjusting the chamber length. However, this may result in varying instability levels. Hence, high-fidelity simulations may be performed by using an upstream forcing together with non-reflecting boundary condition and a sponge zone at the downstream end. While performing this study it would be interesting to study the effects of FTFs at varying amplitude, i.e., the FDF, on the predictive capability of the reduced fidelity model.

The evaluation of the reduced fidelity model to predict the behavior of an unknown multi-element chamber is the final goal of this work. At this point, to perform this simulation, there are several questions that needs to be answered first. What is the effect of FDF on the prediction of NLE-FTF simulation? How to perturb a transverse system to obtain FTFs at varying frequencies and amplitudes? How many injector elements must be modeled to extract the FTF? All these questions must be answered while performing the above two tasks.

The contribution of this thesis to the scientific body is an exploration of a pathway towards a computational tool capable of accurately predicting the combustion instabilities in practical systems through the use of reduced fidelity nonlinear Euler equations and spatially distributed two-dimensional local flame transfer functions. This thesis defined the limitations associated with the combination of non-premixed flames, flame transfer functions, and the nonlinear Euler equations, necessary for further investigations and development of the computational tool.

REFERENCES

REFERENCES

[1] L. Rayleigh, "The explanation of certain acoustical phenomena," *Nature*, vol. 18, pp. 319–321, July 1878. [Online]. Available: http://www.nature.com/nature/journal/v18/n455/pdf/018319a0.pdf

[2] L. Crocco and S.-I. Cheng, "Theory of combustion instability in liquid propellant rocket motors," PRINCETON UNIV NJ, Tech. Rep., 1956.

[3] W. E. Anderson and V. Yang, "Liquid rocket engine combustion instability," *Progress in Astronautics and Aeronautics*, 1995.

[4] P. L. Rijke, "Notiz ber eine neie art, die luft in einer an beiden enden offenen rhre in schwingungen zu versetzen," *Annalender Physik*, vol. 107, p. 339343, 1859.

[5] J. C. Oefelein and V. Yang, "Comprehensive review of liquid-propellant combustion instabilities in f-1 engines," *Journal of Propulsion and Power*, vol. 9, no. 5, pp. 657–677, 1993.

[6] S. Candel, D. Durox, S. Ducruix, A.-L. Birbaud, N. Noiray, and T. Schuller, "Flame dynamics and combustion noise: progress and challenges," *International Journal of Aeroacoustics*, vol. 8, no. 1, pp. 1–56, 2009.

[7] A. P. Dowling, "The challenges of lean premixed combustion," in *Proc. international gas turbine Congress.* Citeseer, 2003.

[8] Z. Ibrahim, F. Williams, and S. Buckley, "A review of previous studies of oscillatory combustion in gas turbines," *University of California–Progress Report, San Diego*, 2005.

[9] J. Fang, "Application of combustion time-lag theory to combustion stability analysis of liquid and gaseous propellant rocket engines," in *22nd Aerospace Sciences Meeting*, 1984, p. 510.

[10] P. Langhorne, "Reheat buzz: an acoustically coupled combustion instability. part 1. experiment," *Journal of Fluid Mechanics*, vol. 193, pp. 417–443, 1988.

[11] H. U. Wisniowski, "Prevention of screeching combustion in jet engines," Mar. 8 1960, uS Patent 2,927,423.

[12] M. Barrere and F. Williams, "Comparison of combustion instabilities found in various types of combustion chambers," in *Symposium (International) on Combustion*, vol. 12, no. 1. Elsevier, 1969, pp. 169–181.

[13] S. M. Candel, "Combustion instabilities coupled by pressure waves and their active control," in *Symposium (International) on Combustion*, vol. 24, no. 1. Elsevier, 1992, pp. 1277–1296.

[14] L. Crocco, “Aspects of combustion stability in liquid propellant rocket motors part i: fundamentals. low frequency instability with monopropellants,” *Journal of the American Rocket Society*, vol. 21, no. 6, pp. 163–178, 1951.

[15] L. . Crocco, “Aspects of combustion stability in liquid propellant rocket motors part ii: Low frequency instability with bipropellants high frequency instability,” *Journal of the American Rocket Society*, vol. 22, no. 1, pp. 7–16, 1952.

[16] E. Zukoski, “Combustion instability sustained by unsteady vortex combustion,” in *21st Joint Propulsion Conference*, 1985, p. 1248.

[17] T. J. Poinsot, A. C. Trouve, D. P. Veynante, S. M. Candel, and E. J. Esposito, “Vortex-driven acoustically coupled combustion instabilities,” *Journal of fluid mechanics*, vol. 177, pp. 265–292, 1987.

[18] L. Baker Jr and F. W. Steffen, “Screaming tendency of the gaseous-hydrogen-liquid-oxygen propellant combination,” 1958.

[19] J. Hulka and J. J. Hutt, “Instability phenomena in liquid oxygen/hydrogen propellant rocket engines,” *Liquid rocket engine combustion instability*, vol. 169, pp. 39–72, 1995.

[20] M. Rocker and T. E. Nesman, “Elimination of high-frequency combustion instability in the fastrac engine thrust chamber,” 1998.

[21] B. Pomeroy, N. Nugent, and W. Anderson, “Measuring transverse stability combustion response at full scale frequencies in a subscale combustor,” in *46th AIAA/ASME/SAE/ASEE Joint Propulsion Conference & Exhibit*, 2010, p. 7146.

[22] Y. Yu, J. C. Sisco, S. Rosen, A. Madhav, and W. E. Anderson, “Spontaneous longitudinal combustion instability in a continuously-variable resonance combustor,” *Journal of Propulsion and Power*, vol. 28, no. 5, pp. 876–887, 2012.

[23] S. Gröning, J. S. Hardi, D. Suslov, and M. Oschwald, “Injector-driven combustion instabilities in a hydrogen/oxygen rocket combustor,” *Journal of Propulsion and Power*, no. 0, pp. 560–573, 2016.

[24] K. Kailasanath, J. Gardner, J. Boris, and E. Oran, “Numerical simulations of acoustic-vortex interactions in a central-dump ramjet combustor,” *Journal of Propulsion and Power*, vol. 3, no. 6, pp. 525–533, 1987.

[25] K. Schadow, E. Gutmark, T. Parr, D. Parr, K. Wilson, and J. Crump, “Large-scale coherent structures as drivers of combustion instability,” *Combustion science and technology*, vol. 64, no. 4-6, pp. 167–186, 1989.

[26] Y. Huang and V. Yang, “Effect of swirl on combustion dynamics in a lean-premixed swirl-stabilized combustor,” *Proceedings of the Combustion Institute*, vol. 30, no. 2, pp. 1775–1782, 2005.

[27] B. Franzelli, E. Riber, L. Y. Gicquel, and T. Poinsot, “Large eddy simulation of combustion instabilities in a lean partially premixed swirled flame,” *Combustion and flame*, vol. 159, no. 2, pp. 621–637, 2012.

[28] M. E. Harvazinski, C. Huang, V. Sankaran, T. Feldman, W. Anderson, C. Merkle, and D. G. Talley, "Combustion instability mechanisms in a pressure-coupled gas-gas coaxial rocket injector," in *49th AIAA/ASME/SAE/ASEE Joint Propulsion-Conference*, 2013, p. 3990.

[29] S. V. Sardeshmukh, S. D. Heister, and W. E. Anderson, "Prediction of combustion instability with detailed chemical kinetics," in *53rd AIAA Aerospace Sciences Meeting*, 2015, p. 1826.

[30] T. Schmitt, G. Staffelbach, S. Ducruix, S. Gröning, J. Hardi, and M. Oschwald, "Large-eddy simulations of a sub-scale liquid rocket combustor: influence of fuel injection temperature on thermo-acoustic stability," in *7th European Conference for Aeronautics ad Aerospace Sciences (EUCASS), July, Milan, Italy*, 2017.

[31] P. Tucker, S. Menon, C. Merkle, J. Oefelein, and V. Yang, "Validation of high-fidelity cfd simulations for rocket injector design," in *44th AIAA/ASME/SAE/ASEE Joint Propulsion Conference & Exhibit*, 2008, p. 5226.

[32] S. J. Brookes, R. S. Cant, I. D. Dupere, and A. P. Dowling, "Computational modelling of self-excited combustion instabilities," in *ASME Turbo Expo 2000: Power for Land, Sea, and Air*. American Society of Mechanical Engineers, 2000, pp. V002T02A024–V002T02A024.

[33] C. Angelberger, D. Veynante, and F. Egolfopoulos, "Les of chemical and acoustic forcing of a premixed dump combustor," *Flow, Turbulence and Combustion*, vol. 65, no. 2, pp. 205–222, 2000.

[34] Y. Huang, H.-G. Sung, S.-Y. Hsieh, and V. Yang, "Large-eddy simulation of combustion dynamics of lean-premixed swirl-stabilized combustor," *Journal of Propulsion and Power*, vol. 19, no. 5, pp. 782–794, 2003.

[35] K. Shipley, "Multi-injector modeling of transverse combustion instability experiments," Master's thesis, Purdue University, 2014.

[36] Y. Yu, L. O'Hara, R. Smith, W. Anderson, and C. Merkle, "Integrated method for combustion stability prediction," *Progress in Propulsion Physics*, vol. 2, pp. 297–316, 2011.

[37] A. P. Dowling, "The calculation of thermoacoustic oscillations," *Journal of sound and vibration*, vol. 180, no. 4, pp. 557–581, 1995.

[38] F. E. Culick and V. Yang, "Overview of combustion instabilities in liquid-propellant rocket engines," *Liquid Rocket Engine Combustion Instability*, vol. 169, pp. 3–37, 1995.

[39] F. Culick, "Some recent results for nonlinear acoustics in combustion chambers," *AIAA journal*, vol. 32, no. 1, pp. 146–169, 1994.

[40] B. Zinn, "A theoretical study of nonlinear combustion instability in liquid-propellant rocket engines." *AIAA journal*, vol. 6, no. 10, pp. 1966–1972, 1968.

[41] B. T. Zinn and M. E. LORES, "Application of the galerkin method in the solution of non-linear axial combustion instability problems in liquid rockets," *Combustion Science and Technology*, vol. 4, no. 1, pp. 269–278, 1971.

[42] T. Poinsot and S. M. Candel, “A nonlinear model for ducted flame combustion instabilities,” *Combustion science and technology*, vol. 61, no. 4-6, pp. 121–153, 1988.

[43] A. P. Dowling and S. R. Stow, “Acoustic analysis of gas turbine combustors,” *Journal of propulsion and power*, vol. 19, no. 5, pp. 751–764, 2003.

[44] B. B. Schuermans, W. Polifke, and C. O. Paschereit, “Modeling transfer matrices of premixed flames and comparison with experimental results,” in *ASME 1999 International Gas Turbine and Aeroengine Congress and Exhibition*. American Society of Mechanical Engineers, 1999, pp. V002T02A024–V002T02A024.

[45] B. B. Schuermans, W. Polifke, C. O. Paschereit, and J. H. van der Linden, “Prediction of acoustic pressure spectra in combustion systems using swirl stabilized gas turbine burners,” in *ASME Turbo Expo 2000: Power for Land, Sea, and Air*. American Society of Mechanical Engineers, 2000, pp. V002T02A025–V002T02A025.

[46] H. Merk, “An analysis of unstable combustion of premixed gases,” in *Symposium (International) on Combustion*, vol. 6, no. 1. Elsevier, 1957, pp. 500–512.

[47] T. Lieuwen, “Modeling premixed combustion-acoustic wave interactions: A review,” *Journal of propulsion and power*, vol. 19, no. 5, pp. 765–781, 2003.

[48] A. Giauque, L. SELLE, L. Gicquel, T. Poinsot, H. Buechner, P. Kaufmann, and W. Krebs, “System identification of a large-scale swirled partially premixed combustor using les and measurements,” *Journal of Turbulence*, no. 6, p. N21, 2005.

[49] R. Balachandran, B. Ayoola, C. Kaminski, A. Dowling, and E. Mastorakos, “Experimental investigation of the nonlinear response of turbulent premixed flames to imposed inlet velocity oscillations,” *Combustion and Flame*, vol. 143, no. 1-2, pp. 37–55, 2005.

[50] A.-L. Birbaud, D. Durox, S. Ducruix, and S. Candel, “Dynamics of confined premixed flames submitted to upstream acoustic modulations,” *Proceedings of the Combustion Institute*, vol. 31, no. 1, pp. 1257–1265, 2007.

[51] R. Kaess, R. Koeglmeiner, R. Behr, and J. Rochhi, “Liquid propellant rocket combustion stability evaluation using singe flame calculations for combustion dynamics,” in *International Symposium on Thermoacoustic Instabilities in Gas Turbines and Rocket Engines, Munich*, 2016.

[52] M. L. Frezzotti, S. DAlessandro, B. Favini, and F. Nasuti, “Numerical issues in modeling combustion instability by quasi-1d euler equations,” *International Journal of Spray and Combustion Dynamics*, vol. 9, no. 4, pp. 349–366, 2017.

[53] F. Duchaine and T. Poinsot, “Sensitivity of flame transfer functions of laminar flames,” in *Proceedings of the Summer Program*, 2010, p. 251.

[54] T. Schuller, D. Durox, and S. Candel, “A unified model for the prediction of laminar flame transfer functions: comparisons between conical and v-flame dynamics,” *Combustion and Flame*, vol. 134, no. 1-2, pp. 21–34, 2003.

[55] C. F. Silva, M. Merk, T. Komarek, and W. Polifke, "The contribution of intrinsic thermoacoustic feedback to combustion noise and resonances of a confined turbulent premixed flame," *Combustion and Flame*, vol. 182, pp. 269–278, 2017.

[56] S. H. Preetham and T. C. Lieuwen, "Response of turbulent premixed flames to harmonic acoustic forcing," *Proceedings of the Combustion Institute*, vol. 31, no. 1, pp. 1427–1434, 2007.

[57] L. Selle, G. Lartigue, T. Poinsot, R. Koch, K.-U. Schildmacher, W. Krebs, B. Prade, P. Kaufmann, and D. Veynante, "Compressible large eddy simulation of turbulent combustion in complex geometry on unstructured meshes," *Combustion and Flame*, vol. 137, no. 4, pp. 489–505, 2004.

[58] K. Truffin and T. Poinsot, "Comparison and extension of methods for acoustic identification of burners," *Combustion and Flame*, vol. 142, no. 4, pp. 388–400, 2005.

[59] T. Lieuwen and Y. Neumeier, "Nonlinear pressure-heat release transfer function measurements in a premixed combustor," *Proceedings of the Combustion Institute*, vol. 29, no. 1, pp. 99–105, 2002.

[60] R. Wang and R. Roncen, "On lean premixed combustion instabilities in a backward-facing step combustor," in *International Symposium on Thermoacoustic Instabilities in Gas Turbines and Rocket Engines, Munich*, 2016.

[61] D. Kim, J. G. Lee, B. D. Quay, D. A. Santavicca, K. Kim, and S. Srinivasan, "Effect of flame structure on the flame transfer function in a premixed gas turbine combustor," *Journal of Engineering for Gas Turbines and Power*, vol. 132, no. 2, p. 021502, 2010.

[62] Paschereit, A. Saurabh, and C. Oliver, "Comparison of flame response to axial transverse (symmetric) forcing," in *International Symposium on Thermoacoustic Instabilities in Gas Turbines and Rocket Engines, Munich*, 2016.

[63] A. Scarpato, L. Zander, R. Kulkarni, and B. Schuermans, "Identification of multiparameter flame transfer function for a reheat combustor," in *ASME Turbo Expo 2016: Turbomachinery Technical Conference and Exposition*. American Society of Mechanical Engineers, 2016, pp. V04BT04A038–V04BT04A038.

[64] D. Larea, K. Prieur, D. Durox, T. Schuller, S. M. Camporeale, and S. Candel, "Flame describing function analysis of standing modes in an annular combustor and comparison with experiments," in *International Symposium on Thermoacoustic Instabilities in Gas Turbines and Rocket Engines: Industry meets Academia, TUM, Garching, Germany*, 2016.

[65] N. Noiray, D. Durox, T. Schuller, and S. Candel, "A unified framework for nonlinear combustion instability analysis based on the flame describing function," *Journal of Fluid Mechanics*, vol. 615, pp. 139–167, 2008.

[66] C. Paschereit, B. Schuermans, and P. Monkewitz, "Non-linear combustion instabilities in annular gas-turbine combustors," in *44th AIAA aerospace sciences meeting and exhibit*, 2006, p. 549.

[67] K. T. Kim, J. G. Lee, B. Quay, and D. Santavicca, "Spatially distributed flame transfer functions for predicting combustion dynamics in lean premixed gas turbine combustors," *Combustion and Flame*, vol. 157, no. 9, pp. 1718–1730, 2010.

[68] V. Kornilov, R. Rook, J. ten Thije Boonkkamp, and L. De Goey, "Experimental and numerical investigation of the acoustic response of multi-slit bunsen burners," *Combustion and Flame*, vol. 156, no. 10, pp. 1957–1970, 2009.

[69] R. Kaess, W. Polifke, T. Poinsot, N. Noiray, D. Durox, T. Schuller, and S. Candel, "Cfd-based mapping of the thermo-acoustic stability of a laminar premix burner," in *Proc. of the summer program.* Citeseer, 2008, pp. 289–302.

[70] L. T. W. Chong, T. Komarek, R. Kaess, S. Foller, and W. Polifke, "Identification of flame transfer functions from les of a premixed swirl burner," in *ASME turbo expo 2010: power for land, sea, and air.* American Society of Mechanical Engineers, 2010, pp. 623–635.

[71] F. Boudy, D. Durox, T. Schuller, G. Jomaas, and S. Candel, "Describing function analysis of limit cycles in a multiple flame combustor," *Journal of Engineering for Gas Turbines and Power*, vol. 133, no. 6, p. 061502, 2011.

[72] X. Han, J. Li, and A. S. Morgans, "Prediction of combustion instability limit cycle oscillations by combining flame describing function simulations with a thermoacoustic network model," *Combustion and Flame*, vol. 162, no. 10, pp. 3632–3647, 2015.

[73] G. M. R. Tamanampudi and W. E. Anderson, "Development of combustion instability analysis tool by incorporating combustion response models," in *51st AIAA/SAE/ASEE Joint Propulsion Conference*, 2015, p. 4165.

[74] M. Gonzalez-Flesca, P. Scouflaire, T. Schmitt, S. Ducruix, S. Candel, and Y. Méry, "Reduced order modeling approach to combustion instabilities of liquid rocket engines," *AIAA Journal*, vol. 56, no. 12, pp. 4845–4857, 2018.

[75] C. Huang, W. E. Anderson, M. E. Harvazinski, and V. Sankaran, "Analysis of self-excited combustion instabilities using decomposition techniques," *AIAA Journal*, pp. 2791–2807, 2016.

[76] R. Garby, L. Selle, and T. Poinsot, "Large-eddy simulation of combustion instabilities in a variable-length combustor," *Comptes Rendus Mécanique*, vol. 341, no. 1-2, pp. 220–229, 2013.

[77] P. J. Schmid, "Dynamic mode decomposition of numerical and experimental data," *Journal of fluid mechanics*, vol. 656, pp. 5–28, 2010.

[78] K. Miller, J. Sisco, N. Nugent, and W. Anderson, "Combustion instability with a single-element swirl injector," *Journal of Propulsion and Power*, vol. 23, no. 5, pp. 1102–1112, 2007.

[79] J. C. Sisco, Y. Yu, V. Sankaran, and W. E. Anderson, "Examination of mode shapes in an unstable model combustor," *Journal of Sound and Vibration*, vol. 330, no. 1, pp. 61–74, 2011.

[80] S. C. Rosen, "Combustion instabilities in the transition region of an unstable model rocket combustor," Ph.D. dissertation, Purdue University, 2011.

[81] M. E. Harvazinski, W. E. Anderson, and C. L. Merkle, "Analysis of self-excited combustion instabilities using two-and three-dimensional simulations," *Journal of Propulsion and Power*, vol. 29, no. 2, pp. 396–409, 2013.

[82] A. R. Madhav, "Efficacy of a nonlinear acoustic model for combustion stability prediction," Ph.D. dissertation, Purdue University, 2011.

[83] R. Garby, "Simulations of flame stabilization and stability in high-pressure propulsion systems," Ph.D. dissertation, INPT, 2013.

[84] L. Selle, R. Blouquin, M. Théron, L.-H. Dorey, M. Schmid, and W. Anderson, "Prediction and analysis of combustion instabilities in a model rocket engine," *Journal of Propulsion and Power*, vol. 30, no. 4, pp. 978–990, 2014.

[85] S. Srinivasan, R. Ranjan, and S. Menon, "Flame dynamics during combustion instability in a high-pressure, shear-coaxial injector combustor," *Flow, Turbulence and Combustion*, vol. 94, no. 1, pp. 237–262, 2015.

[86] M. E. Harvazinski, D. G. Talley, and V. Sankaran, "Influence of boundary condition treatment on longitudinal mode combustion instability predictions," in *49th AIAA/ASME/SAE/ASEE Joint PropulsionConference*, 2013, p. 3994.

[87] M. E. Harvazinski, "Modeling self-excited combustion instabilities using a combination of two-and three-dimensional simulations," Ph.D. dissertation, Purdue University, 2012.

[88] G. Berkooz, P. Holmes, and J. L. Lumley, "The proper orthogonal decomposition in the analysis of turbulent flows," *Annual review of fluid mechanics*, vol. 25, no. 1, pp. 539–575, 1993.

[89] A. Chatterjee, "An introduction to the proper orthogonal decomposition," *Current science*, pp. 808–817, 2000.

[90] J. Hardi, W. Z. Hallum, C. Huang, and W. E. Anderson, "Development of validation approaches for numerical simulation of combustion instability using flame imaging," in *50th AIAA/ASME/SAE/ASEE Joint Propulsion Conference*, 2014, p. 3775.

[91] C. Huang, "Fundamental insights into combustion instability predictions in aerospace propulsion," Ph.D. dissertation, Purdue University, 2015.

[92] C. Huang, K. Duraisamy, and C. Merkle, "Challenges in reduced order modeling of reacting flows," in *2018 Joint Propulsion Conference*, 2018, p. 4675.

[93] G. M. R. Tamanampudi, "Reduced order modeling and analysis of combustion instabilities," Master's thesis, 2015.

[94] B. D. Bellows, Y. Neumeier, and T. Lieuwen, "Forced response of a swirling, premixed flame to flow disturbances," *Journal of propulsion and power*, vol. 22, no. 5, pp. 1075–1084, 2006.

[95] D. You, Y. Huang, and V. Yang, "A generalized model of acoustic response of turbulent premixed flame and its application to gas-turbine combustion instability analysis," *Combustion Science and Technology*, vol. 177, no. 5-6, pp. 1109–1150, 2005.

[96] K. I. Matveev, "Thermoacoustic instabilities in the rijke tube: experiments and modeling," Ph.D. dissertation, California Institute of Technology, 2003.

[97] G. M. R. Tamanampudi, C. Huang, S. V. Sardeshmukh, and W. E. Anderson, "Integration of spatially distributed flame transfer functions with the non-linear euler equations," in *2018 AIAA Aerospace Sciences Meeting*, 2018, p. 0148.

[98] G. M. R. Tamanampudi, S. V. Sardeshmukh, and W. E. Anderson, "Sensitivity analysis of implementing cfd-based distributed flame transfer functions in a nonlinear euler solver," in *2018 Joint Propulsion Conference*, 2018, p. 4773.

VITA

VITA

Gowtham Manikanta Reddy Tamanampudi was born on 17th of July 1992 in Penugonda, India. He obtained a Bachelor of Technology degree in Aerospace Engineering from SRM University, Kattankulathur, India in 2013. He joined Purdue University in fall 2013 to pursue MS in Aeronautics and Astronautics with major in propulsion. He obtained MSAAE degree in 2015 under the guidance of Dr. William Anderson. He continued research and obtained his Doctor of Philosophy in 2019 in Aeronautics and Astronautics under the advisor Dr. William Anderson. At Purdue, he worked on exploration of a path-way towards a computational tool capable of accurately predicting the combustion instabilities in practical systems through the use of reduced fidelity nonlinear Euler equations and spatially distributed two-dimensional local flame transfer functions. Following Purdue he will begin working at Robert Bosch LLC located at Sunnyvale, California.